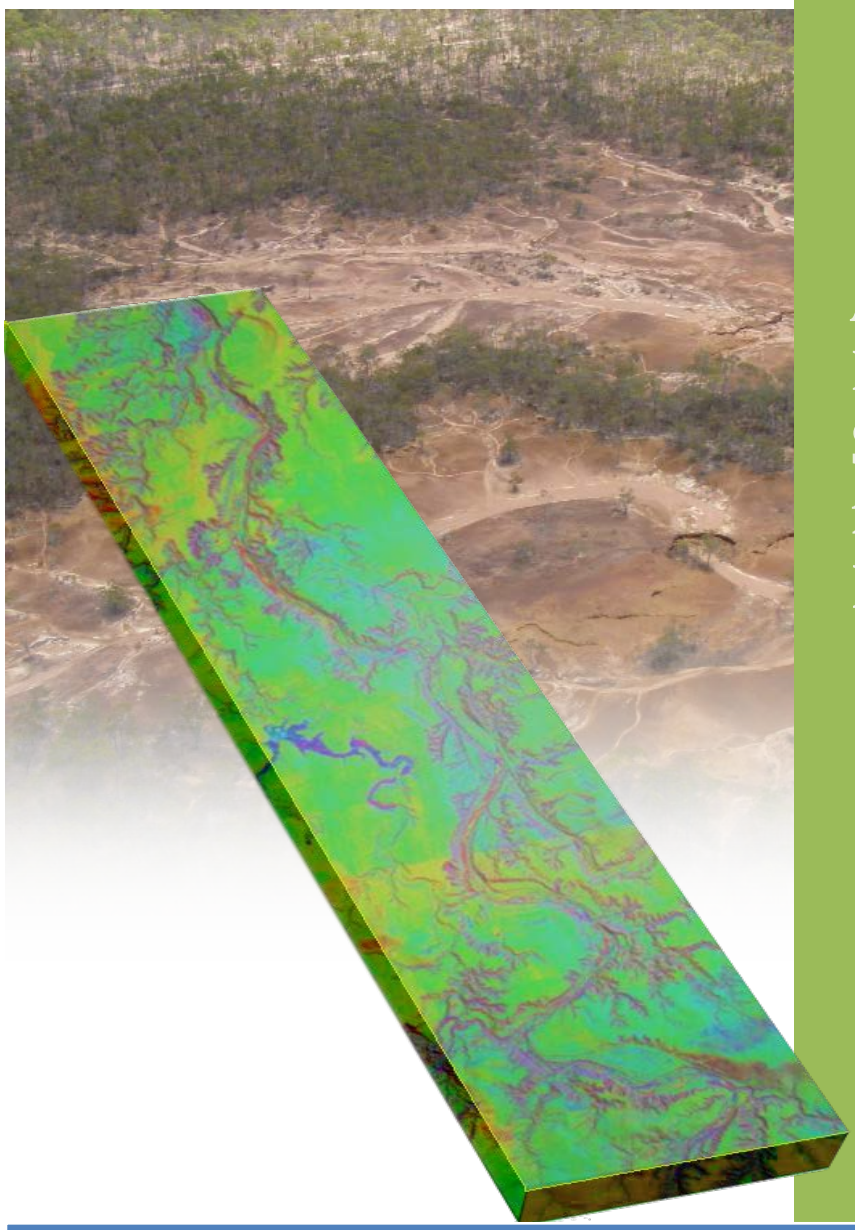

An Empirically-based Sediment Budget for the Normanby Basin

Andrew Brooks, John Spencer, Jon Olley, Tim Pietsch, Daniel Borombovits, Graeme Curwen, Jeff Shellberg, Christina Howley, Angela Gleeson, Andrew Simon, Natasha Bankhead, Danny Klimetz, Leila Eslami-Endargoli, Anne Bourgeault

Australian Rivers Institute

Griffith University

Appendix 09: Validation and Calibration of BSTEM for select sites on the East Normanby River

Griffith UNIVERSITY

CARING FOR OUR COUNTRY

Appendix to the Final Report prepared for the Australian Government's Caring for our Country - **Reef Rescue initiative**

IMPORTANT

This document is current at the date noted. Due to the nature of collaborative academic publishing, this content is subject to change and revision. Please see the Cape York Water Quality website for more info:

http://www.capeyorkwaterquality.info

This Version: 3/03/2013

CAPE YORK WATER QUALITY

Appendix 9

Validation and Calibration of BSTEM for select sites on the East Normanby River, QLD, Australia

Prepared by

Cardno ENTRIX

1223 Jackson Ave. E., Suite 301, Oxford, MS 38655

Tel 662 236 6983 Fax 662 281 9942Toll-free 800 368 7511

www.cardnoentrix.com

Table of Contents

Tables

Figures

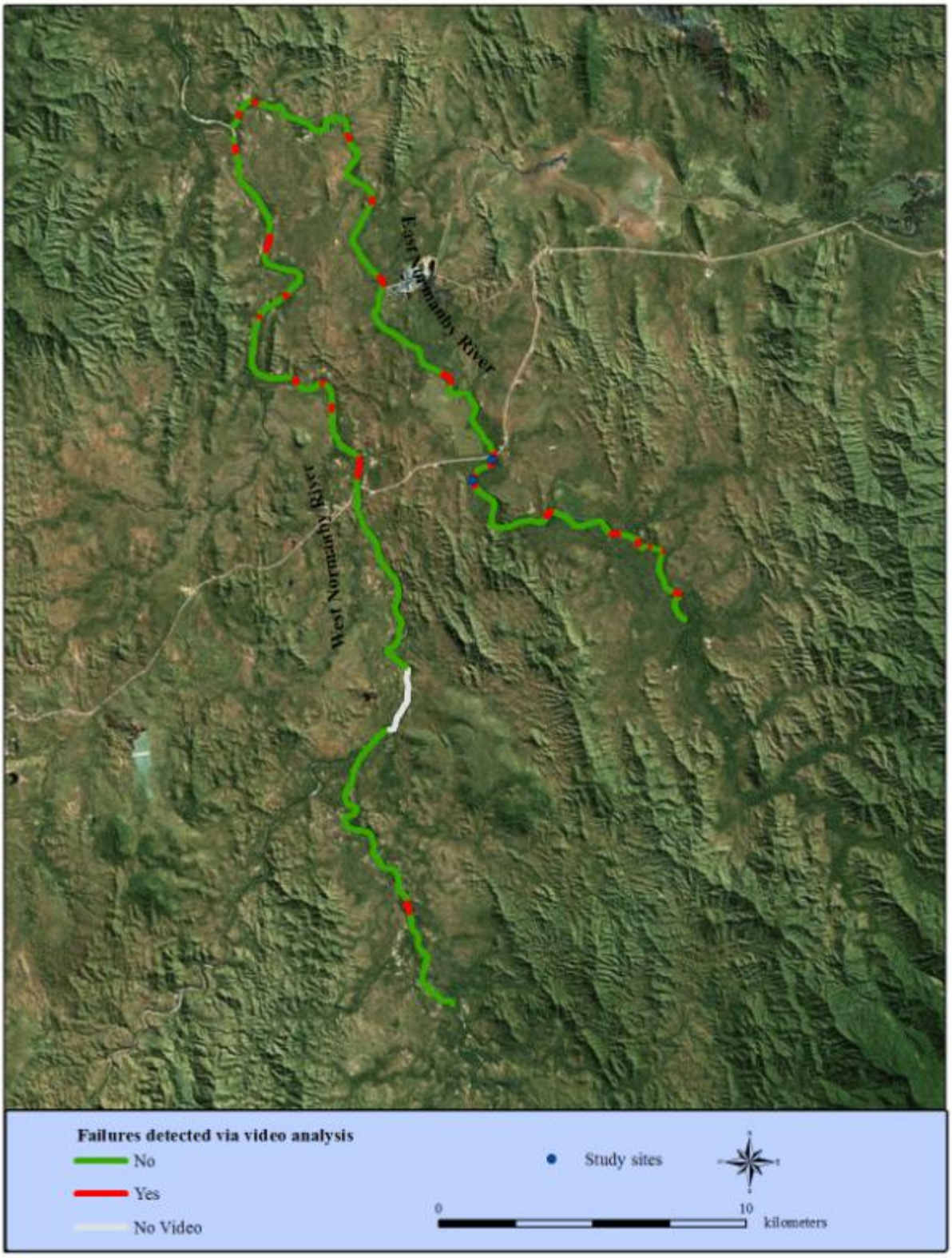

List of Prepares

Cardno ENTRIX staff

Management Staff

Principal-in-Charge ..... Andrew Simon

Project Manager ..... Andrew Simon

Deputy Project Manager ..... Natasha Bankhead

Key Staff

Field Data Collection ..... Andrew Simon, Danny Klimetz

Data Management ..... Lauren Klimetz

Geographical Information Systems (GIS) ..... Danny Klimetz

Hydrology / Water Quality ..... Natasha Bankhead, Danny Klimetz

Technical Editing ..... Natasha Bankhead

Chapter 1 Introduction

The delivery of fine-grained sediment and nutrients to the Great Barrier Reef (GBR) is posing a threat to the sustainability of the reef and bay ecosystems. Of this fine-grained sediment, streambank erosion from unstable stream systems can be a dominant source.

Streambank retreat and erosion take place by a combination of processes including hydraulic erosion of the bank surface and bank toe, and by geotechnical, or mass failure of the bank mass. The Bank-Stability and Toe Erosion Model (BSTEM) is a simple spreadsheet tool to simulate hydraulic and geotechnical processes in a completely mechanistic framework. It has been successfully used in a range of alluvial environments all over the globe in both static mode to simulate bank-stability conditions and the design of streambank-stabilization measures, and dynamically over periods of up to 100 years to evaluate hydraulic erosion, bank-failure frequency and thus, the volume of sediment eroded from a bank over a given period of time. Streambank loadings by particle-size class derived from BSTEM (using time steps from days to months) have been successfully integrated with both channel and catchment flow- and sediment-transport routing models. Reducing sediment loads from streambanks can be accomplished using a variety of mitigation measures that vary in cost and effectiveness. The reinforcing effects of riparian vegetation are quantified and included in analysis of mitigation strategies with the sub-model RipRoot. The role of the above-ground and below-ground biomass of riparian vegetation on hydraulic erosion of the surface materials is accounted for through grain roughness and the increase in critical shear stress for root-permeated soils, respectively. BSTEM has been shown to be very useful in testing the effect of potential mitigation measures to reduce the frequency of bank instability and decrease sediment loadings emanating from streambanks. These results can then be used to spatially extrapolate bank-derived volumes of sediment from individual sites to entire stream lengths when used in conjunction with Rapid Geomorphic Assessments (RGAs) of the study stream

1.1 Objectives

The overall objective of the larger study being conducted by Cardno's partners, is to develop a new sediment budget for the Normanby catchment. This progress report details the calibration and validation of the Bank Stability and Toe Erosion Model (BSTEM), which will be used to determine streambank sediment loadings, a key part of this overall sediment budget. Field data collected within the Normanby catchment pertaining to soil shear strength and hydraulic erodibility are detailed in this report, along with data collected on rooting characteristics of common riparian species found in this catchment.

1.2 Field site locations

Field data was collected at sites on Crocodile Creek, the East Normanby and on a gully in the Crocodile Creek watershed (Figure 1).

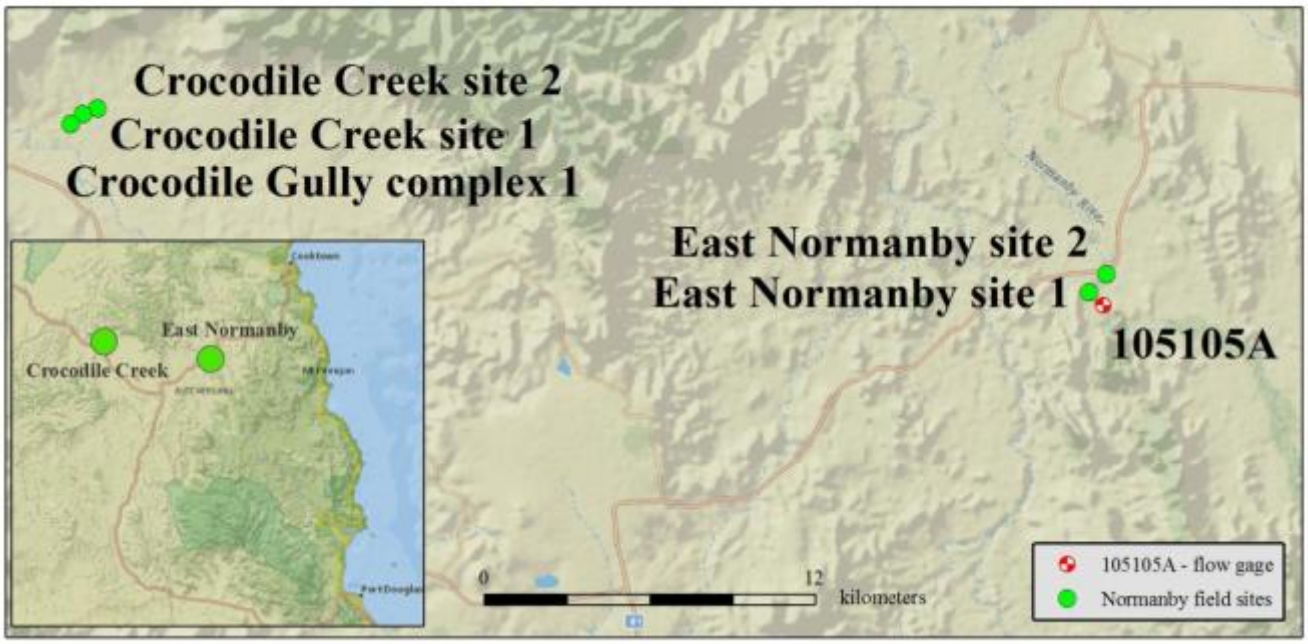

Figure 1 - Fieldsite locations for BSTEM geotechnical, hydraulic and root data collection.

Chapter 2
The Bank Stability and Toe Erosion Model (BSTEM-Dynamic)

Conceptual models of bank retreat and the delivery of bank sediments to the flow, emphasize the importance of interactions between hydraulic forces acting at the bed and bank toe, and gravitational forces acting on *in situ* bank materials (Carson and Kirkby, 1972; Thorne, 1982; Simon *et al*., 1991). Failure occurs when erosion of the bank toe and possibly the channel bed adjacent to the bank, increase the height and angle of the bank to the point that gravitational forces exceed the shear strength of the bank material. After failure, failed bank materials may be delivered directly to the flow and deposited as bed material, dispersed as wash load, or deposited along the toe of the bank as intact blocks, or as smaller, dispersed aggregates (Simon *et al*., 1991).

Bank materials do not maintain constant shear strength (resistance to failure) throughout the year. Strength varies with the moisture content of the bank and the elevation of the saturated zone in the bank mass. The wetter the bank and the higher the water table, the weaker the bank mass becomes and the more prone it is to failure. Bank failures, however, do not occur frequently during high flows because the water in the channel is providing a buttressing, or confining force to the bank mass. This is true even though it is during high-flow events that the bank may be undercut by hydraulic forces. It is upon recession of the flow when the bank loses the confining force but still maintains a high degree of saturation when it is most likely to fail. This is why changes in flow regime can be very important in determining trends of bank stability over time.

Analyzing streambank stability is a matter of characterizing the gravitational forces acting on the bank and the geotechnical strength of the *in situ* bank material. Field data are required to quantify those parameters controlling this balance between force and resistance. If we initially envision a channel deepened by bed degradation in which the streambanks have not yet begun to fail, the gravitational force acting on the bank cannot overcome the resistance (shear strength) of the *in situ* bank material. Shear strength is a combination of frictional forces represented by the angle of internal friction (ϕ'), and effective cohesion (c'). Pore-water pressures in the bank serve to reduce the frictional component of shear strength. A factor of safety (F_s) is expressed then as the ratio between the resisting and driving forces. A value of unity (or the critical case) indicates the driving forces are equal to the resisting forces and that failure is imminent.

The forces resisting failure on the saturated part of the failure surface are defined by the Mohr-Coulomb equation:

$$S_r = c' + (\sigma - \mu) \tan \phi' \quad (1)$$

where μ is the pore pressure and ϕ' is the angle of internal friction.

The geotechnical driving force is given by the term:

$$F = W \sin\beta \quad (2)$$

where, F = driving force acting on bank material (N), W = weight of failure block (N), and β = angle of the failure plane (degrees).

In the part of the streambank above the "normal" level of the groundwater table, bank materials are unsaturated, pores are filled with water and with air, and pore-water pressure is negative. The difference ($\mu_a - \mu_w$) between the air pressure (μ_a) and the water pressure in the pores (μ_w) represents matric-suction (ψ). This force acts to increase the shear strength of the material and with effective cohesion produces apparent cohesion (c_a). The increase in shear strength due to an increase in matric suction is described by the angle ϕ^b. This effect has been incorporated into the standard Mohr-Coulomb equation normally used for saturated soils by Fredlund *et al*. (1978), with a maximum value of ϕ' under saturated conditions (Fredlund and Rahardjo, 1993). The effect of matric suction on shear strength is reflected in the apparent or total cohesion (c_a) term:

$$c_a = c' + (\mu_a - \mu_w) \tan \phi^b = c' + \psi \tan \phi^b \quad (3)$$

As can be seen from equation 1, negative pore-water pressures (positive matric suction; ψ) in the unsaturated zone provide for cohesion greater than the effective cohesion, and thus, greater shearing resistance. This is often manifest in steeper bank slopes than would be indicated by ϕ'.

Thus, for the unsaturated part of the failure surface the resisting forces as modified by Fredlund *et al.* (1978) are used:

$$S_r = c' + (\sigma - \mu_a) \tan \phi' + (\mu_a - \mu_w) \tan \phi^b \quad (4)$$

where S_r is shear strength (kPa), c' is effective cohesion (kPa), σ is normal stress (kPa), μ_a is pore air pressure (kPa), μ_w is pore-water pressure (kPa), (μ_a-μ_w) is matric suction, or negative pore-water pressure (kPa), and tan ϕ^b is the rate of increase in shear strength with increasing matric suction.

2.1.1 The Dynamic Bank Stability and Toe Erosion Model (BSTEM-Dynamic)

The Bank Stability and Toe-Erosion Model (BSTEM; Simon *et al*. 1999) combines three limit-equilibrium methods that calculate the Factor of Safety (F_s) of multi-layer streambanks. The methods employed within BSTEM are horizontal layers (Simon *et al*., 1999), vertical slices with tension crack (Morgenstern and Price, 1965) and cantilever failures (Thorne and Tovey, 1981). All three methods account for the strength of up to five soil layers, the effect of pore-water pressure (both positive and negative (matric suction)), confining pressure due to streamflow and soil reinforcement due to vegetation. This description will focus upon the first and third methods as the second method has not been used herein due to the absence of observed tension cracks in the field. All model runs are for one bank only, with each site being independent of each other. Additionally, the model does not contain sediment transport or routing functions.

2.1.1.1 *Assessing Geotechnical Failure*

The enhanced bank-stability sub-model in the current version of BSTEM-Dynamic incorporates a random walk search algorithm for the minimum Factor of Safety, F_s. F_s is the ratio between the resisting and driving forces acting on a potential failure block. A value of unity indicates that the driving forces are equal to the resisting forces and that failure is imminent (F_s = 1.0). Instability exists under any condition where the driving forces exceed the resisting forces (F_s < 1.0), conditional stability is indicated by F_s values between 1.0 and 1.3, with stable bank conditions having a F_s value of >1.3. The Factor of Safety (F_s) of the horizontal layer method is given by:

$$F_s = \frac{\sum_{i=1}^{I}\left(\left[c_i^{'} + c_r\right]L_i + \left(\mu_a - \mu_w\right)_i L_i \tan\phi_i^b + \left[W_i\cos\beta - \mu_{ai}L_i + P_i\cos(\alpha-\beta)\right]\tan\phi_i^{'}\right)}{\sum_{i=1}^{I}\left(W_i\sin\beta - P_i\sin[\alpha-\beta]\right)} \quad (5)$$

where c_i' = effective cohesion of i^{th} layer (kPa), L_i = length of the failure plane incorporated within the i^{th} layer (m), W_i = weight of the i^{th} layer (kN), P_i = hydrostatic-confining force due to external water level (kN m^{-1}) acting on the i^{th} layer, β = failure-plane angle (degrees from horizontal), α = local bank angle (degrees from horizontal), and I = number of layers.

The cantilever shear failure algorithm results from inserting β = 90° into equation 5. F_s is given by:

$$F_s = \frac{\sum_{i=1}^{I}\left(c_i' L_i + \left(\mu_a - \mu_w\right)_i L_i \tan\phi_i^b + \left[P_i \sin\alpha - \mu_{ai} L_i\right]\tan\phi_i'\right)}{\sum_{i=1}^{I}\left(W_i + P_i \cos\alpha\right)} \quad (6)$$

The F_s is the ratio of the shear strength of the soil to the weight of the cantilever. The inclusion of α-terms in equation 6 ensures that if the bank is partially or totally submerged, the weights of the layers affected by water are correctly reduced irrespective of the geometry of the basal surface of the overhang.

2.1.2 Modeling Movement of the Groundwater Table

It is apparent from equations 3, 4, 5 and 6 that the elevation of the groundwater table is an important parameter controlling soil shear strength. For the purposes of this study, a simplified one-dimensional (1-D) groundwater model, based on the 1-D Richards Equation, was developed to simulate the motion of the groundwater table. This model assumes that the dominant pressure gradient within a streambank is the difference between the groundwater table elevation and the in-channel water surface elevation (i.e. it neglects the influence of infiltrating precipitation). Assuming that water infiltrates either into or out of the bank along a horizontal plane of unit length and computing distance-weighted mean soil properties between these two elevations, the simplified equation can be written as:

$$\frac{\partial h}{\partial t} - K_r K_{sat} = 0 \quad (7)$$

where h = groundwater elevation (m), t = time (s), and K_rK_{sat} = relative permeability × saturated hydraulic conductivity. K_r is evaluated as $K_r = \Theta^{1/2}\left[1-\left(1-\Theta^{1/b}\right)^b\right]^2$, where Θ = soil saturation and, following van Genuchten (1980), Θ is evaluated as:

$$\Theta = \Theta_r + \frac{\Theta_s - \Theta_r}{\left[1+\left(\frac{[z-h]}{l}\right)^{1/1-m}\right]^m} \quad (8)$$

where the subscripts r and s denote the residual moisture content and saturated moisture content, l and m are curve-fitting parameters and z is the water surface elevation (m). If $h \geq z$, $K_r = 1$.

2.1.3 Assessing Hydraulic Erosion

The magnitude of bank-face and bank-toe erosion and the extent of bank steepening by hydraulic forces are calculated using an algorithm that computes the hydraulic forces acting on either the left or right near-bank zone during a particular flow event.

The boundary shear stress exerted by the flow on each node is estimated by dividing the flow area at a cross-section into segments (Figure 2) that are affected only by the roughness of the bank or the bed and then further subdividing to determine the flow area affected by the roughness on each node (e.g. Einstein, 1942). The hydraulic radius of a segment, R_i, is the area of the segment, A_i, divided by the wetted perimeter of the segment. The boundary shear stress active at the node *i* may then be estimated as:

$$\tau_{oi} = \rho g R_i S \qquad (9)$$

where S = channel gradient (m m^{-1}).

Flow resistance in an open channel is a result of viscous and pressure drag over its wetted perimeter. For a vegetated channel, this drag may be conceptually divided into three components: (1) the sum of viscous drag on the ground surface and pressure drag on particles or aggregates small enough to be individually moved by the flow (grain roughness); (2) pressure drag associated with large non-vegetal boundary roughness (form roughness); and (3) drag on vegetal elements (vegetal roughness) (Temple *et al*., 1987). As energy lost to the flow represents work done by a force acting on the moving water, the total boundary shear stress may also be divided into three components:

$$\tau_o = \tau_{og} + \tau_{of} + \tau_{ov} \qquad (10)$$

where the subscripts *g*, *f* and *v* signify the grain, form and vegetal components of the boundary shear stress, respectively.

If it is assumed that these components may be expressed in terms of a Manning's coefficient for each, and Manning's equation is assumed to apply for each component, equation 9 can be rewritten as (Temple, 1980):

$$n^2 = n_g^2 + n_f^2 + n_v^2 \qquad (11)$$

where n = Manning's roughness coefficient (s m$^{-1/3}$). Grain roughness is estimated for each node on the bank profile using the equation of Strickler (Chow, 1959):

$$n_g = 0.0417 (D_{50}^{1/6}) \qquad (12)$$

Combining equations 10 and 11, the effective boundary shear stress, the component of the boundary shear stress acting on the boundary in the absence of form and vegetal roughness, may be computed as:

$$\tau_g = \tau_o (n_g^2 / n^2) \qquad (13)$$

The rate of erosion of bank-face and bank-toe materials can then be calculated using an excess shear approach (Partheniades, 1965).

An average erosion rate (in m/s) is computed for each node and time-step where the boundary shear stress exceeds the critical shear stress of the bank or toe material. This erosion rate is then integrated with respect to time to yield an average erosion distance. This method is similar to that employed in the CONCEPTS model (Langendoen, 2000):

$$E = k \Delta t (\tau_o - \tau_c) \qquad (14)$$

where E = erosion distance (cm), k = erodibility coefficient (cm^3/N-s), Δt = time step (s), and τ_c = critical shear stress (Pa).

Resistance of bank-toe and bank-surface materials to erosion by hydraulic shear is handled differently for cohesive and non-cohesive materials. For cohesive materials the relation developed by Simon *et al*. (2010) using a submerged jet-test device (Hanson, 1990) is used:

$$k = 1.6 \tau_c^{-0.8264} \qquad (15)$$

For non-cohesive materials the following relation is used:

$$k = 0.1 \tau_c^{-0.5} \qquad (16)$$

This relationship was analytically compared with excess shear stress-based bedload transport functions proposed by Du Boys (1879), Schoklitsch (1914), O'Brien and Rindlaub (1934), Shields (1936), Bagnold (1956), van Rijn (1984) and Wu et al. (2000) and was found to provide reasonable estimates of k for particles in the medium to coarse sand range.

During the dynamic simulations described herein, the erosion distance during a time-step is computed by integrating the erosion rate within the time-step by the time-step size. It must be stressed that the model is incapable of routing flow and sediment, so that estimates of erosion are only valid for "clear-water" conditions where the amount of sediment being transported by the flow is lower than sediment transport capacity. Field observations suggest that this is likely to be a reasonably safe assumption for the study reaches.

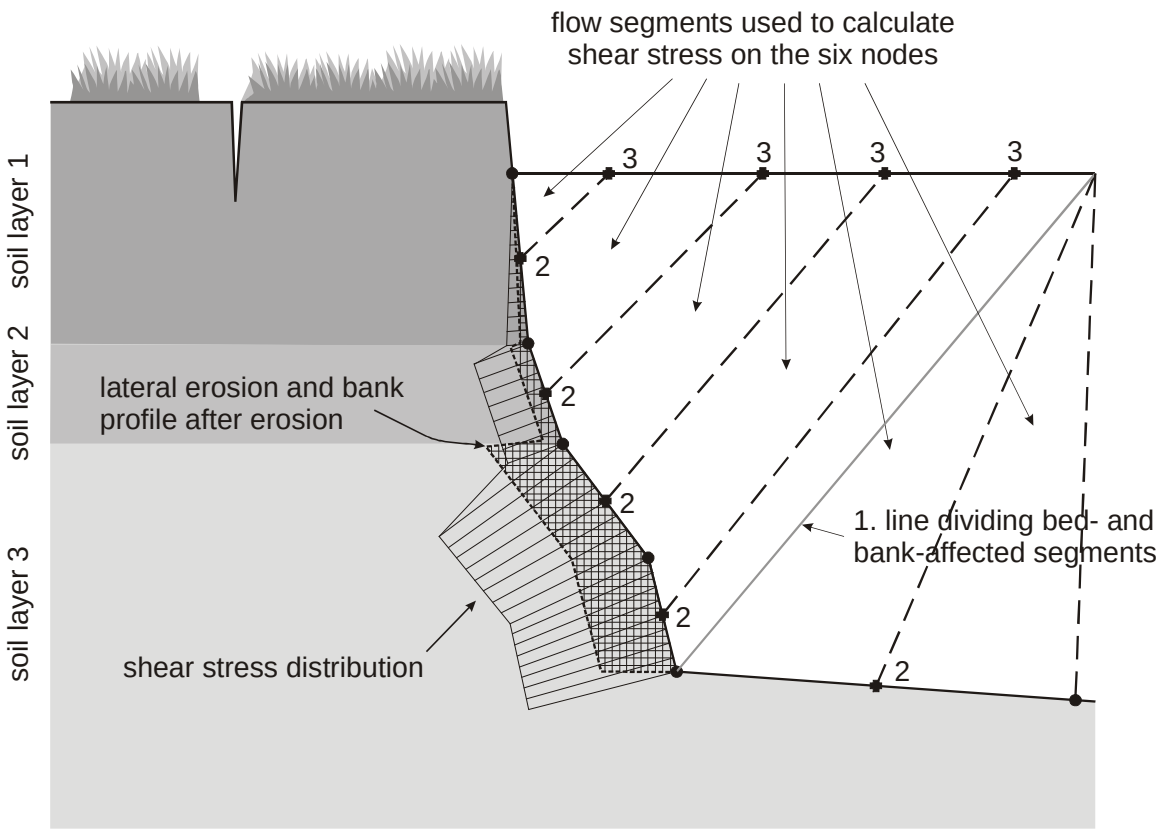

Figure 2 - Segmentation of local flow areas and hydraulic radii

2.1.4 Assessing Root-Reinforcement by Riparian Vegetation

Soil is generally strong in compression, but weak in tension. The fibrous roots of trees and herbaceous species are strong in tension but weak in compression. Root-permeated soil, therefore, makes up a composite material that has enhanced strength (Thorne, 1990). Numerous authors have quantified this reinforcement using a mixture of field and laboratory experiments. Endo and Tsuruta (1969) used in situ shear boxes to measure the strength difference between soil and soil with roots. Gray and Leiser (1982) and Wu (1984) used laboratory-grown plants and quantified root strength in large shear boxes.

Many studies have found an inverse power relationship between ultimate tensile strength, T_r, and root diameter, d (examples include but are not limited to: Waldron and Dakessian, 1981; Riestenberg and Sovonick-Dunford, 1983; Coppin and Richards, 1990; Gray and Sotir, 1996; Abernethy and Rutherfurd, 2001; Simon and Collison, 2002; Pollen and Simon, 2005; Fan and Su, 2008):

$$T_r = e(1000d)^f \tag{17}$$

where e = multiplier (MPa m^{-f}), and f = exponent (dimensionless) in the root tensile strength-diameter function, respectively. Note that f is always negative. Root strength (in kN) can therefore be evaluated as the product of the root area, A_r ($\pi d^2/4$), and the ultimate tensile strength, T_r:

$$T_r A_r = \frac{e\pi\left(1000^{1+f}\right)d^{2+f}}{4} \tag{18}$$

Smaller roots are stronger per unit area (higher ultimate tensile strength), but the larger cross-sectional area of larger diameter roots means that the peak load they can withstand before breaking, is higher than that of small roots.

Wu et al. (1979, after Waldron, 1977) developed a widely-used equation that estimates the increase in soil strength (c_r) as a function of root areal density and root distortion during shear:

$$c_r = \frac{1}{A}\sum_{i=1}^{i=I}\left(A_r T_r\right)_i\left[sin(90-\zeta)+cos(90-\zeta)tan\phi'\right] \tag{19}$$

where c_r = cohesion due to roots (kPa), T_r = tensile strength of roots (kPa), A_r = area of roots in the plane of the shear surface (m^2), A = area of the shear surface (m^2), I = total number of roots crossing the shear plane, the subscript $i = i^{th}$ root, and

$$\zeta = \tan^{-1}\left(\frac{1}{\tan\theta + \cot\chi}\right) \tag{20}$$

where θ = angle of shear distortion (degrees), and χ = initial orientation angle of fiber relative to the failure plane (degrees).

Pollen et al. (2004) and Pollen and Simon (2005) found that models based on equation 19 tend to overestimate root reinforcement because it is assumed that the full effect of each root is mobilized during soil shearing and that the roots all break simultaneously. This overestimation was largely corrected by Pollen and Simon (2005) by developing a fiber-bundle model (RipRoot) to account for progressive breaking during mass failure. RipRoot was validated by comparing results of root-permeated and non-root-permeated direct-shear tests. These tests revealed that, relative to results obtained with the perpendicular model of Wu et al. (1979), accuracy was improved by an order of magnitude, but some error still existed (Pollen and Simon, 2005).

One explanation for the remaining error in root-reinforcement estimates lies in the fact that observations of incised streambanks suggest that, when a root-reinforced soil shears, two mechanisms of root failure occur: root breaking and root pullout. The anchorage of individual leek roots was studied by Ennos (1990), who developed a function for pullout forces based on the strength of the bonds between the roots and soil:

$$F_P = \pi d \tau_s L_r \tag{21}$$

where F_P = pullout force for an individual root (N), and L_r = root length (m), which can be estimated in the absence of field data using $L_r = 123.1\ d^{0.7}$ (Pollen, 2007).

The pullout force was not accounted for in the original version of RipRoot (Pollen and Simon, 2005) and so the role played by spatio-temporal variations in soil shear strength was neglected. Pollen (2007) tested the appropriateness of equation 21 by making field measurements of the forces required to pull out roots. Pullout forces were then compared with breaking forces obtained from field testing and the RipRoot model was modified to account for both breaking and pullout.

A second explanation is that, following the work of Wu *et al*. (1979), it has commonly been assumed that the $\sin(90-\zeta) + \cos(90-\zeta)\tan\phi'$ term in equation 19 takes an approximately constant value of 1.2. Sensitivity analysis indicates that this assumption is flawed as this term varies from -1 when $\zeta = 180°$ to a maximum as $\zeta \rightarrow \phi'$. A series of Monte Carlo simulations was undertaken, assuming that θ was uniformly distributed between 0° and 90° and assuming that χ was uniformly distributed between ±90° from the vertical, approximating a heartroot network. Friction angle was varied from 0° to 44° and failure plane angle was varied from 10° to 90°. For this assumed distribution, the $\sin(90-\zeta) + \cos(90-\zeta)\tan\phi'$ term was found to be independent of failure plane angle. In addition, for a given friction angle, the distribution of values was highly skewed, with the median and 84th percentile being approximately equal but the 16th percentile being much smaller. It was found that it was possible to predict the median value of the $\sin(90-\zeta) + \cos(90-\zeta)\tan\phi'$ term using a cubic polynomial involving only the friction angle.

Chapter 3
BSTEM Data Collection

3.1 Geotechnical Data Collection: Borehole Shear Tests

To gather data on the internal shear strength properties of the banks, *in-situ* Borehole Shear Test (BSTs) devices were used (Figure 3; Figure 4). To properly determine the resistance of cohesive materials to erosion by mass movement, data must be acquired on those characteristics that control shear strength; that is cohesion, angle of internal friction, pore-water pressure, and bulk unit weight. Cohesion and friction angle data can be obtained from standard laboratory testing (triaxial shear or unconfined compression tests), or by *in-situ* testing with a borehole shear-test (BST) device (Lohnes and Handy 1968; Thorne *et al.* 1981; Little *et al*. 1982; Lutenegger and Hallberg 1981).

The BST provides direct, drained shear-strength tests on the walls of a borehole (

Figure 3). To use the BST, a 0.069 m (2.75 in) diameter hole is bored using an auger, from the floodplain above a channel bank into the middle of the bank layer to be tested. The shear head is then placed in the borehole to the desired depth and expanded, using CO_2 gas connected to the Normal Stress console, under a known initial pressure (generally about 40 kPa on the normal stress gauge) to the walls of the borehole. After initial consolidation, the pulling assembly is used to apply an axial stress to the shear head, measured on the shearing gauge, until failure beyond the walls of the borehole occurs. The axial stress is released, the normal pressure is raised in increments of about 10 kPa, and an additional 5-30 minutes of consolidation is provided, depending on the soil. The shearing process is repeated to generate a series of data points providing the shear stress to fail the material for each associated normal stress that is applied to the walls of the borehole. The data points are then plotted with normal stress on the x-axis and shear stress on the y-axis. The gradient of the resulting linear relationship represents the friction angle of the soil layer tested, and the intercept with the y-axis represents the apparent cohesion of the soil layer. Effective cohesion (*c'*) is then calculated using the apparent cohesion value and the result of a pore-water pressure reading of a soil sample taken from the BST location. Advantages of the instrument include:

1. The test is performed *in situ* and testing is, therefore, performed on undisturbed material.

2. Cohesion and friction angle are evaluated separately with the cohesion value representing apparent cohesion (c_a). Effective cohesion (*c'*) is then obtained by adjusting c_a according to measured pore-water pressure and ϕ^b.

3. A number of separate trials are run at the same sample depth to produce single values of cohesion and friction angle based on a standard Mohr-Coulomb failure envelope.

4. Data and results obtained from the instrument are plotted and calculated on site, allowing for repetition if results are unreasonable; and

5. Tests can be carried out at various depths in the bank to locate weak strata (Thorne *et al*. 1981).

At each testing depth, a small core of known volume was removed and sealed to be returned to the laboratory. The samples were weighed, dried and weighed again to obtain values of moisture content and bulk unit weight, both required for analysis of streambank stability.

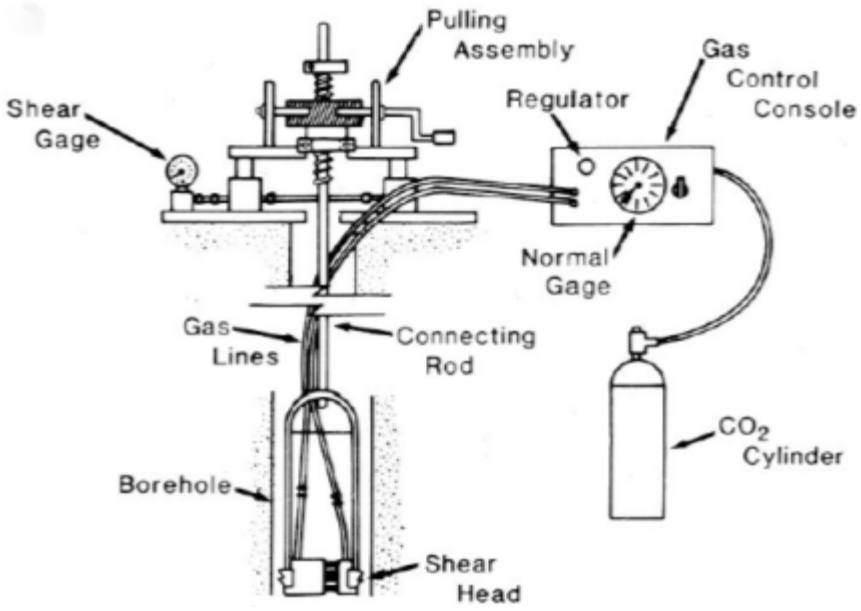

Figure 3 – Schematic representation of borehole shear tester (BST) used to determine cohesive and frictional strengths of *in-situ* streambank materials. Modified from Thorne *et al.*, 1981.

Figure 4 - Conducting a BST at the Normanby 1 site.

3.2 Geotechnical Data Collection: Submerged Jet Tests

Resistance properties of the bank-toe and face are input properties of the bank stability model. Where materials are non-cohesive, a bulk particle size or particle count are sufficient to describe resistance properties. However, cohesive materials are not entrained into the water column predictably due to particle size, as a result of electro-chemical bonds between particles. In order to test *in situ* erodibility of cohesive materials, a submerged jet-test has been developed by the Agricultural Research Service (

Figure 5; Hanson, 1990; ASTM, 1995). This device was developed based on knowledge of the hydraulic characteristics of a submerged jet and the characteristics of soil-material erodibility. The Mini-Jet used throughout this project is a scaled-down version of this instrument; side-by-side testing of the mini-jet and the standard submerged jet are reported in Simon *et al.*, 2011. Depth-of-scour is measured manually using a point gauge at known increments over time (Figure 6). As the scour depth increases with time, the applied shear stress decreases, due to increasing dissipation of jet energy within the plunge pool. Detachment rate is initially high and asymptotically approaches zero as applied shear stress approaches the critical shear stress of the bed material. The difficulty in determining equilibrium scour depth is that the length of time required to reach equilibrium can be large. It was found that fitting time series scour data to the logarithmic-hyperbolic method described in Hanson and Cook (1997) predetermines critical shear stress, τ_c. The erodibility coefficient, k, is then determined by curve fitting measured values of scour depth versus time and minimizing the error of the measured time versus the predicted time.

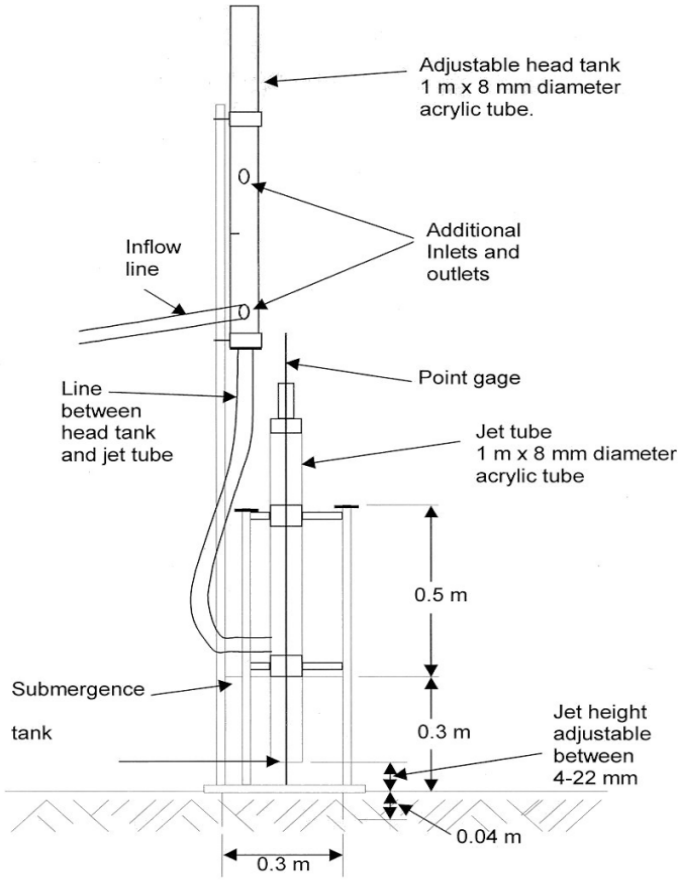

Figure 5 – Schematic of jet-test device (from Hanson and Simon, 2001).

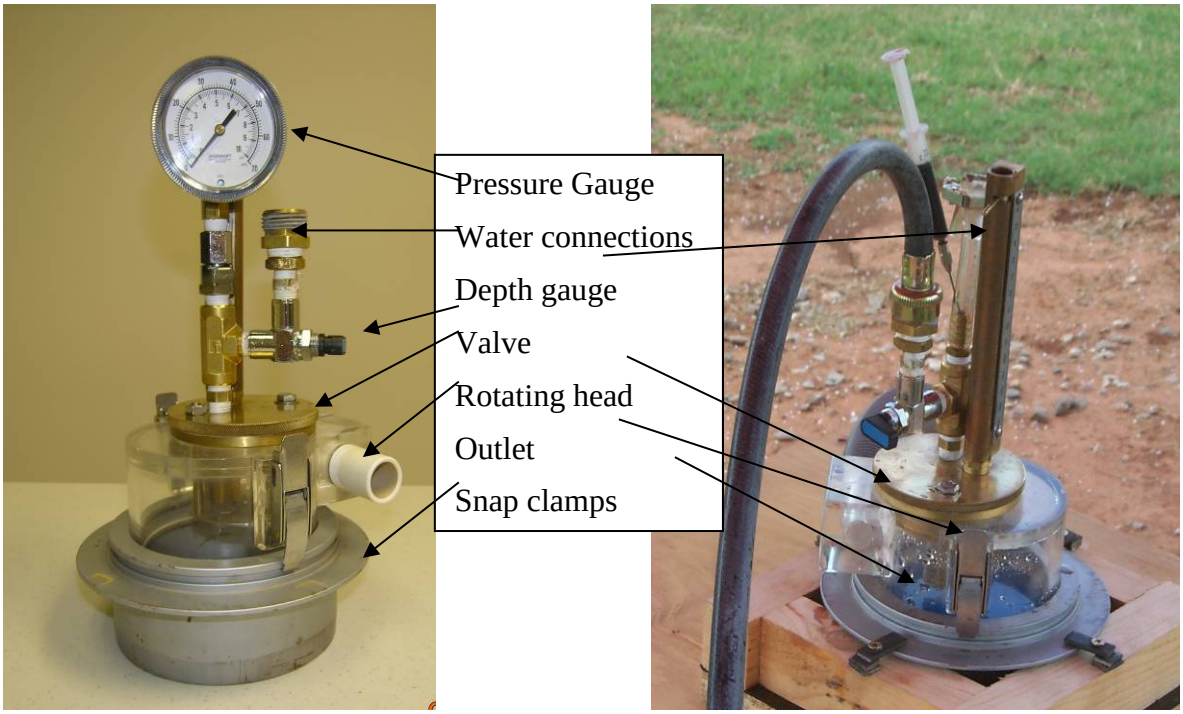

Figure 6 – Photographs of the scaled-down mini-jet submerged jet test device, used *in situ* to measure soil erodibility.

Figure 7 - Conducting jet tests at Normanby 1 and Crocodile Creek

3.3 Geotechnical Data Collection: Results

BST results showed that effective cohesion values at the sites tested ranged from 0 to 18.7 kPa (Table 1), with the materials tested generally being described as silty sands. The wide variability in effective cohesion values suggests that the inherent strength of the bank materials can vary considerably both with depth at individual sites, and between sites along the same river. The effective cohesion within each soil layer is a function on both the electrochemical bonding between the clay and silt particles, and possible cementation between particles following successive wetting and drying events. Jet test data collected at the Crocodile Creek and East Normanby sites ranged from 0.008 Pa (indicative of a very fine sand) to 2.7 Pa (typical of a silt).

Table 1. BST data collected at Crocodile Creek and East Normanby sites

Site	Test	Depth m	c_a Pa	c' Pa	c' used Pa	ϕ degrees	Suction kPa	ϕ^b degrees	Field Eval.
Crocodile 1	1	0.6	17.5	5.15	5.15	21.6		10	sandy silt
Crocodile 1	2	0.5	13.7	1.35	1.35	28.3		10	sandy silt
Crocodile 2	2	0.6	20.8	8.49	8.49	22.1		10	sandy silt
Crocodile 2	1	1.4	16.7	4.37	4.37	33.5		10	sandy silt
Crocodile 2	3	2.2	16.5	4.16	4.16	30.1		10	sandy silt
E. Normanby 1	1	1.4	0.40	-11.95	0.0	29.2	850	10	silt
E. Normanby 1	2	4.5	15.0	0.94	0.94	25.7	800	10	silt
E. Normanby 1	3	6.1	28.8	15.6	15.6	17.4	751	10	silt
E. Normanby 2	1	2.0	6.2	-6.14	0.0	30.1		10	sandy silt
E. Normanby 2	2	5.1	16.9	4.51	4.51	29.9		10	sandy silt
Crocodile Gully	3	0.35	4.33	-8.01	0.0	32.2		10	sandy silt
Crocodile Gully	1	0.35	31.0	18.65	18.65	7.3		10	sandy silt
Crocodile Gully	4	0.90	10.8	-1.54	0.0	37.2		10	sandy silt
Crocodile Gully	5	2.0	9.7	-2.67	0.0	33.7		10	clayey silt

Table 2. Jet test data collected at Crocodile Creek and East Normanby sites.

Channel	Site	Bank	Mini-J - Blaisdell	
			τ_c in Pa	k in $cm^3/N\text{-}s$
Crocodile Creek	1	Bank face	0.2452	8.17096
Crocodile Creek	1	Bank face	0.2227	23.6076
Crocodile Creek	2	LBFace 0.7 m	0.1497	36.1654
Crocodile Creek	2	LBFace 0.7 m	0.2812	17.78
Crocodile Creek	2	Toe	0.3473	25.978
Crocodile Creek	2	Toe	0.0833	24.8276
Crocodile Creek	2	Toe	1.453	33.0989
Crocodile Creek	2	Toe	2.371	15.3871
Crocodile Gully	Gully	Layer1 0.3 m	0.0381	51.4776
Crocodile Gully	Gully	Layer2 1.3 m	0.4836	3.39409
Crocodile Gully	Gully	Layer3 2 m	0.0387	4.59982
East Normanby	Site 2 at Bridge	LBFace bench	0.00836	27.5098
East Normanby	Site 2 at Bridge	LBFace bench	2.7168	8.14904
East Normanby	Site 2 at Bridge	LBFace bench	0.3568	41.6329
East Normanby	Site 2 at Bridge	LBFace bench	0.171	28.3349
East Normanby	Site 2 at Bridge	LBFace bench	0.013	35.1203
East Normanby	Site 1 DSGage	Lower layer	0.1454	15.222
East Normanby	Site 1 DSGage	Lower layer	0.0302	19.5232
East Normanby	Site 1 DSGage	Upper layer	0.2044	3.51198
East Normanby	Site 1 DSGage	Upper layer	0.3344	16.9115
East Normanby	Site 1 DSGage	Upper layer	0.7826	2.19684

Chapter 4
Riparian Vegetation Data Collection

4.1 Methodology

Root diameter distributions were measured on exposed bank faces at several locations within the Normanby watershed as per the wall profile method of Bohm (1979). Data were analyzed to determine typical rooting depth and diameter distributions for various riparian tree species and assemblages by measuring the diameters of roots protruding from 0.5m depth increments along exposed bank faces (Figure 8). The length of bank studied was also recorded so that root densities per meter length of bank could be calculated and compared to other data sources. The root system, leaves, canopy and bark of each tree studied were also photographed to allow for identification of species.

Figure 8 - Collecting root diameter distribution data at the Normanby 1 site. Left shows pink flagging identifying 0.5m depths. Right shows data collection using digital caliper.

4.2 Results

Several trends were seen within the root distribution data collected. First, root densities tended to decline non-linearly with depth, a common trend within root architecture studies (Pollen-Bankhead and Simon, 2009; Canadell *et al.*, 1996; Jackson *et al.*, 1996; Schenk and Jackson, 2002; Shields and Gray, 1992). The plots in Figure 9 show an example from a *Casuarina* tree studied at the Normanby 2 site, with plots for the remaining trees studied being shown in Appendix A. In addition, the frequency of smaller diameter roots was generally higher than larger diameter roots (Figure 9 B and C). This is to be expected also, because tree root architectures tend to develop in a similar way to drainage networks, with many small "first order" roots whose role is predominantly to extract moisture and nutrients from the soil matrix, and fewer "higher order" roots whose primary roles are to provide anchorage to the tree, and extract water from greater depths.

It has been hypothesized (Hubble and Hull, 1996; Abernethy and Rutherfurd, 2000; 2001; Docker and Hubble, 2001; Hubble 2001, 2004) that Australian riparian tree species have root architectures that act to enhance bank strength more than riparian tree species in other parts of the world. Root densities per meter of bank were therefore calculated to be used as a comparison with data collected for North American riparian species, to see if similarities or differences existed between the data sets. Rooting densities per square meter of bank face were quite low in many cases (Figure 10) when compared to the typical root-growth curve developed for US riparian species (Pollen-Bankhead and Simon, 2009). Of the four points from the Australian dataset that fall near the average US curve, three of these were for *Melaleuca* trees. The remaining trees or assemblages studied had approximately 50 roots per meter square of bank, even for older trees.

In addition to root density, it is however, important to consider rooting depths. Although the lateral roots measured from the bank face were concentrated in the top meter of the bank, in some cases roots were recorded on the bank face as deep as 2.5 m. It should be noted here that these roots represent only the lateral roots that can be seen on exposed bank faces, and deeper vertical roots were likely missed. A review by Hubble et al. (2010) noted that other studies of Australian riparian species have reported rooting depths of 5 to 20 m, with these deep root networks significantly increasing bank stability and mitigating against mass failure events. Indeed, it appears from the data collected here that it is not necessarily the density of roots that provides superior root-reinforcement in Australian riverine environments, but the ability of the riparian tree species present to root to such great depths. The effects of this deep rooting are two-fold. First the deeper roots act like vertical reinforcing piles within the bank, that cross potential planar and circular failure planes within the banks. Second, the removal of water by roots to great depths throughout the banks decreases pore-water pressures within the banks and thus increases the geotechnical stability of the banks. This effect on pore-water pressure varies both spatially, according to rooting depths, and temporally. Whilst the effect on pore-water pressures can be significant during dry periods, (Simon and Collison, 2002), once the banks have recharged at the start of the wet season, this effect is likely to be less important than that of woody root-reinforcement, which varies less seasonally (Bankhead and Simon, 2010).

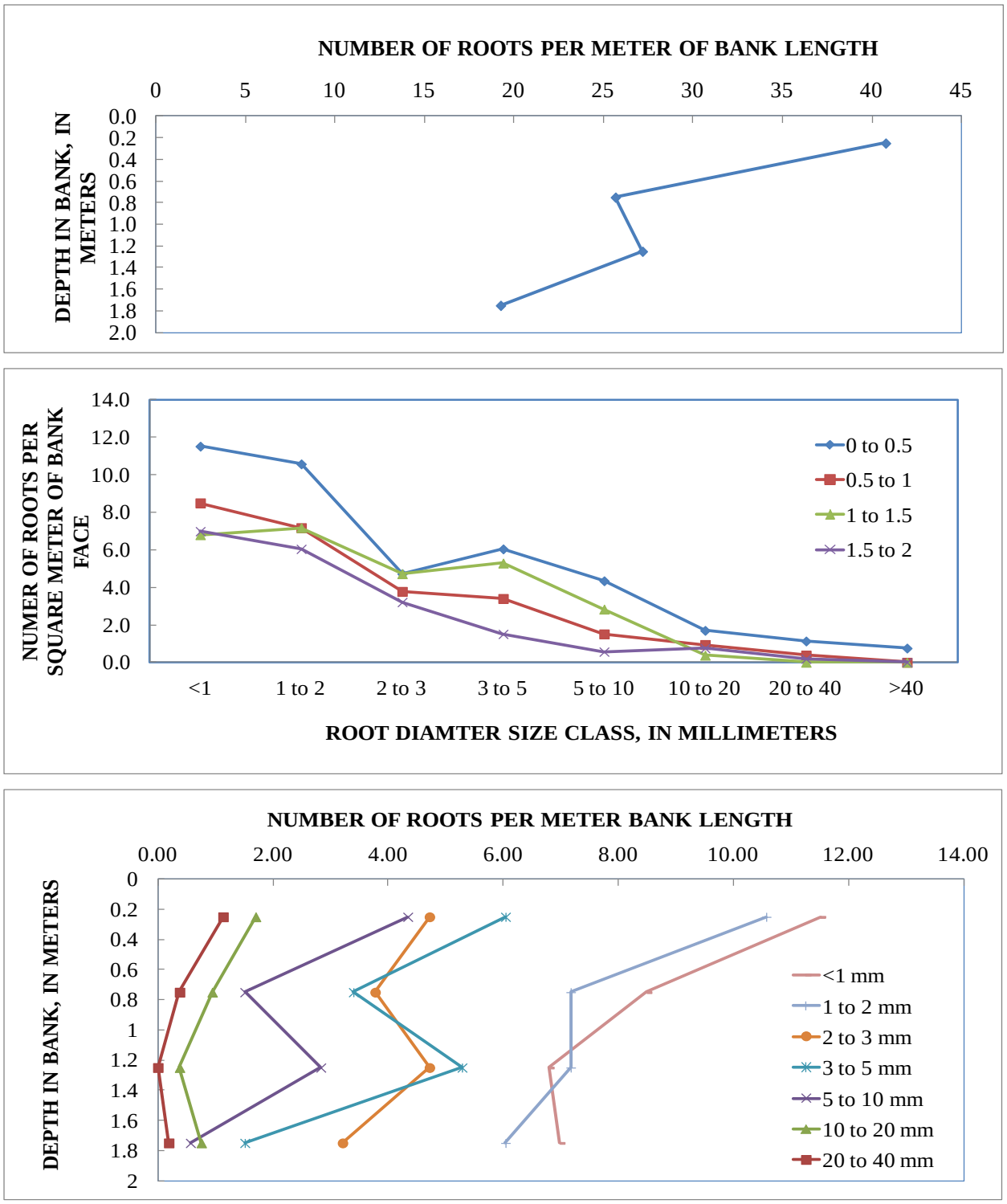

Figure 9 - Example of root-diameter distribution data for a *Casuarina* tree studied at the Normanby 2 site showing A) Total number of roots within each 0.5m bank layer B) Number of roots within each size class, separated by soil layer and C) Number of roots at each depth within each diameter size class.

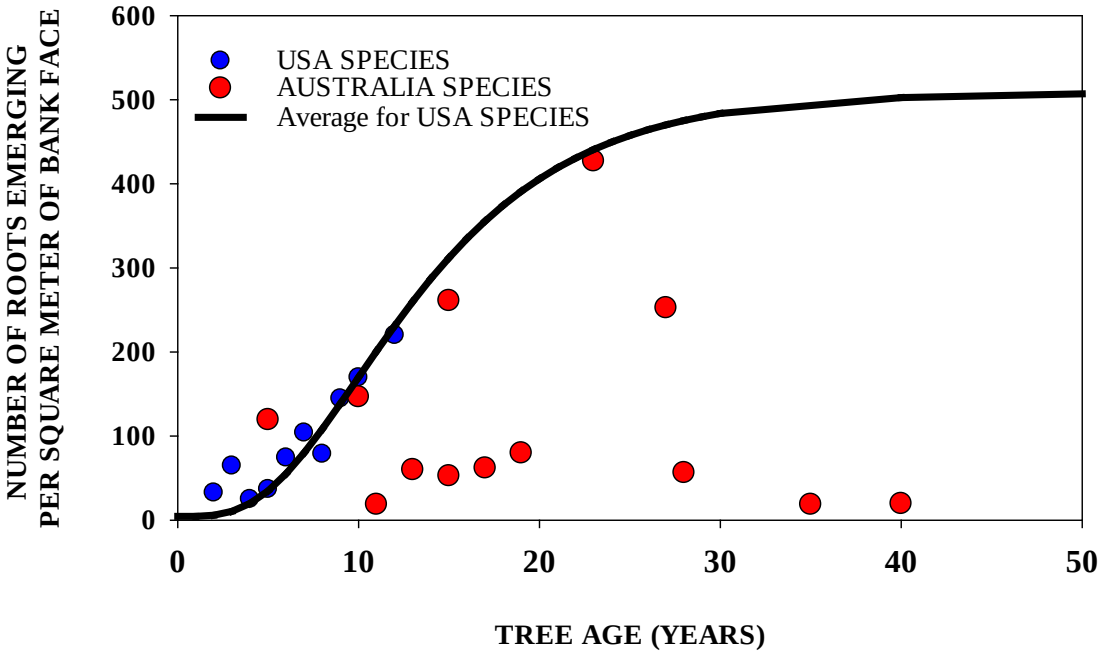

Figure 10 - Comparison of the number of roots exposed per meter square of bank face for USA riparian species and trees measured in the Normanby catchment. N.B. Age estaimtes for the Australia species were based on tree diameter alone. A relationship between stem diameter and tree age likely has a considerable degree of error associated with it.

Chapter 5
BSTEM Calibration Runs

5.1 Normanby 1 Site

Calibration was performed using BSTEM for the 2009 to 2011 flow record at the Normanby 1 site, using discharge data from gauge 105105A. As shown in the photos in

Figure **11** A and B, this site has a steep bank, with a riparian cover of *Eucalyptus* spp. and *Corymbia clarksonia* on the bank top. The bank face itself is largely bare of vegetation, with exposed roots on the upper 1-3 meters of the bank face. At the base of the bank, established riparian trees are present on the bank toe, providing some protection from hydraulic scour, and actually encouraging accretion in some areas. Areas of accretion can be seen in the

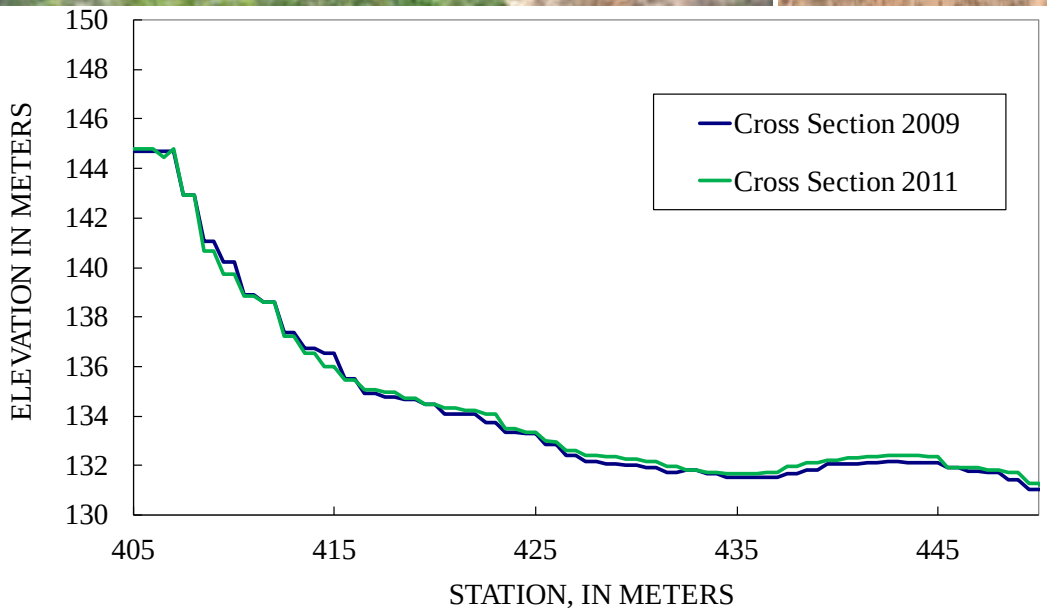

before and after cross sections of this profile in

Figure **11** C.

C

Figure 11 - A) and B) show photos of the Normanby 1 site, C) shows the 2009 and 2011 bank profiles (taken from LiDAR data), being used to calibrate BSTEM.

The 2009 and 2011 profiles also showed that no banktop erosion occurred during the calibration period although some erosion did occur on the bank face and toe region. The 2009 and 2011 cross sections were obtained from LiDAR data and are only accurate to ± 30 cm vertically and ± 50 cm horizontally. This means that whilst this data can be used to capture the occurrence of mass failure events between two dates, fluvial scour is likely below the level of detection.

The discharge data for the calibration period from 2009 to 2011 are shown in Figure 12. The annual peaks for 2010 and 2011 included in the BSTEM run were 143 and 235 cms respectively. When compared to the longterm flow record at this gauge (Figure 13), these values represent the 46th and 68th percentiles for peak annual discharges. The calibration period therefore represents a fairly average set of flow years, but does not encompass the full range of high discharges historically experienced at this site. For calibration purposes this is not problematic though as long as the model can be calibrated to correctly predict the bank changes seen between the 2009 and 2011 cross sections.

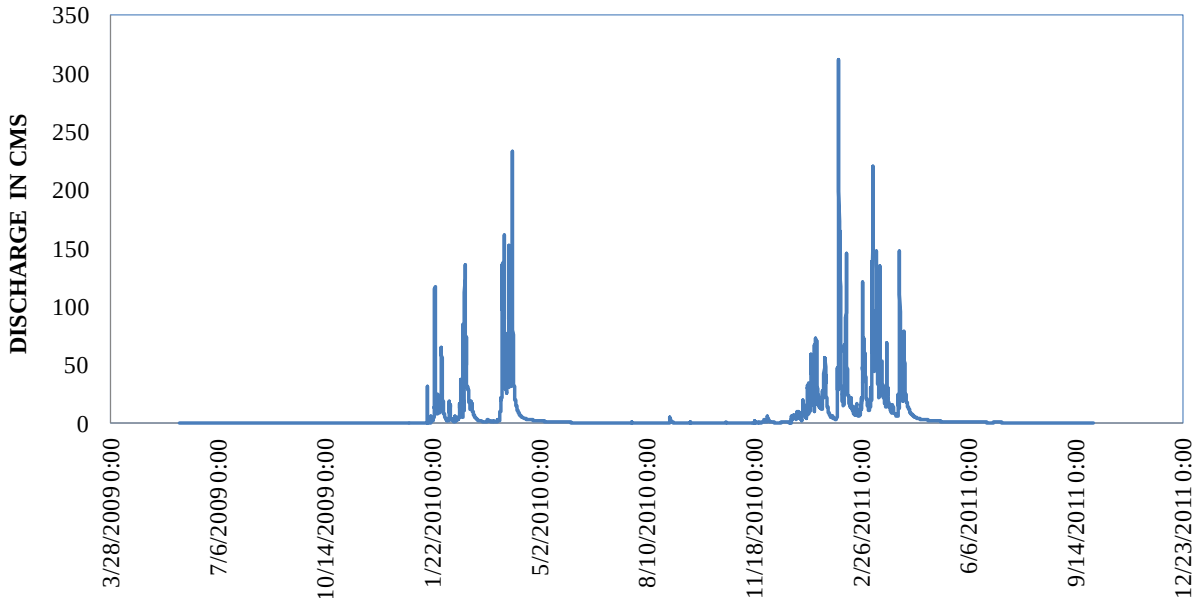

Figure 12 - Discharge data from gauge 105105A for calibration period 2009 to 2011

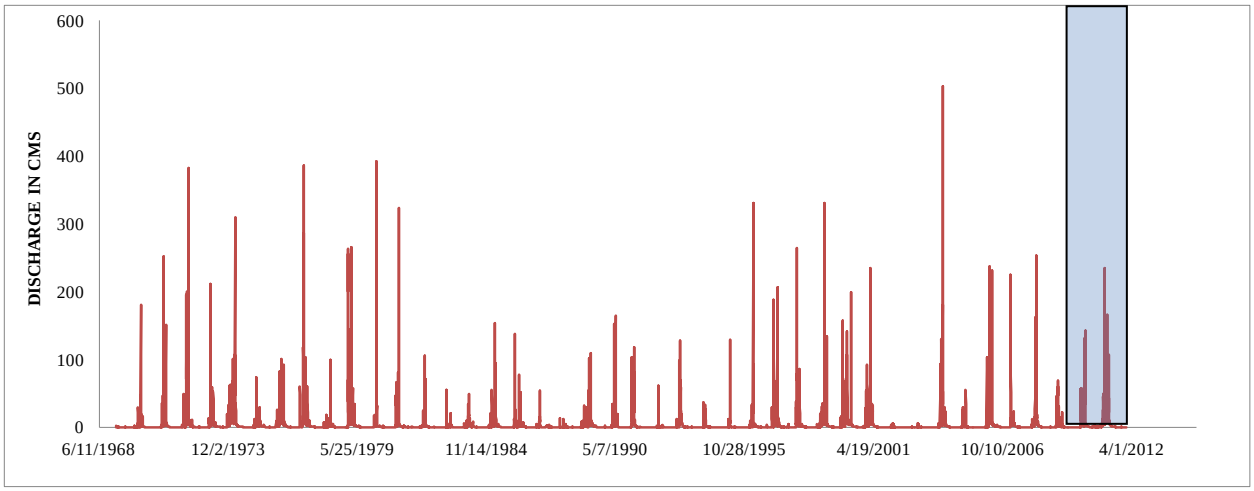

Figure 13 - Discharge data from gauge 105105A from 1968 to 2012.

The discharge record for the calibration period was converted to flow stage using a normal-depth spreadsheet tool, that estimated flow stage over the range of discharges input to the channel cross section at the Normanby 1 site, using a range of Manning's n values. To use this tool, the full cross section, and channel slope obtained from the 2009 LIDAR data were used (0.0011; Figure 14).

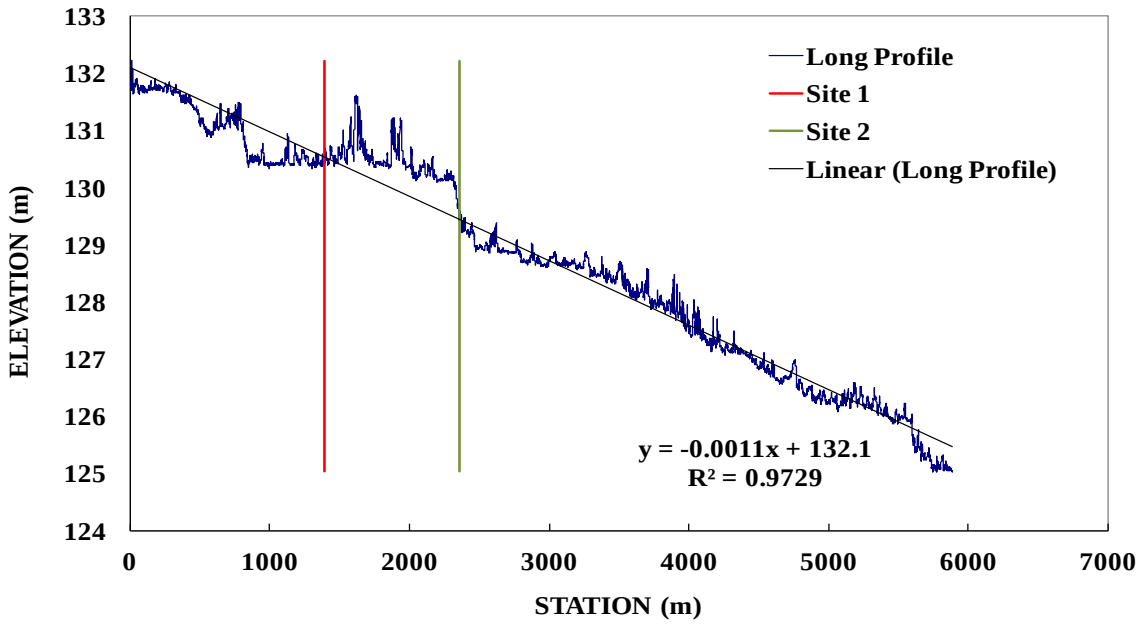

Figure 14 - Slope obtained from LIDAR thalweg data

Bank geometry was obtained from the 2009 LIDAR data provide in

Figure **11**. Bank material layering, geotechnical and hydraulic parameters were taken from field data collected *in situ*_at the site (Table 1; Table 2). This information was input to BSTEM-Dynamic (Figure 15; Figure 16). Root-reinforcement was estimated using the RipRoot submodel within BSTEM-Dynamic; the root-diameter distribution curves obtained in the field for *Eucalyptus* spp. and *Corymbia clarksonia* trees were used as input to RipRoot in conjunction with recorded rooting depths and percent vegetation cover at the site being modeled. Root-tensile strength data were not collected during this stage of fieldwork so the

root-tensile strength curve published by Abernethy and Rutherfurd (2001) for Eucalyptus and Meleleuca species was used:

$$T_r = 49.391 d^{-0.773}$$

Where T_r = root tensile strength, and d = root diameter in mm.

The only modification made to the field data collected was to increase the critical shear stress (τ_c) of the toe material to account for the trees that were present at the base of the bank, which act to reduce the applied shear stress in this region of the bank. The jet test τ_c value was increased by a factor of ten (Simon and Thomas, 2009) to account for vegetation in this zone, and corresponding k value applied.

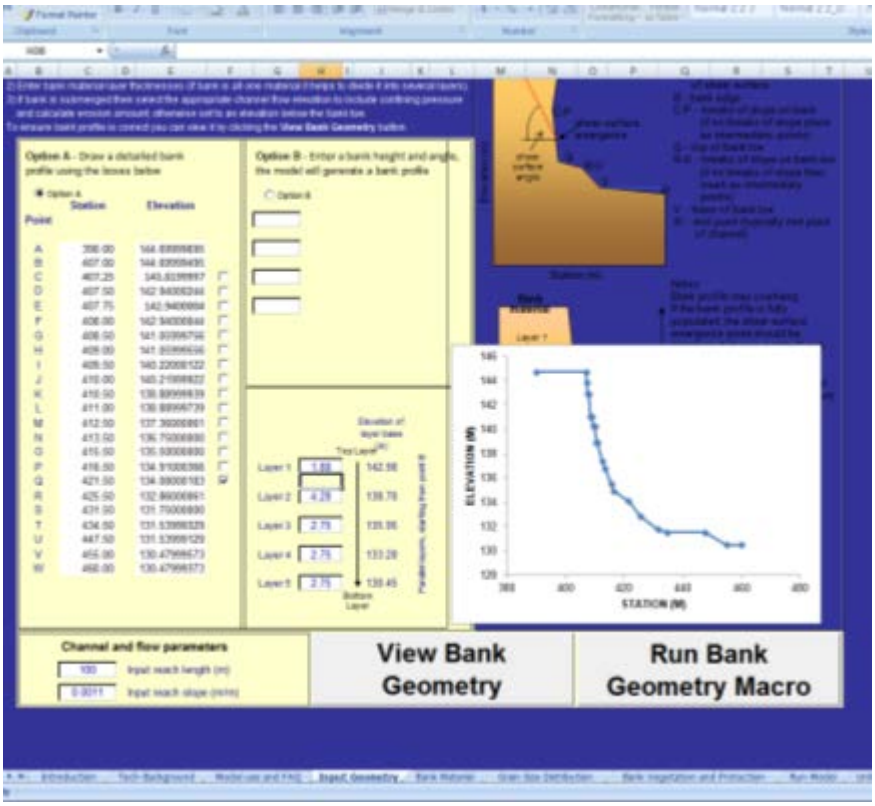

Figure 15 - Input cross section and layering for Normanby 1 site in BSTEM.

Bank and bank-toe material data tables.

These are the default parameters used in the model. Changing the values or descriptions will change the values used when selecting soil types from the list boxes above. Add your own data using the white boxes.

Material Descriptors			Bank Model Input Data					Groundwater Model Input Data			Toe Model Input Data	
Bank material type	Description	Mean grain size, D_{50} (m)	Friction angle ϕ' (degrees)	Cohesion c' (kPa)	Saturated unit weight (kN/m^3)	ϕ^b (degrees)	Chemical concentration (kg/kg)	Hydraulic Conductivity K_{sat} (m/s)	van Genuchten α (1/m)	van Genuchten n	τ_c (Pa)	k (cm^3/N/s)
1	Boulders	0.512	42.0	0.0	20.0	15.0	-	1.745E-03	3.5237	2.3286	498	0.004
2	Cobbles	0.128	42.0	0.0	20.0	15.0	-	1.745E-03	3.5237	2.3286	124	0.009
3	Gravel	0.0113	36.0	0.0	20.0	15.0	-	3.160E-03	3.5237	2.3286	11.0	0.030
4a and 4b	Angular sand	0.00035	36.0	0.0	18.0	15.0	-	7.439E-05	3.5237	3.1769	Coarse (0.71 mm) or	
5a and 5b	Rounded sand	0.00035	27.0	0.0	18.0	15.0	-	1.130E-06	4.0563	2.3286	Fine (0.18 mm)	
6a, 6b and 6c	Silt	-	30.0	3.0	18.0	15.0	-	5.064E-06	0.6577	1.6788	Erodible (0.100 Pa),	
7a, 7b and 7c	Soft clay	-	25.0	10.0	18.0	15.0	-	9.473E-07	1.5812	1.4158	Moderate (5.00 Pa), or	
8a, 8b and 8c	Stiff clay	-										
	Own data layer 1		25.7	5.9	18.0	10.0		5.064E-06	0.6577	1.6788	0.44	3.153
	Own data layer 2		25.7	0.9	18.0	10.0		5.064E-06	0.6577	1.6788	0.44	3.153
9	Own data layer 3		17.4	15.6	18.0	10.0		5.064E-06	0.6577	1.6788	0.15	7.670
	Own data layer 4		17.4	15.6	18.0	10.0		5.064E-06	0.6577	1.6788	0.15	7.670
	Own data layer 5		17.4	15.6	18.0	10.0		5.064E-06	0.6577	1.6788	0.15	7.670
	Own data Bank Toe				18.0						1.50	1.144

Figure 16 - Bank material property input parameters for Normanby 1 site in BSTEM.

Manning's n values ranging from 0.07 to 0.09 were run through the normal-depth worksheet with corresponding changes in the stage record then being tested in a set of calibration runs in BSTEM-Dynamic. The resulting before and after bank profiles from the BSTEM runs for the calibration period are shown in

Figure 17. The profiles show no bank retreat, but some erosion in the bank toe region, ranging from 5.06 m^2 for an n-value of 0.09 to 10.67 m^2 for an n-value of 0.07. These resulting bank profiles show good agreement with the changes in the bank profile seen in the 2009 and 2011 LIDAR data (

Figure **11** C), bearing in mind that these bank profiles are based on repeat LiDAR data, in which the observed changes are approaching the detection limit of the method. The exception is that in the LIDAR data, some accretion can be seen within the toe region, because the trees act to reduce flow velocity in this region. BSTEM is unable to predict accretion and so this is not shown in the resulting BSTEM profiles at the end of the calibration period. To model a 40-year period for this site, a Manning's n value of 0.07 will be used. This n-value best approximates the roughness characteristics seen in the field at this site, and the enhanced erosion seen under this condition is likely to occur at higher discharges when flow is routed behind the trees on the flatter part of the bank toe. The presence of both aggradation, and some active widening are both indicative of a channel in Stage V of the channel evolution model of Simon and Hupp (1986) and Simon (1989).

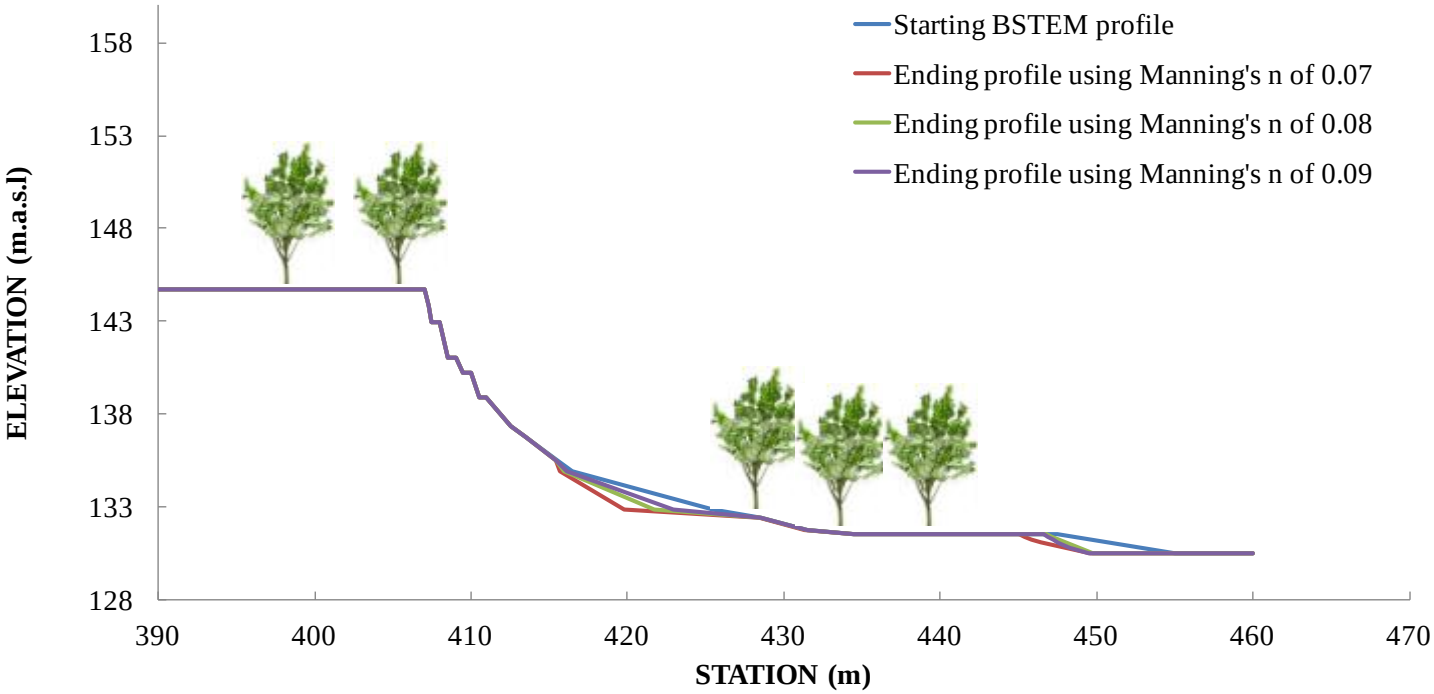

Figure 17 - BSTEM profiles for Normanby 1 before and after calibration period, using varying Manning's n values, and trees located at the bank toe.

5.2 Crocodile Creek Site 1

Calibration at this site was not possible because repeat cross section data was unavailable. A 3-year run was performed in BSTEM prior to running the 40-year flow period, to check for reasonable annual erosion rates. Flow data for this site was obtained through model results provided by Griffith University. The flow period modeled by Griffith University did not coincide with the flow period used for calibration at the E. Normanby site, but a 3-year period with similar frequency, magnitude and duration flow events was selected: 2007 – 2009, and lateral retreat rates were compared to the 2009 to 2011 period for which repeat LiDAR was available.

Figure 18 – Crocodile Creek 1 fieldsite.

The streambank sites on Crocodile Creek were lower in height than the E. Normanby site (2.56 m vs 14.22 m) (Figures 18, and 19). Riparian trees were present on the bank top, with roots permeating the top 1-2 m of the upper bank. As with the Normanby site, bank geometry was obtained from the 2009 LIDAR data. Bank material layering, geotechnical and hydraulic parameters were taken from field data collected *in situ* at the site (Table 1; Table 2). This information was input to BSTEM-Dynamic (Figure 19 and Figure 20).

A Manning's n value of 0.03 was selected for this site, based on the relatively smooth toe and bank surfaces where roots were not present. The critical shear stress (τ_c) values of the top two layers of the bank were modified to account for the bank top tree roots permeating the bank, which act to reduce the applied shear stress in this region. The jet test τ_c value for critical shear stress was increased by a factor of ten (Simon and Thomas, 2009) to account for vegetation in this zone, and corresponding *k* value applied.

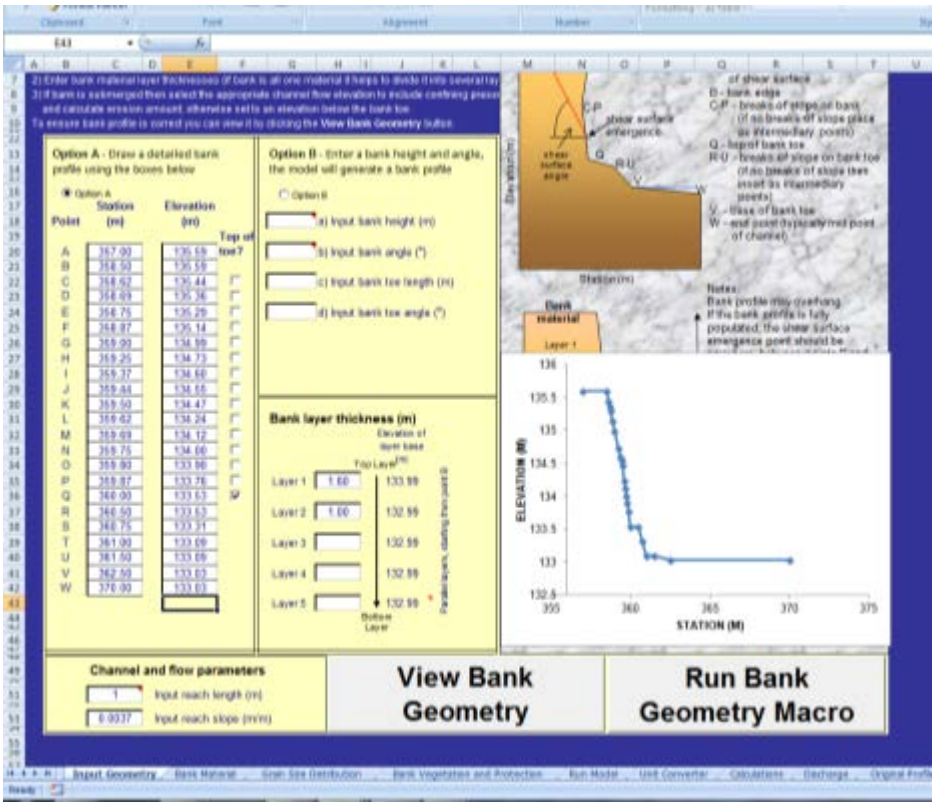

Figure 19 - Input cross section and layering for Crocodile Creek 2 site in BSTEM.

Bank and bank-toe material data tables.

These are the default parameters used in the model. Changing the values or descriptions will change the values used when selecting soil types from the list boxes above. Add your own data using the white boxes.

Material Descriptors			Bank Model Input Data					Groundwater Model Input Data			Toe Model Input Data	
Bank material type	Description	Mean grain size, D_{50} (m)	Friction angle ϕ^b (degrees)	Cohesion c^b (kPa)	Saturated unit weight (kN/m^3)	ϕ^g (degrees)	Chemical concentration (kg/kg)	Hydraulic Conductivity k_s	van Genuchten α (1/m)	van Genuchten n	τ_c (Pa)	k (cm^3/N/s)
1	Boulders	0.512	42.0	0.0	20.0	15.0	-	1.745E-03	3.5237	2.3286	498	0.004
2	Cobbles	0.128	42.0	0.0	20.0	15.0	-	1.745E-03	3.5237	2.3286	124	0.009
3	Gravel	0.0113	36.0	0.0	20.0	15.0	-	3.160E-03	3.5237	2.3286	11.0	0.030
4a and 4b	Angular sand	0.00035	36.0	0.0	18.0	15.0	-	7.439E-05	3.5237	3.1769	Coarse (0.71mm) or	
5a and 5b	Rounded sand	0.00035	27.0	0.0	18.0	15.0	-	1.130E-06	4.0563	2.3286	Fine (0.18 mm)	
6a, 6b and 6c	Silt	-	30.0	3.0	18.0	15.0	-	5.064E-06	0.6577	1.6788	Erodible (0.100 Pa),	
7a, 7b and 7c	Soft clay	-	25.0	10.0	18.0	15.0	-	9.473E-07	1.5812	1.4158	Moderate (5.00 Pa), or	
8a, 8b and 8c	Stiff clay	-	20.0	15.0	18.0	15.0	-	1.708E-06	1.4962	1.2531	Resistant (50.0 Pa)	
	Own data layer 1		27.8	6.43	18.0	10.0		1.130E-06	4.0563	2.3286	2.150	0.850
	Own data layer 2		30.1	4.16	18.0	10.0		1.130E-06	4.0563	2.3286	2.150	0.850
9	Own data layer 3											
	Own data layer 4											
	Own data layer 5											
	Own data Bank Toe										1.91	0.937

Figure 20 - Bank material property input parameters for Crocodile Creek 2 site in BSTEM.

Calibrating the 1.0 m of lateral retreat shown in the 2009 to 2011 LiDAR period, for the 2007 to 2009 period modeled in BSTEM, required a Manning's n value of 0.035 (Figure 21). This value was then used in the 40-year simulation to predict longterm and annual sediment loadings.

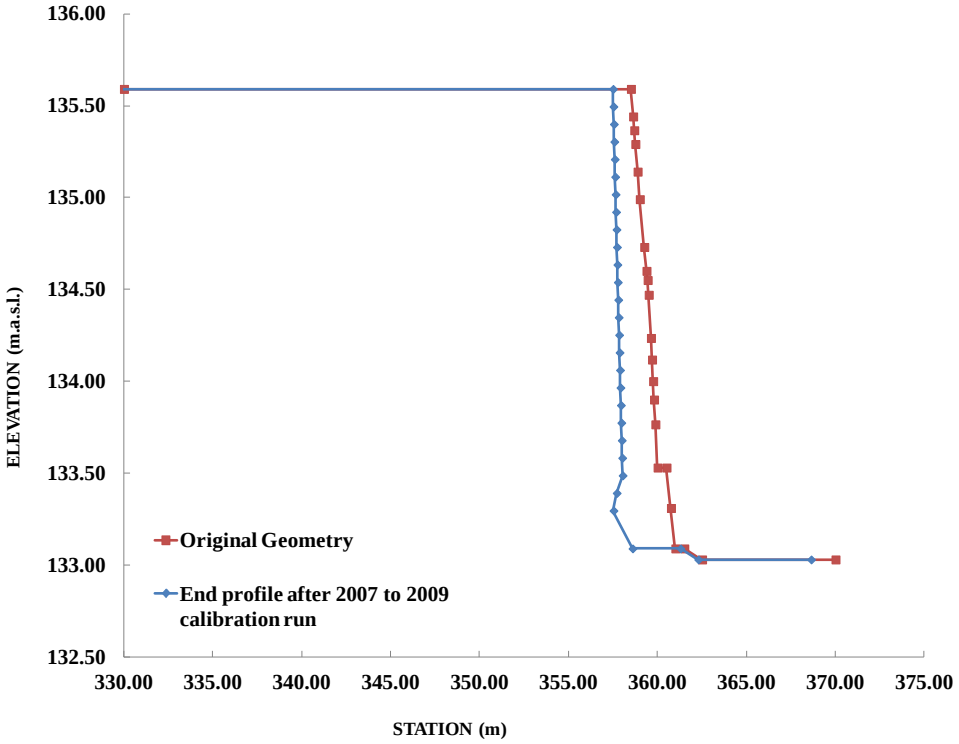

Figure 21 – Before and after profiles for Crocodile Creek 2 site for the BSTEM modeling period 2007 to 2009.

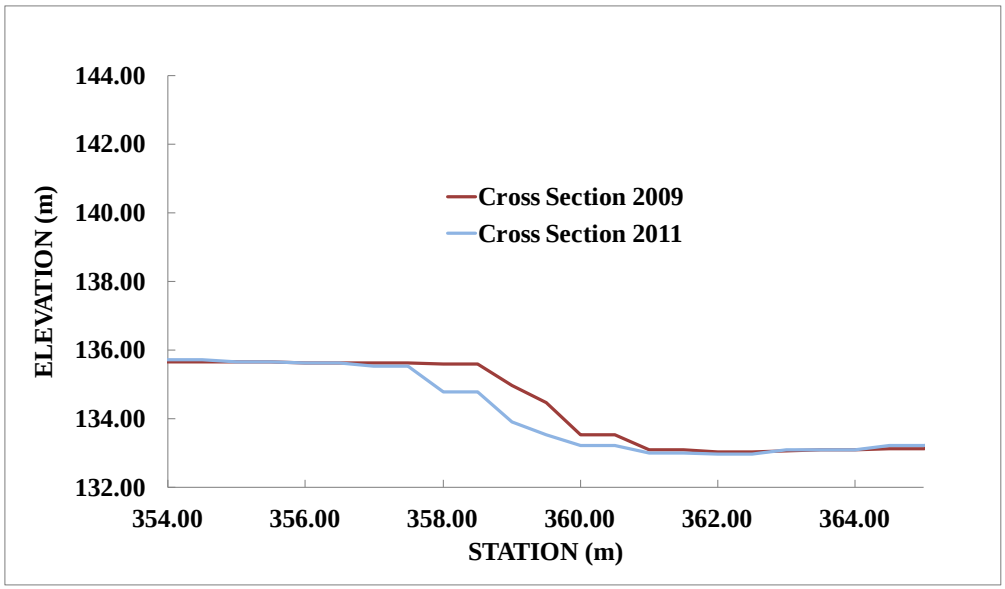

Figure 22 – Before and after profiles for Crocodile Creek 2 site for repeat LiDAR cross sections from 2009 and 2011.

Chapter 6 40-year BSTEM runs

A 40-year flow period was run for each of the two sites. For the Normanby 1 site the last forty years of flow record from gauge 105105A was used (1971 to 2011). Less flow data was available for the Crocodile Creek 2 site, so a 20-year flow period was selected (1986 to 2006) and run twice, to create a 40-year flow series. The discharge data used for this site was created using a mflow model and provided to us by Griffith University.

6.1 Normanby 1 Site

Lateral retreat at the Normanby 1 site was predicted to be 51.9 m over the 40-year flow period modeled in BSTEM (Figure 22). The predicted volume of eroded sediment from this bank was 209 m^3, of which 58.1 % (121 m^3) was estimated to be fines (Source: particle size sample analysis performed by Griffith University). Of the eroded sediment, 96 % of the eroded volume emanated from geotechnical failures of the bank, with just 4 % resulting from hydraulic erosion. Geotechnical failures occurring during drawdown conditions delivered the vast majority of the sediment from the modeled site.

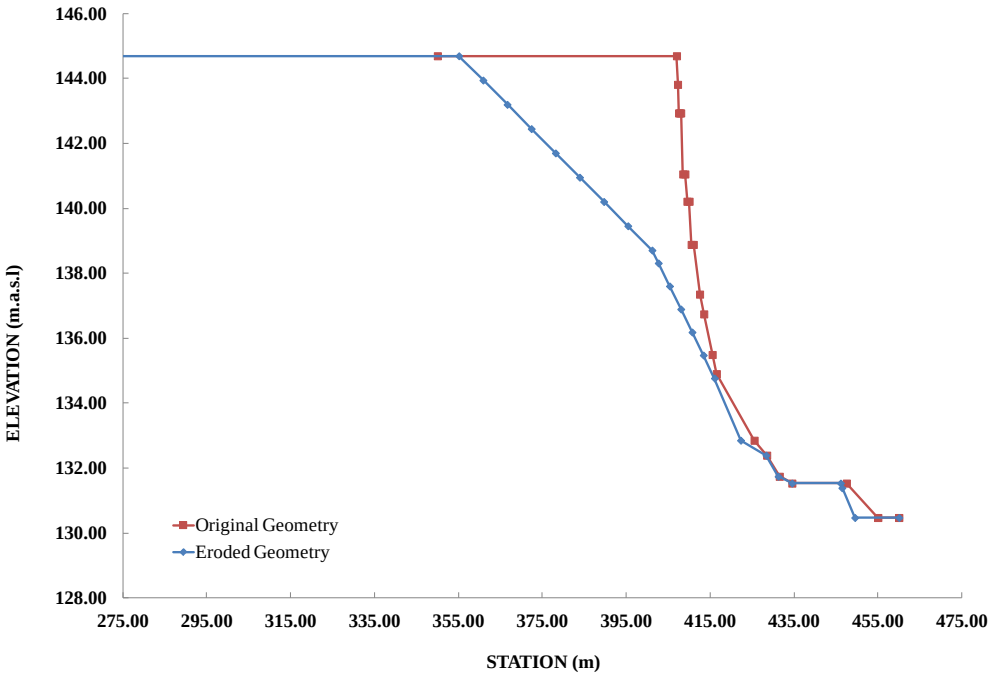

Figure 23 – Before and after profiles for Normanby 1 site for the 40 years modeled in BSTEM.

6.2 Crocodile Creek 2 Site

Lateral retreat at the Crocodile Creek 2 site was predicted to be 12.5 m over the 40-year flow period modeled in BSTEM (Figure 23). The predicted volume of eroded sediment from this bank was 32.5 m^3, of which 34 % (11.1 m^3) was estimated to be fines (Source: particle size sample analysis performed by Griffith University). Of the eroded sediment volume, 82.0 % emanated from geotechnical failures, whilst 18.0 % resulted from hydraulic erosion of the bank toe and bank face. Although hydraulic erosion accounted for a relatively small portion of the overall erosion, it can be seen in the eroded bank profile below, that it is hydraulic erosion and undercutting at the base of the bank, that decreases bank stability, resulting in geotechnical failures.

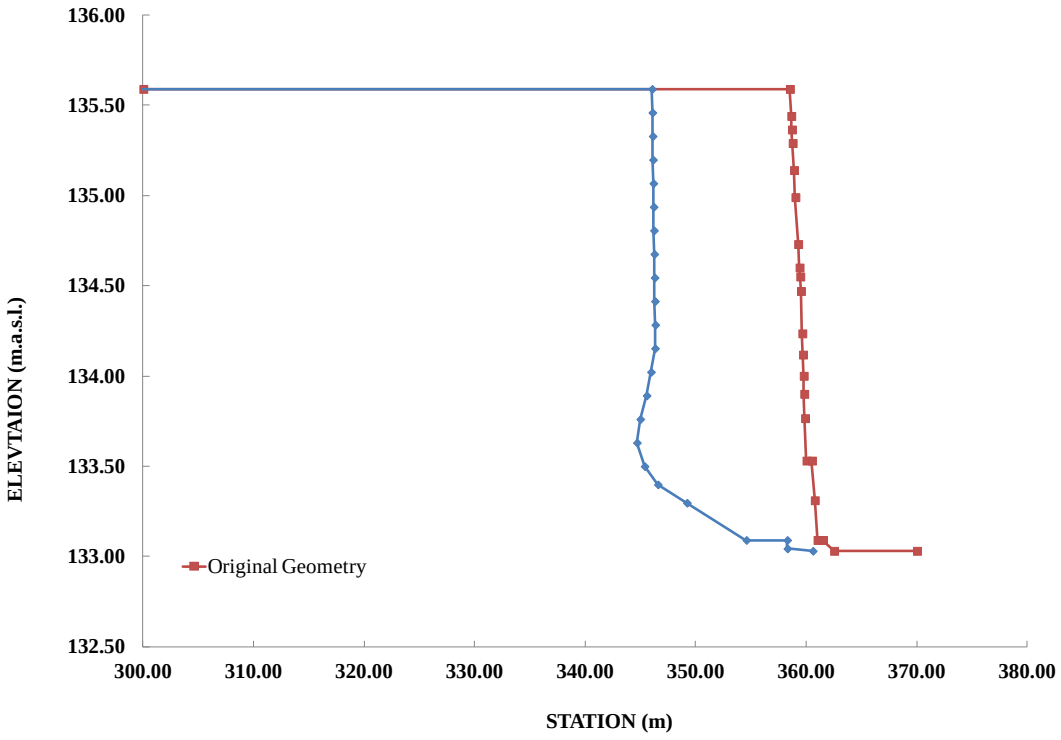

Figure 24 – Before and after profiles for Crocodile Creek 2 site for the 40 years modeled in BSTEM.

6.3 9Model Sensitivity

The BSTEM runs carried out for the calibration runs in this chapter highlighted the sensitivity of the model output to Manning's n values. For the Normanby site, a change in Manning's n of 0.02 caused a change of 7 m of lateral erosion over the 40-year time period (52 vs 59 m of erosion). At the Crocodile 2 site, a change in Manning's n of just 0.005, from 0.03 to 0.035, produced a decrease in lateral erosion over the 40-year modeled period, from 33.9 to 12.5 m of lateral erosion. This sensitivity stresses the importance of the calibration process, as large variations in predicted lateral retreat rates, and associated sediment volumes, can result if this step is bypassed. A small error at the site level will be magnified by several orders of magnitude once the sediment loading extrapolations have been calculated.

Chapter 7
Video Analysis of Percent Reach Failing

Video recorded along the study reach during helicopter reconnaissance was analyzed to provide the percent of each 2-km reach that was considered to have active bank failures. Video recorders were geo-referenced with GPS, enabling locations to be accurate to within ± 15 m. From these videos it was possible to characterize active geomorphic processes and relative stability along different sections of the study reach, for example, by observing bank failures, and areas of significant aggradation. Modified Rapid Geomorphic Assessments (RGAs; Bankhead and Simon, 2009) were conducted on 2-mile reaches, establishing the longitudinal extent of recent streambank failures. This is quantified as the percent of the reach failing as estimated from the video taken during air reconnaissance. These percentages are broken into classes (0-10, 11-25, 25-50, 51-75 and 76-100%) and used as a measure of the severity of bank instability and when mapped, the extent of that instability.

The aerial video analysis showed a dense vegetation canopy present along long stretches of the study reaches. The presence of well-developed riparian forests and corridors reaching all the way down to low-flow lines tended to be indicative of fairly stable geomorphic areas. Locations where erosion was more active were seen in the video, and typically had a more open vegetative canopy, exposed bank faces and fallen trees within the channel itself.

Maps showing the average and maximum percent of each 2 km reach failing are shown in Figure 24 These maps indicate that the banks along the majority of the study reach lengths were relatively stable, as indicated by dense vegetation to the low flow line. It should be noted however, that in places the dense vegetative canopy made it difficult to see the banks of the channel, so additional locations of bank failures may actually exist. Areas of the banks where bank failures were clearly seen on the aerial video are highlighted in Figure 25 (Crocodile Creek) and Figure 27 (East and West Normanby). On Crocodile Creek areas of mass wasting occurred along the entire study reach, but bank erosion became more concentrated, and extended over longer stretches of the creek, towards the downstream end of the study reach (Figures 25 and 26). On the East and West Normanby there were also locations of bank failures along the entire study reach. The upstream portion of the West Normanby had just one location of bank erosion that was clearly visible from the video analysis, with more regular occurrences of bank erosion being visible in the lower half of the study reach (Figures 27 and 28). Areas of bank erosion along the East Normanby were seen along the entire study reach, but were more concentrated in the upper and mid-sections of the reach (Figures 27 and 29).

The results provided by this video analysis will be used in further calculations, to extrapolate at-a-site sediment loadings, to potential streambank sediment loadings along the length of the study reaches.

A)

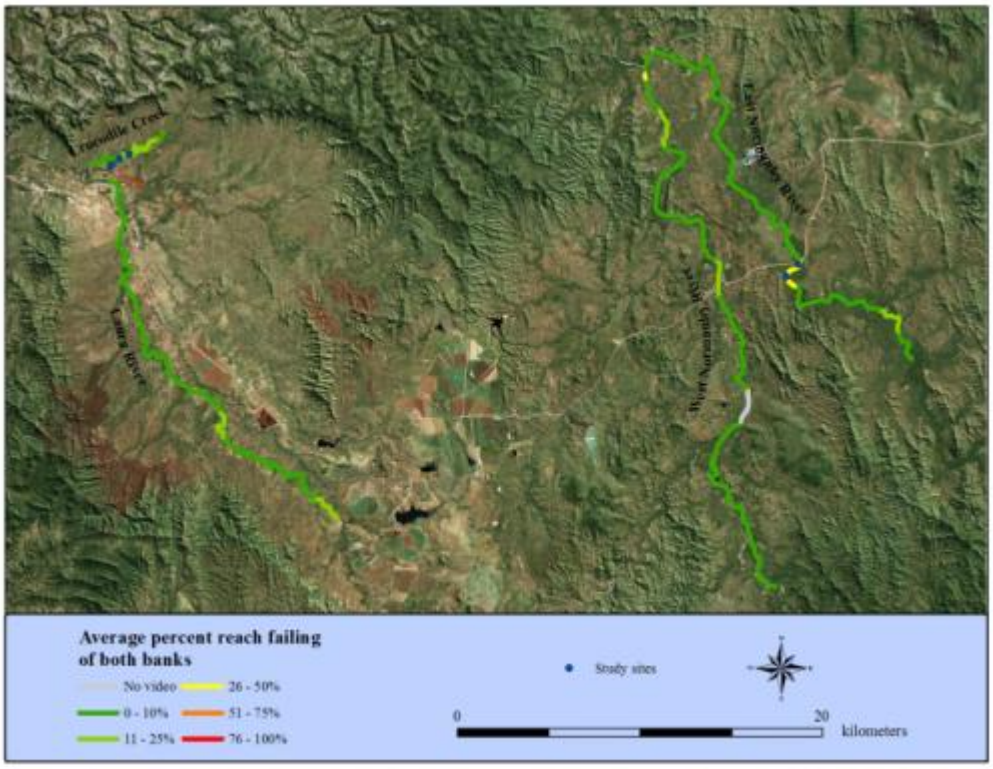

B)

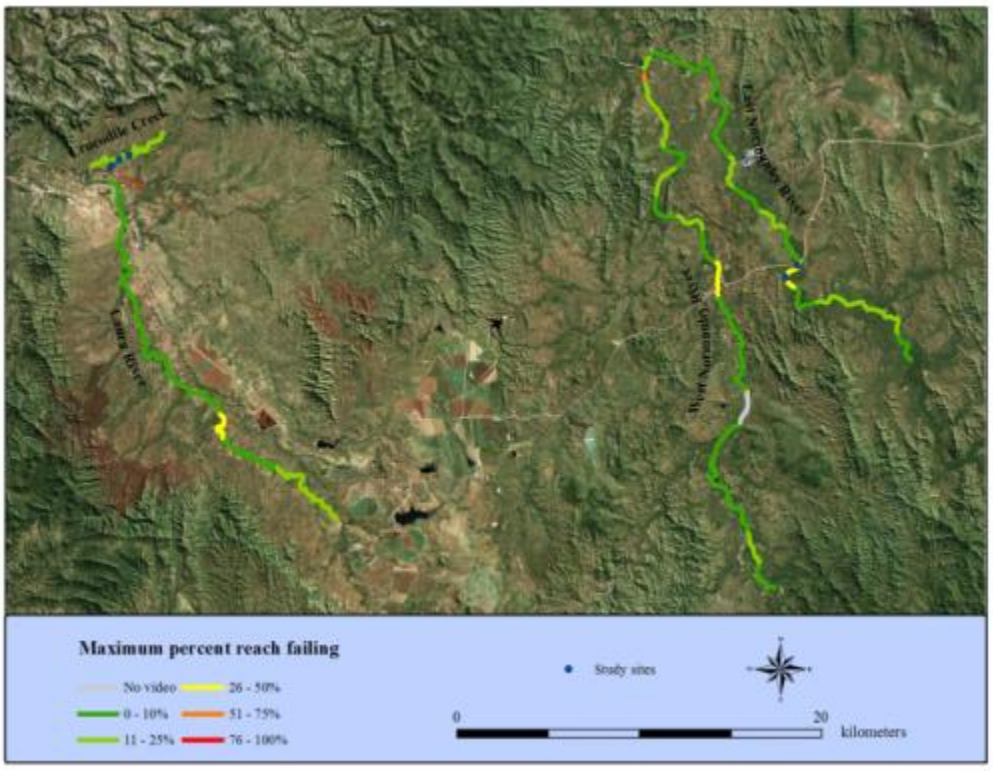

Figure 25 – Maps of East and West Normanby Rivers and Crocodile Creek and Laura River, showing A) average percent of both banks failing along each 2km reach, and B) Maximum percent of banks failing along each 2km reach.

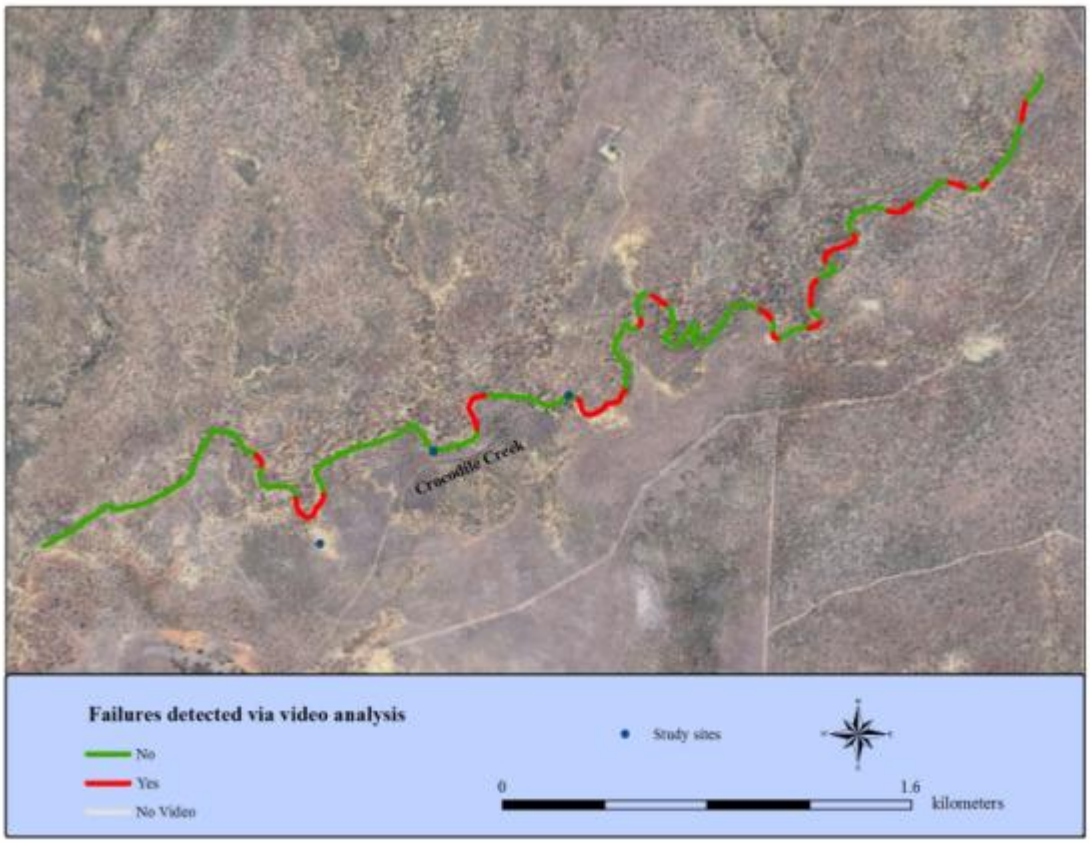

Figure 26 – Failures detected from aerial video along Crocodile Creek.

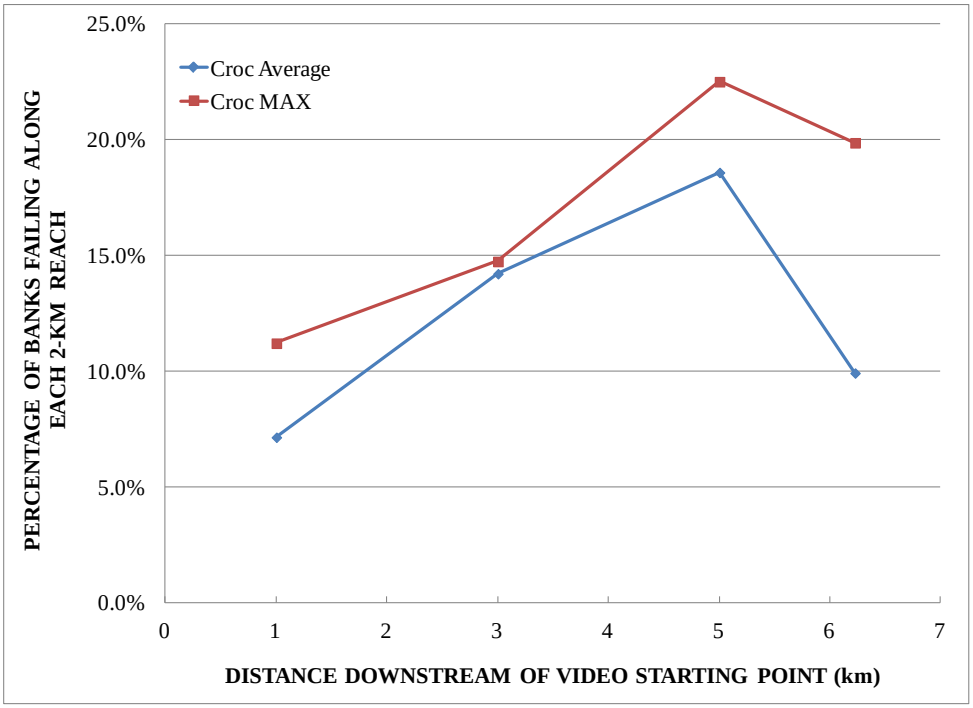

Figure 27 – Percent of banks failing along the Crocodile Creek study reach.

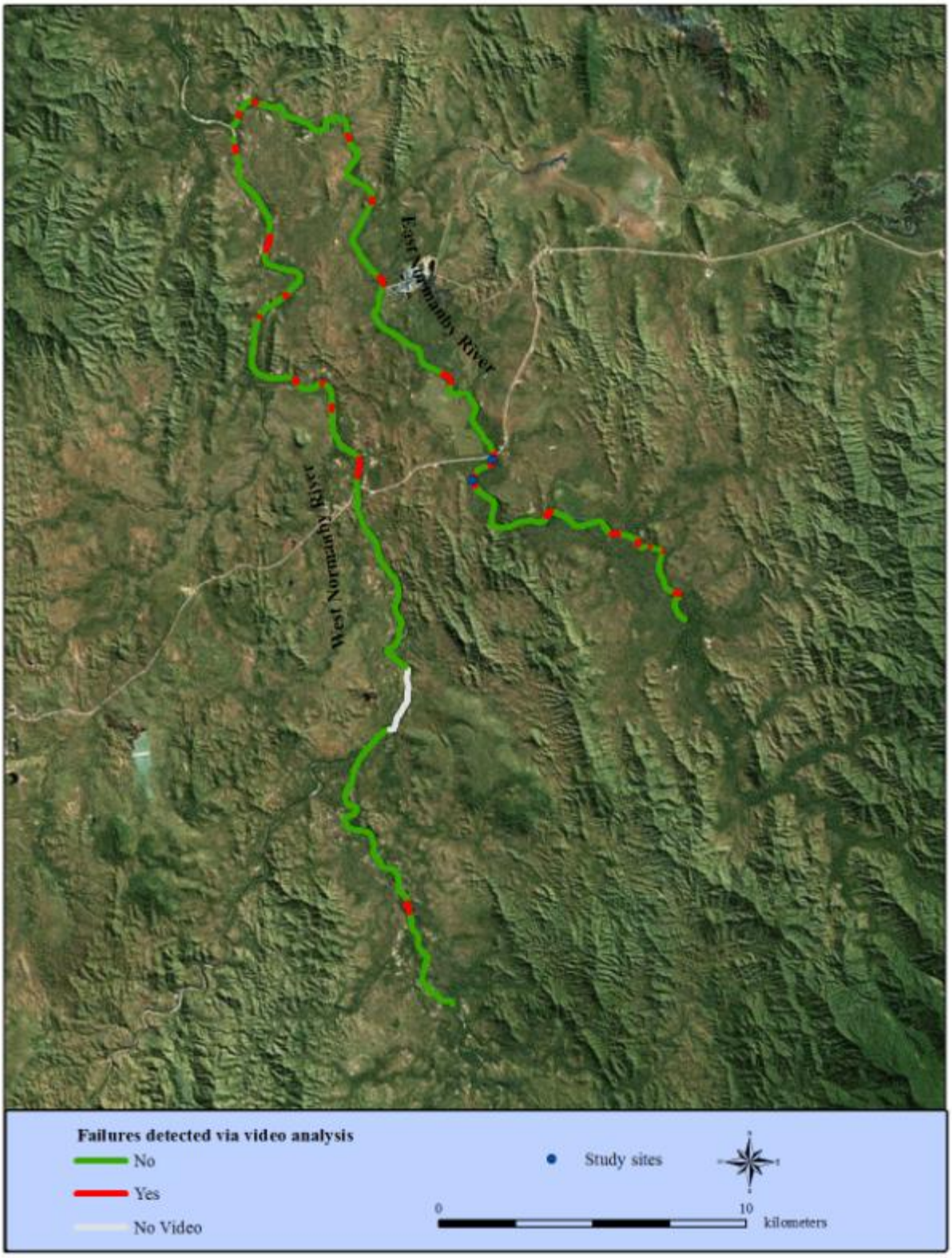

Figure 28 – Locations of bank failures detected along the East and West Normanby.

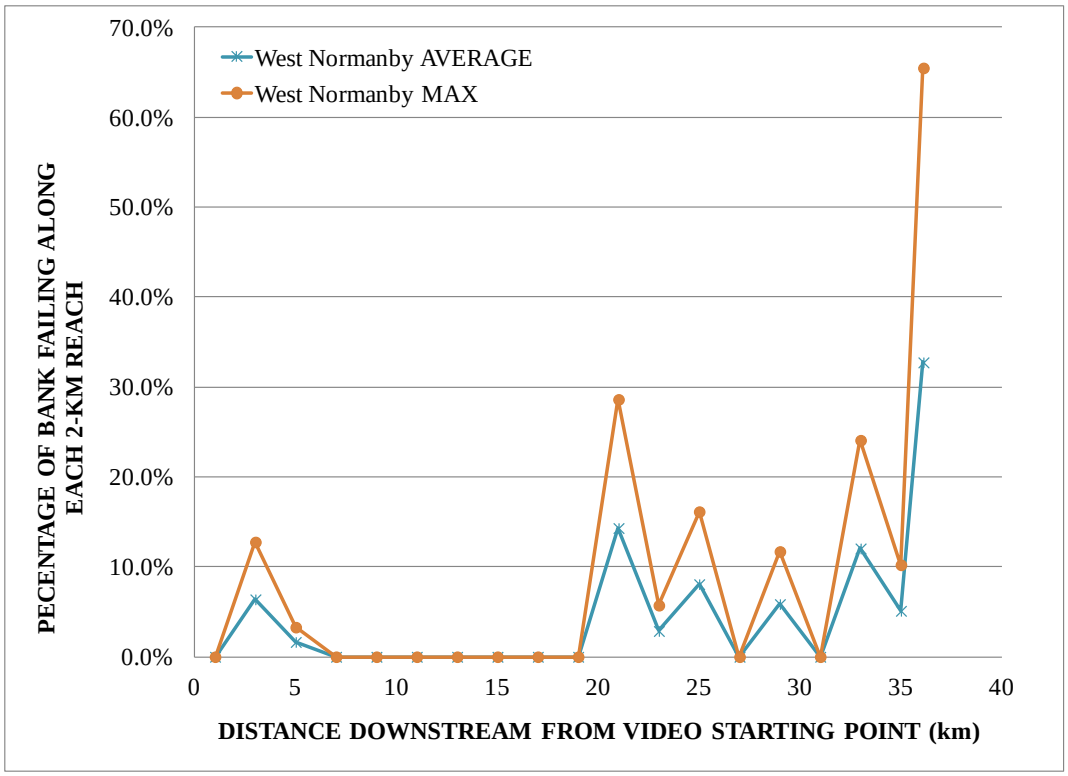

Figure 29 – Percent of banks failing along the West Normanby study reach.

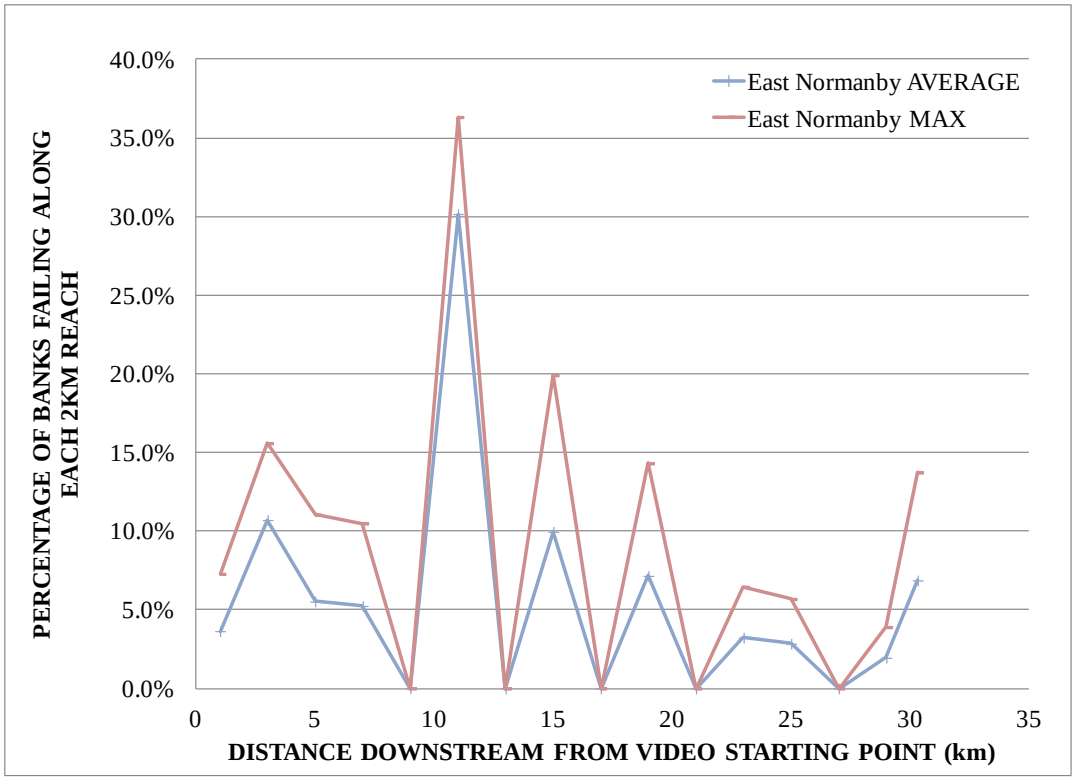

Figure 30 – Percent of banks failing along the East Normanby study reach.

Chapter 8 Extrapolation of Sediment Loadings from Modeled Sites to Watershed Scale

The eroded volumes from the BSTEM runs were combined with the percent reach failing data presented in Chapter 7, and bank height data provided from LIDAR data collected by Griffith University, to develop a spreadsheet to extrapolate eroded sediment volumes throughout the study watershed. Particle size data were also applied so as to be able to distinguish the fraction of this eroded volume that was fine sediment. This fine sediment could be easily entrained and transported from the river system into open water, thus ultimately affecting the Great Barrier Reef. To extrapolate the at-a-site values to watershed scale, the following steps were taken:

1) Take the bank height for the sites modeled, to create a relation between bank height and eroded volume.
2) Use a look up table to select volume of erosion for a given reach according to the bank height by RKm data obtained from LIDAR
3) Multiply the eroded volume by the average percent of the reach that is failing
4) Multiply the volume of sediment by the percent fines
5) Multiply by 2 to account for both banks
6) Annualize to get a volume per year
7) Unitize to get a volume per km per year

8.1 Bank Heights

Bank heights (Figure 30) were obtained from LiDAR data where available, and through modeling for those reaches not covered by LIDAR (Figure 31). Bank heights on the smaller secondary channels (Laura and Crocodile Creek) were much lower than those on the East and West Normanby Channels, with heights ranging from 1.50 to 2.70 m for Crocodile Creek, 7.50 to 12.3 m for Laura RiverRiver, 24.0 to 27.1 m on the West Normanby, and 12.5 to 23.2 m on the East Normanby. Because the gravitational forces acting on streambanks increase with increasing bank height, the banks of the E. and W. Normanby channels, have greater potential for mass wasting than the banks of the secondary channels. It should be noted, however, that the occurrence of mass wasting failures is also controlled by other factors affecting the driving and resisting forces of the banks, such as bank material strength, the extent of roots and the hyadraulic conductivity of the bank materials (i.e. as to whether it can be assumed that the banks are fully saturated during the post-flood draw down phase).

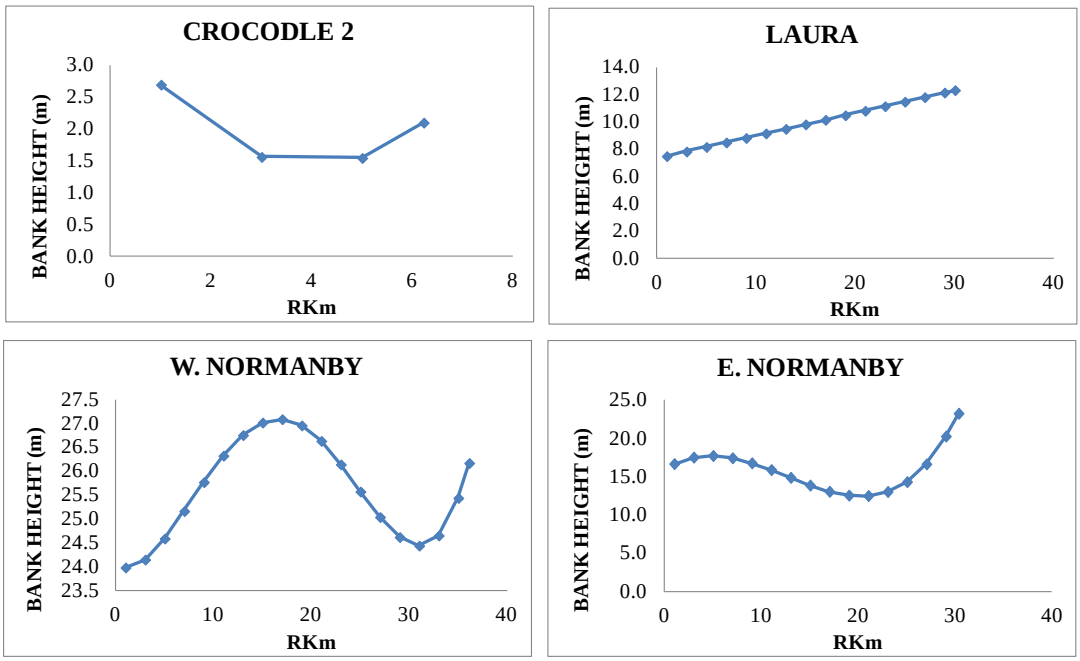

Figure 31 – Bank heights measured in LIDAR blocks and modeled between LIDAR blocks according to empirically derived relationships.

Figure 32 – Availability of LIDAR data over the study reaches extrapolated for sediment loadings. Green lines show reaches used for sediment loading analysis, grey areas show reaches with LIDAR data. 1 = Laura River, 2 = Crocodile Creek, 3 = E. Normanby, 4 = W. Normanby.

8.2 Developing a relation between eroded volume and bank height

To extrapolate loadings from the two sites modeled in BSTEM it was necessary to develop a relation between bank height and the volume of sediment eroded in the model simulations. To achieve this, the two sites were modeled in BSTEM Static 5.4, using the same bank materials modeled in BSTEM Dynamic, but for varying bank heights. The top bank layer depth was kept constant, and the lower layer increased with bank height. Failure volume was recorded and then plotted against modeled bank height, to develop a relation for each site. This relation showed predicted geotechnical erosion for an individual failure event. To determine the extent of loading over the 40-year period modeled in BSTEM Dynamic, the relation was scaled to the known eroded volume from the BSTEM Dynamic runs. The resulting two relations (Figure 32) were then applied to the bank height data presented in Section 8.1, to calculate the predicted amount of erosion for each 2 km reach over the 40 year modeled period. In each case the relation between bank height and failure volume was a power function, indicating that eroded volume increased non-linearly with increasing bank height.

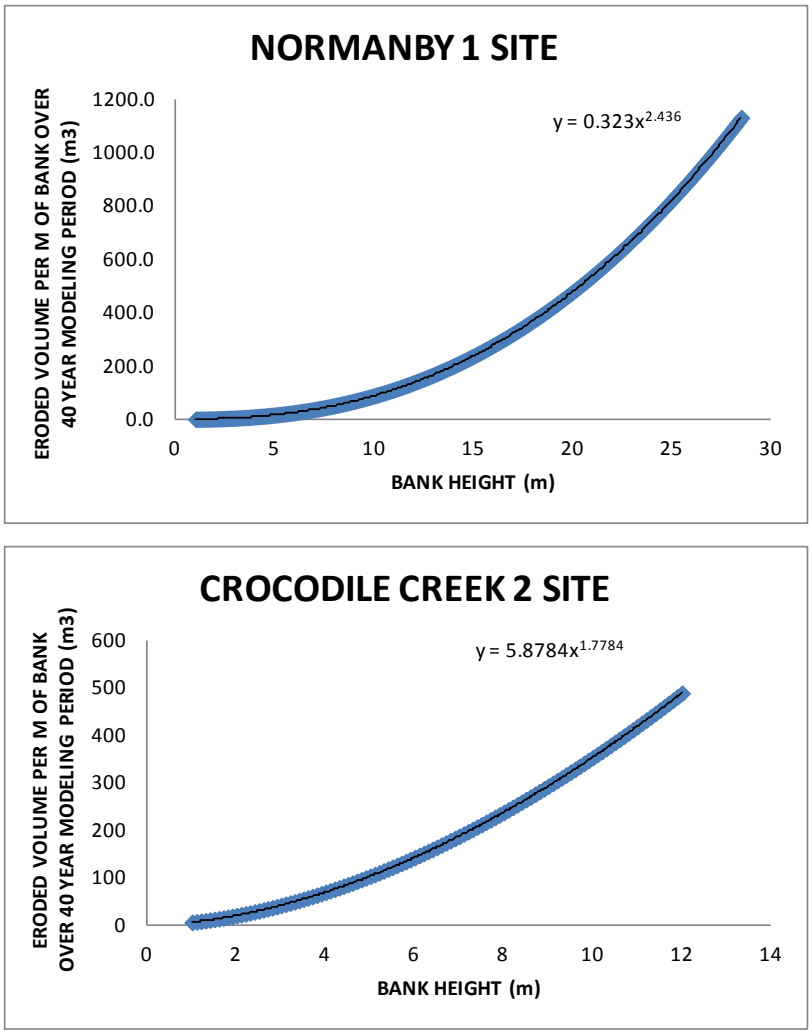

Figure 33 – Relation between bank height and eroded sediment volume, based on BSTEM Static 5.4 runs.

8.3 Volume of Erosion

The volumes of eroded sediment calculated in Section 8.2 for each 2 km reach were then multiplied by the percent of reach failing data presented in Chapter 7 to estimate the volume of sediment predicted to be delivered to each channel system, from each 2km reach. Finally, these values were divided by the model period of 40 years to obtain annualized values. Total values for each channel, and per km were also calculated (Table 3). In addition, all loads were multiplied by the percent fines measured in the particle size samples taken along these reaches. This is important because it is these fines that are most easily carried in suspension, and transported through the channel system towards the Great Barrier Reef.

Annualized total and fine sediment loads per 2km reach are shown for each of the study channels in Figures 33 – 36. From the plots it can be seen that overall, estimated sediment loads from the secondary channels (Laura and Crocodile Creek) were considerably lower than those estimated for the E. and W. Normanby. This result is largely a function of the bank heights present within the different channel systems; as shown in Section 8.1, the bank heights in the Normanby channels are much higher than those within the secondary channels systems of Laura and Crocodile Creeks. In addition, although the average percent of reach failing over the study reach length is actually highest for Crocodile Creek (12% compared to 4%, 5%, and 5% respectively for Laura, W.Normanby and E. Normanby), there are locations within the East and West Normanby Rivers, where percent of reach failing increases dramatically, reaching up to 30% (Figures 28 and 29) in places. These areas of high erosion, combined with tall bank heights, produce higher estimates of sediment loading emanating from banks within the main channels, compared to the secondary channels. It should be noted here that per unit of channel cross sectional area, the secondary channels actually seem to be producing more sediment than the large channels; the relations in Figure 32 show higher sediment volumes for comparable bank heights, for the site on Crocodile Creek. Bearing in mind that as in any drainage network, there are more small channels than larger channels, the sum of the loadings from these secondary channels may actually be the dominant source of sediment in the catchment.

For Crocodile Creek, estimated loadings increased from upstream to downstream. Loadings were predicted to be fairly constant along the length of reach studied in this channel. In Laura River, estimated sediment loadings emanating from streambanks were higher in the upstream parts of the reach studied, with the downstream sections of this channel being predicted to have no erosion because these reaches were recorded from the video analysis as having 0 % of the banks failing. It should be noted here that parts of the video showed heavily vegetated banks, and it was difficult to see the banks in some areas. It is possible, therefore, that in Laura River, and some other locations on the other channels with dense vegetation, localized areas of bank erosion may have been overlooked. In general, it is thought that this potential underestimation in percent reach failing should be minimal, as in general, if mature, dense vegetation is present, this suggests that the banks are relatively stable, and have been there for a significant period of time.

The West Normanby channel showed an area of high predicted sediment loadings from banks, about 4 km downstream of the start of the video analysis. A section of channel about 14km long with little to no bank erosion is then shown, before estimated sediment loadings increase steeply in the downstream half of the study reach, reaching a peak of approximately 25,000 tonnes per 2 km reach at the 21 km mark. In the E. Normanby channel, predicted

sediment loadings from banks were highest in the upstream half of the reach, peaking at the 10-12 km reach downstream of the start of video analysis, at approximately 16,000 tonnes per year from this section of the channel. The downstream half of the E. Normanby channel studied had much lower estimated sediment loading rates, similar in magnitude to those predicted for the secondary channels.

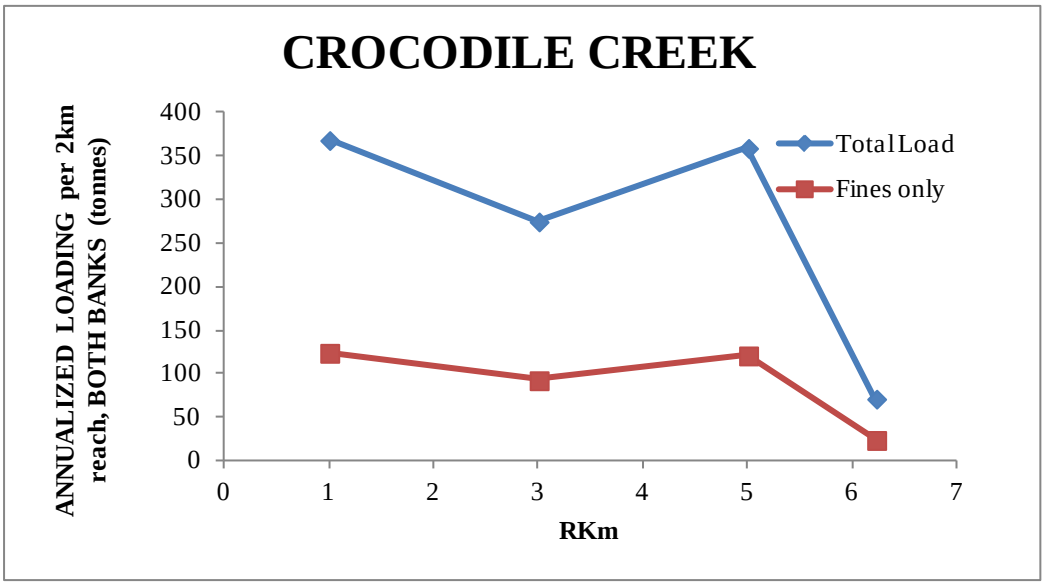

Figure 34 – Annualized total and fine load estimates per 2km reach of Crocodile Creek.

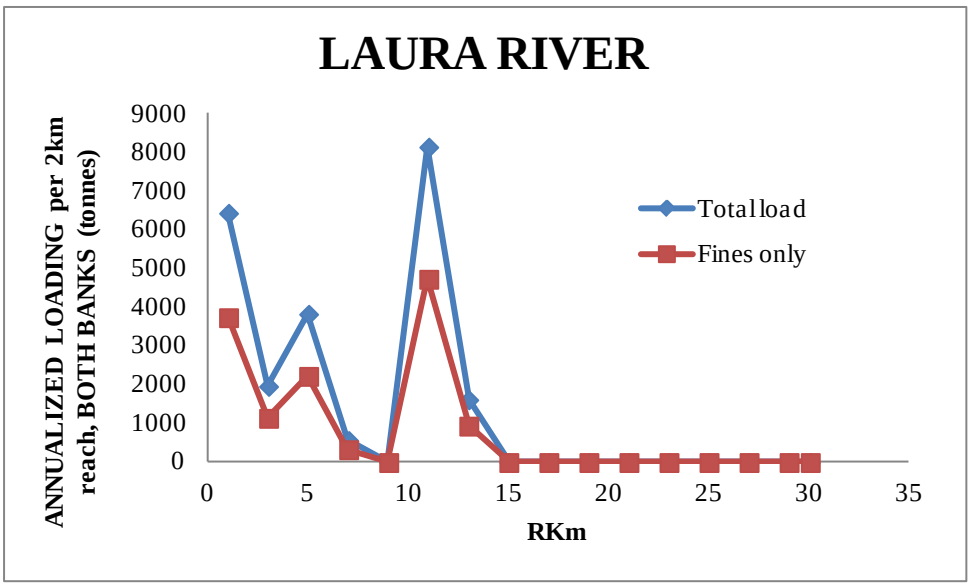

Figure 35 – Annualized total and fine load estimates per 2km reach of Laura River.

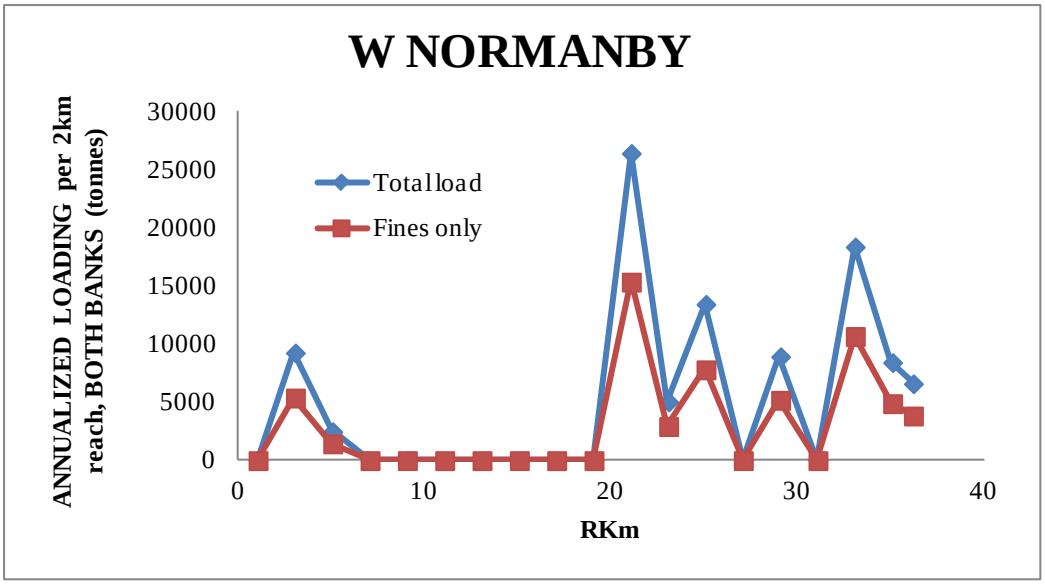

Figure 36 – Annualized total and fine load estimates per 2km reach of the W. Normanby.

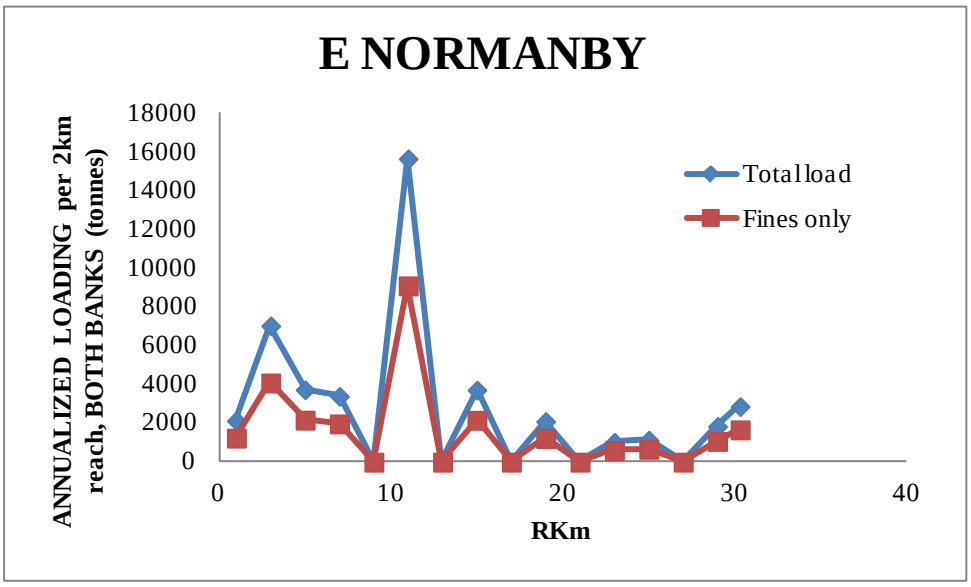

Figure 37 – Annualized total and fine load estimates per 2km reach of the E. Normanby.

Table 3. Annualized total and fine sediment loads per channel and per km of channel.

	ANNUALIZED SEDIMENT LOAD (tonnes) both banks	ANNUALIZED FINE SEDIMENT LOAD (tonnes) both banks	ANNUALIZED TOTAL SEDIMENT LOAD per Km (tonnes) both banks	ANNUALIZED FINE SEDIMENT LOAD per Km (tonnes) both banks
Crocodile	1,076	363	167	56.3
Laura	22,600	13,100	751	436
W. Normanby	99,300	57,700	2,740	1,590
E. Normanby	44,800	26,000	1,461	849

Total estimated annual sediment loading from streambanks for each channel ranged from 1,076 tonnes from Crocodile Creek to 99,300 tonnes from West Normanby (Table 3). Of this load, 58% was assumed to be fine sediment in the Laura and Normanby channels, and 34 % in Crocodile Creek. These percentages were based on particle size data provided by Griffith University.

Finally, the contributions to estimated sediment loads from geotechnical and hydraulic erosion in the BSTEM runs were separated out (Figures 37 and 38). These plots clearly show that geotechnical erosion dominates the sediment delivered to the channel systems, making up 82% of the sediment load on the secondary channels, and 96% of the load in the Normanby channels.

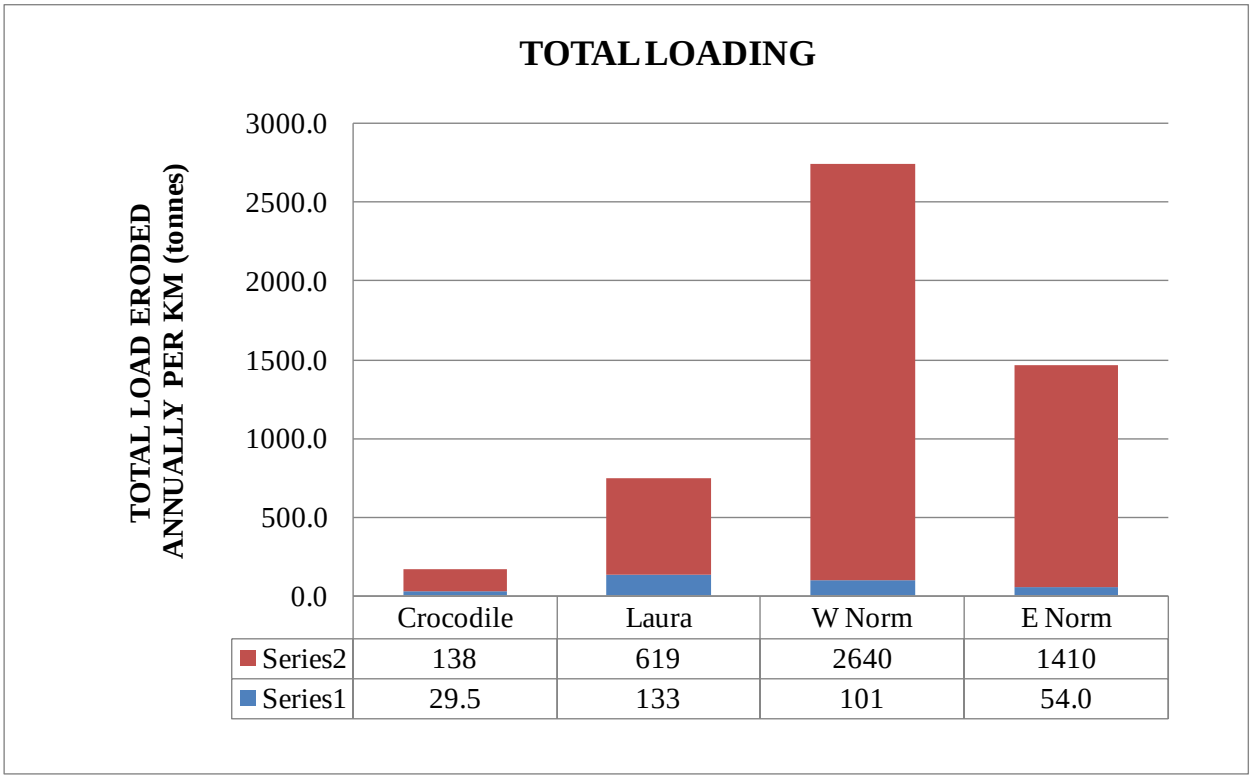

Figure 38 – Annualized total load per km of each channel, divided up by geotechnical and hydraulic erosion.

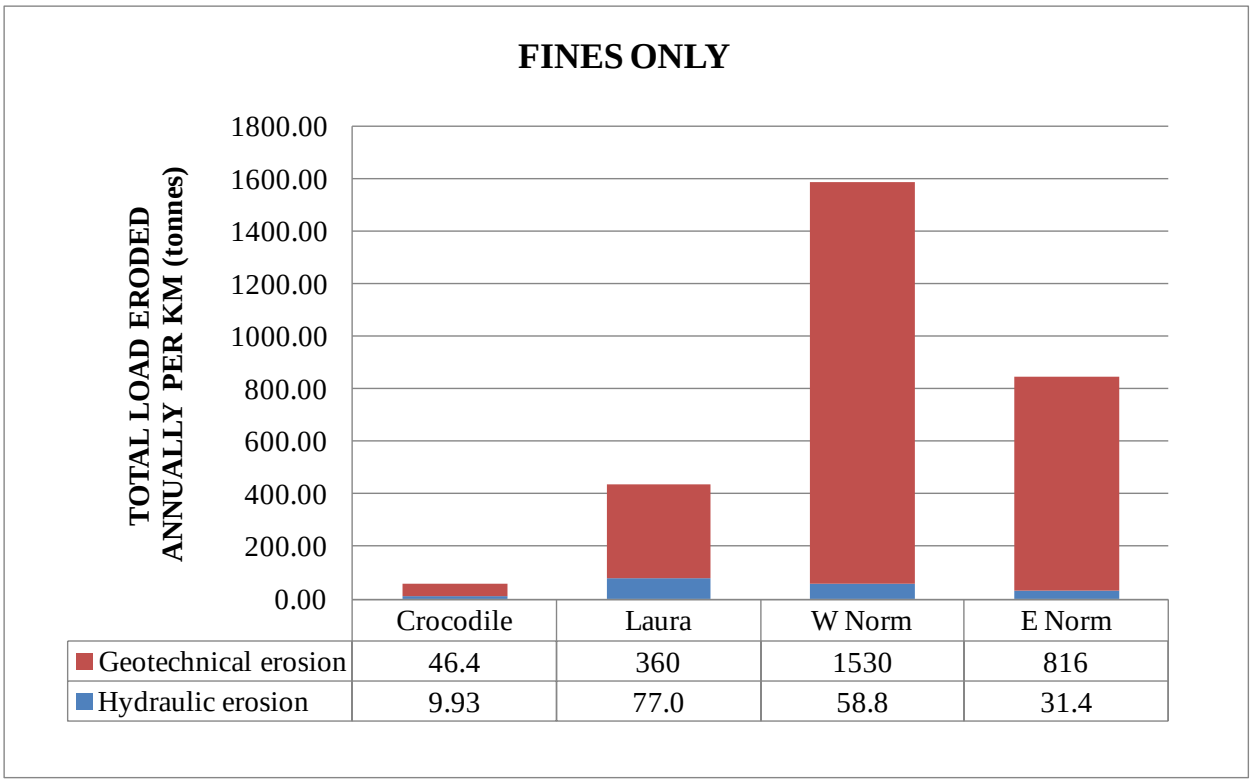

Figure 39 – Annualized fine load per km of each channel, divided up by geotechnical and hydraulic erosion.

Chapter 9 Discussion and Conclusions

This report details the calibration and validation of the Bank Stability and Toe Erosion Model (BSTEM), for sites along the East Normanby River and Crocodile Creek. Field data collection has been conducted at sites on the E. Normanby and Crocodile Creek to obtain the bank layering, geotechnical, and hydraulic erodibility parameters necessary for input to BSTEM. In addition, root architecture data was obtained for a range of riparian trees found at the field sites. The field data collected *in situ* were input to BSTEM-Dynamic, which was run for a calibration period at the Normanby 1 site, from June 1st 2009 to October 1st 2011. LIDAR cross-sections at this site were used to compare the predicted changes in bank geometry due to modeled hydraulic and geotechnical erosion, with actual changes that occurred during this calibration period. To test the model fully, a range of Manning's n values were used 1) to create the flow stage series input to BSTEM and 2) to apply a grain roughness factor to account for channel roughness elements, in particular the established riparian trees growing at the bank toe at the Normanby 1 site. It was found that for the calibration period BSTEM correctly predicted no bank top retreat, instead predicting between 5.06 m^2 of erosion in the bank toe region for an n-value of 0.09 and 10.67 m^2 for an n-value of 0.07. The resulting bank profiles from BSTEM-Dynamic show good agreement with the changes in the bank profile seen in the 2009 and 2011 LIDAR data, with the exception that in the LIDAR data, some accretion can be seen within the toe region, because the trees act to reduce flow velocity in this region. BSTEM is unable to predict accretion and so this is not shown in the resulting BSTEM profiles at the end of the calibration period. The accuracy of predicted bank geometry changes compared to the LIDAR data for the Normanby 1 site over the calibration period, lends support to the use of BSTEM-Dynamic to run both longer flow periods, and extrapolate these at-a-site-loadings to longer reach scales, to aid in the development of a more accurate sediment budget for these study reaches.

Calibration at the Crocodile Creek 2 site was not possible because repeat cross section data was unavailable. A 3-year run was performed in BSTEM prior to running the 40-year flow period, to check for reasonable annual erosion rates. To model a 40-year period for this site, a Manning's n value of 0.07 was used for the East Normanby site and a value of 0.03 for the Crocodile Creek site. These n-values best approximates the roughness characteristics seen in the field at these sites. Lateral retreat at the Normanby 1 site was predicted to be 51.9 m over the 40-year flow period modeled in BSTEM. The predicted volume of eroded sediment from this bank was 209 m^3, of which 58.1 % (121 m^3) was estimated to be fines. Lateral retreat at the Crocodile Creek 2 site was predicted to be 12.5 m over the 40-year flow period modeled in BSTEM. The predicted volume of eroded sediment from this bank was 32.5 m^3, of which 34 % (11.1 m^3) was estimated to be fines.

To extrapolate the at-a-site loadings predicted at the two BSTEM sites, BSTEM erosion volumes were used in conjunction with bank height data obtained from LIDAR, percent reach failing data from the video analysis highlighted the locations and potential extent of bank failures occurring along these channels, bulk density data, and particle size data, to establish estimates for annualized total and fine sediment loads emanating from the banks of each channel, and amounts per km of each channel. Estimated sediment loads from the secondary channels (Laura and Crocodile Creek) were considerably lower than those estimated for the E. and W. Normanby. This result is largely a function of the bank heights present within the

different channel systems. Per unit cross section area, the secondary channels actually produce more sediment than the larger channels. Total estimated annual sediment loading from streambanks for each channel ranged from 1,076 tonnes from Crocodile Creek to 99,300 tonnes from West Normanby. Of this load, 58% was assumed to be fine sediment in the Laura and Normanby channels, and 34 % in Crocodile Creek. These percentages were based on empirical data collected within the catchment for another part of this project. Analysis of the BSTEM simulations also suggests that the vast majority of this sediment results from geotechnical failures of the banks. It is however, important to point out that although hydraulic erosion accounts for just 6 to 18 % of the estimated sediment loadings from the banks, if this hydraulic erosion did not occur, in many cases the banks would not become oversteepened and/or undercut, a condition that contributes to many geotechnical failures.

Assumptions and Uncertainty

A number of assumptions were made in this study. First, it should be noted that BSTEM does not have a way of accounting for the deposition of materials after a failure event; as such, the model assumes that any failed material is removed immediately by flowing water, regardless of volume of material or particle size breakdown. This assumption could have led to overestimation of bank toe erosion, bank geotechnical failures and resulting predictions of lateral bank retreat.

Another assumption was that the materials tested at the two sites on the Normanby River and Crocodile Creek, were representative of the catchment as a whole. It was necessary to make this assumption so that the BSTEM erosion rates at these two sites could be extrapolated to the rest of the reaches in the study area. This assumption could lead to either over or under-estimation, depending on the spatial variability of bank materials in the catchment. A higher resolution of sampling locations could reduce the uncertainty associated with this assumption in future studies.

Finally, assumptions were made about groundwater levels and moisture content within the streambanks modeled. A permeability of 5.06×10^{-6} ms^{-1} was assumed, which meant that groundwater and surface water tracked each other with little lag time. Banks may not actually become as saturated as BSTEM predicted, so some underestimation of streambank Factor of Safety could have occurred in the BSTEM runs for the two sites modeled. In addition, the effect of vegetation and evapotranspiration (ET) on matric suction values within the streambanks was not accounted for in this study. If this process had been accounted for Factor of Safety values could have been higher, and the predicted bank erosion rates lower. The effects of ET are however, seasonal, and antecedent soil moisture conditions vary temporally throughout the catchment. The modeling and extrapolation of loadings do not take into account the spatial (according to vegetation type, age, density, and rooting depth) and temporal variability in the ET process.

Chapter 10 References

Abernethy, B., Rutherfurd, I.D., 2000. The effect of riparian tree roots on the mass-stability of riverbanks. Earth Surface Processes and Landforms 25, 921–937.

Abernethy, B., Rutherfurd, I.D., 2001. The distribution and strength of riparian tree roots in relation to riverbank reinforcement. Hydrological Processes 15, 63–79.

ASTM, 1995. Annual Book of ASTM Standards: Section 4, Construction, v. 04-09. American Society for Testing and Materials: West Conshohocken, PA.

Blaisdell, F.W., Clayton, L.A., and Hebaus, G.G., 1981. Ultimate dimension of local scour, Journal of the Hydraulics Division, Proceedings of the American Society of Civil Engineers, 107(HY3), 327-337.

Bohm, W., 1979. Methods of Studying Root Systems. Berlin: Springer-Verlag.

Canadell J, Jackson RB, Ehleringer JR, Mooney HA, Sala OE, Schulze ED. 1996. Maximum rooting depth of vegetation types at the global scale. *Oecologia* **108**: 583–595.

Carson, M.A. and Kirkby, M. J., 1972. Hillslope Form and Process. Cambridge

Chow, V.T., 1959. Open Channel Hydraulics. McGraw-Hill: New York, NY.

Coppin, N.J., and Richards, I.G., 1990. Use of Vegetation in Civil Engineering. Butterworths: London, UK.

Docker, B.B., Hubble, T.C.T., 2001. Riverbank collapse on the Nepean River in the Wallacia Valley: assessing possible causes by historical and geomechanical methods. Journal of the Royal Society of New South Wales 134, 65–78.

Einstein, H.A. (1942). Formulas for the Transport of Bed Sediment. Trans. American Society of Civil Engineers, Vol. 107, pp. 561-574

Endo, T., and Tsuruta, T., 1969. On the effect of tree roots upon the shearing strength of soil. Annual report of the Hokkaido branch, Forest Place Experimental Station: Sapporo, Japan; pp.167-183.

Fan, C.-C., and Su, C.-F., 2008. Role of roots in the shear strength of root-reinforced soils with high moisture content. Ecological Engineering, 33(2), 157-166.

Fredlund, D.G. and Rahardjo, H., 1993. Soil Mechanics of Unsaturated Soils. John Wiley and Sons, New York.

Fredlund, D.G., Morgenstern, N.R., and Widger, R.A., 1978. The shear strength of unsaturated soils. *Canadian Geotechnical Journal*. 15, 313-321.

Gray, D.H., and Leiser, A.T., 1982. Biotechnical Slope Protection and Erosion Control. Van Nostrand Reinhold Company: New York, NY.

Gray, D.H., and Sotir, R.B., 1996. Biotechnical and Soil Bioengineering Slope Stabilization: A Practical Guide for Erosion Control. John Wiley & Sons, Inc.: New York, NY.

Hanson, G.J., and Simon, A., 2001. Erodibility of cohesive streambeds in the loess area of the midwestern USA, Hydrological Processes, 15(1), 23-38.

Hanson, G.J., 1990, Surface erodibility of earthen channels at high stress, Part II - Developing an in situ testing device, Transactions of the American Society of Agricultural Engineers, 33(1), 132-137.

Hanson, G.J., and Cook, K.R., 1997. Development of excess shear stress parameters for circular jet testing, American Society of Agricultural Engineers Paper No. 97-2227. American Society of Agricultural Engineers: St. Joseph.

Hubble, T.C.T. 2001. The history and causes of riverbank failure on the upper Nepean River between 1947 and 1992. Ph.D. Thesis, University of Sydney, Australia.

Hubble, T.C.T., 2004. Slope stability analysis of potential bank failure as a result of toe erosion on weir-impounded lakes: an example from the Nepean River, New South Wales, Australia. Marine and Freshwater Research 55, 57–65.

Hubble, T.C.T., Hull, T., 1996. A model for bank collapse on the Nepean River, Camden Valley, New South Wales, Australia. Australian Geomechanics 29, 80–98.

Jackson RB, Canadell J, Ehleringer JR, Mooney HA, Sala OE, Schulze ED. 1996. A global analysis of root distributions for terrestrial biomes. *Oecologia* **108**: 389–411.

Langendoen, E.J., 2000. CONCEPTS – Conservational channel evolution and pollutant transport system software manual, USDA-ARS National Sedimentation Laboratory Research Report, 16.

Langendoen, E.J., 2010. Assessing post-dam removal sediment dynamics using the CONCEPTS computer model. In: Proceedings of the 2nd Joint Federal Interagency Conference, Las Vegas, NV, June 27-July 1, 2010, 12 p.Little, W.C., Thorne, C.R., and Murphy, J.B., 1982. Mass bank failure analysis of selected Yazoo Basin streams. Transactions of the American Society of Agricultural Engineers, 25, 1321-1328.

Lohnes, R.A., Handy, R.L., 1968. Slope angles in friable loess. J. Geol. 76 _3., 247–258.

Lutenegger, J.A., and Hallberg, B.R., 1981. Borehole shear test in geotechnical investigations. ASTM Special Publication 740, 566-578.

Mehta, A.J., 1991. Review notes on cohesive sediment erosion. In: N.C. Kraus, K.J. Gingerich, and D.L. Kriebel, (eds.), Coastal sediment '91, Proceedings of Specialty Conference on Quantitative Approaches to Coastal Sediment Processes, ASCE; pp.40-53.

Morgenstern, N. R. & Price, V. E. 1965. The analysis of the stability of general slip surfaces. Ge´otechnique 15, No. 1, 79–93.

Parchure, T.M., and Mehta, A.J., 1985. Erosion of soft cohesive sediment deposits. Journal of Hydraulic Engineering, ASCE, 110(10), 1308-1326.

Partheniades, E., 1965. Erosion and deposition of cohesive soils. Journal of the Hydraulics Division, ASCE, 91(HY1), 105-139.

Pollen-Bankhead, N. and Simon, A. 2010. Hydrologic and hydraulic effects of riparian root networks on streambank stability: Is mechanical root-reinforcement the whole story? Geomorphology 116, 353-362.

Pollen, N., 2007. Temporal and spatial variability in root reinforcement of streambanks: Accounting for soil shear strength and moisture. Catena, 69(3), 197-205.

Pollen, N., and Simon, A., 2005. Estimating the mechanical effects of riparian vegetation on streambank stability using a fiber bundle model. Water Resources Research, 41, W07025, doi:10.1029/2004WR003801.

Pollen, N., Simon, A., and Collison, A.J.C., 2004. Advances in assessing the mechanical and hydrologic effects of riparian vegetation on streambank stability. In: S. Bennett and A. Simon, (eds.), Riparian Vegetation and Fluvial Geomorphology, Water Science and Applications 8. AGU: Washington, DC; pp.125-139.

Riestenberg, M., and Sovonick-Dunford, S.S., 1983. The role of woody vegetation in stabilizing slopes in the Cincinnati area. Ohio, Geological Society of America Bulletin, 94(4), 506-518.

Schenk HJ, Jackson RB. 2002. The global biogeography of roots. *Ecological Monographs* **72**(3): 311–328.

Shields FD Jr, Gray DH. 1992. Effects of woody vegetation on sandy levee integrity. *Water Resources Bulletin* **28**(5): 917–931.

Simon, A., 1989. A model of channel response in disturbed alluvial channels. *Earth Surface Processes and Landforms*, 14(1): 11-26.

Simon, A., and Hupp, C. R., 1986. Channel evolution in modified Tennessee channels, Proceedings of the *Fourth Federal Interagency Sedimentation Conference*, March 1986, Las Vegas, Nevada, v. 2, Section 5, 5-71 to 5-82.

Simon, A., and Collison, A.J.C., 2002. Quantifying the mechanical and hydrologic effects of riparian vegetation on stream-bank stability, Earth Surface Processes and Landforms, 27(5), 527-546.

Simon, A., and Thomas, R.E., 2009. The fate of failed bank material and implications for lateral retreat: Lake Tahoe Basin. (Abs.) American Geophysical Union, Fall Meeting, San Francisco, CA.

Simon, A., Wolfe, W. J. and Molinas, A., 1991. Mass Wasting Algorithms in an Alluvial Channel Model. Proceedings of the 5th Federal Interagency Sedimentation Conference. Las Vegas, NV. Volume 2, 8-22 to 8-29 p.

Simon, A., Curini, A., Darby, S., and Langendoen, E., 1999. Stream-bank mechanics and the role of bank and near-bank processes in incised channels. *In*: S. Darby and A. Simon, eds. Incised River Channels. John Wiley and Sons, New York, 123-152.

Simon, A., Pollen-Bankhead, N. and Thomas, R.E., 2011. Development and Application of a Deterministic Bank Stability and Toe Erosion Model for Stream Restoration, In: Simon, A., S.J. Bennett, and J. Castro (eds.), Stream Restoration in Dynamic Systems: Scientific Approaches, Analyses, and Tools. AGU: Washington, DC, p. 453-474.

Stein, O.R., Julien, P.Y., and Alonso, C.V., 1993. Mechanics of jet scour downstream of a headcut. Journal of Hydraulic Research, 31, 723-738.

Stein, O.R., and Nett, D.D., 1997. Impinging jet calibration of excess shear sediment detachment parameters, Transactions of the American Society of Agricultural Engineers 40 (6), 1573-1580.

Temple, D.M., 1980. Tractive force design of vegetated channels. Transactions of the American Society of Agricultural Engineers, 23(4), 884-890.

Temple, D.M., Robinson, K.M., Ahring, R.M., and Davis, A.G., 1987. Stability Design of Grass-Lined Open Channels. USDA ARS Agriculture Handbook Number 667. US Government Printing Office: Washington, DC.

Thorne, C.R., 1990. Effects of vegetation on riverbank erosion and stability, In: J.B. Thornes, (ed.), Vegetation and Erosion. John Wiley & Sons Ltd.: Chichester, UK; pp.125-144.

Thorne, C.R., 1982. Processes and Mechanisms of River Bank Erosion. In, Hey, R.D., Bathurst, J.C. and Thorne, C.R., (Eds.). Gravel-Bed Rivers, John Wiley and Sons, Chichester, England. 227-271 p.

Thorne C.R, Tovey N.K., 1981. Stability of composite river banks. *Earth Surface Processes and Landforms* 6: 469- 484

Thorne, C.R., Murphey, J.B., and Little, W.C., 1981. Bank stability and bank material properties in the bluffline streams of Northwest Mississippi, Stream Channel Stability, Appendix D, Section 32 Program, Work Unit 7, U. S. Army Corps of Engineers, Vicksburg District: Vicksburg, Mississippi.

Wu, T.H., 1984. Effect of vegetation on slope stability, Transportation Research Record, 965, 37-46.

Waldron, L.J., and Dakessian, S., 1981. Soil reinforcement by roots: Calculation of increased soil shear resistance from root properties. Soil Science, 132(6), 427-435.

Appendix A

Root Distribution Graphs

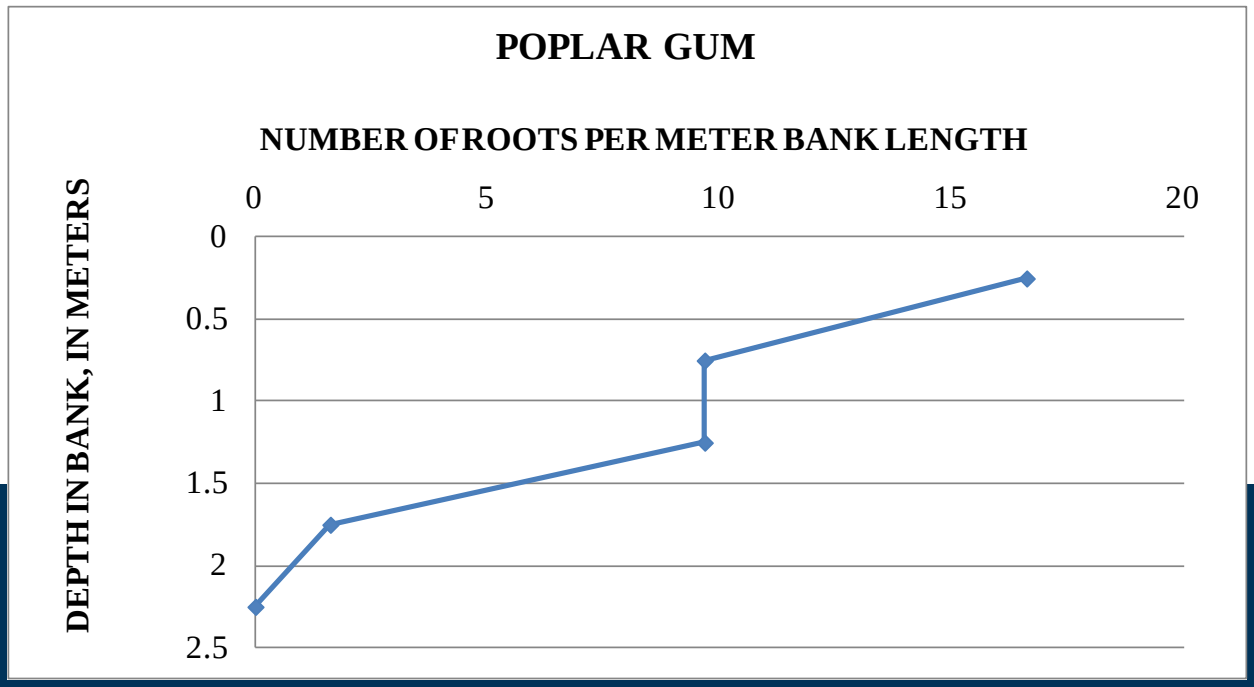
POPLAR GUM
NUMBER OF ROOTS PER METER BANK LENGTH
DEPTH IN BANK, IN METERS
0
5
10
15
20
0
0.5
1
1.5
2
2.5

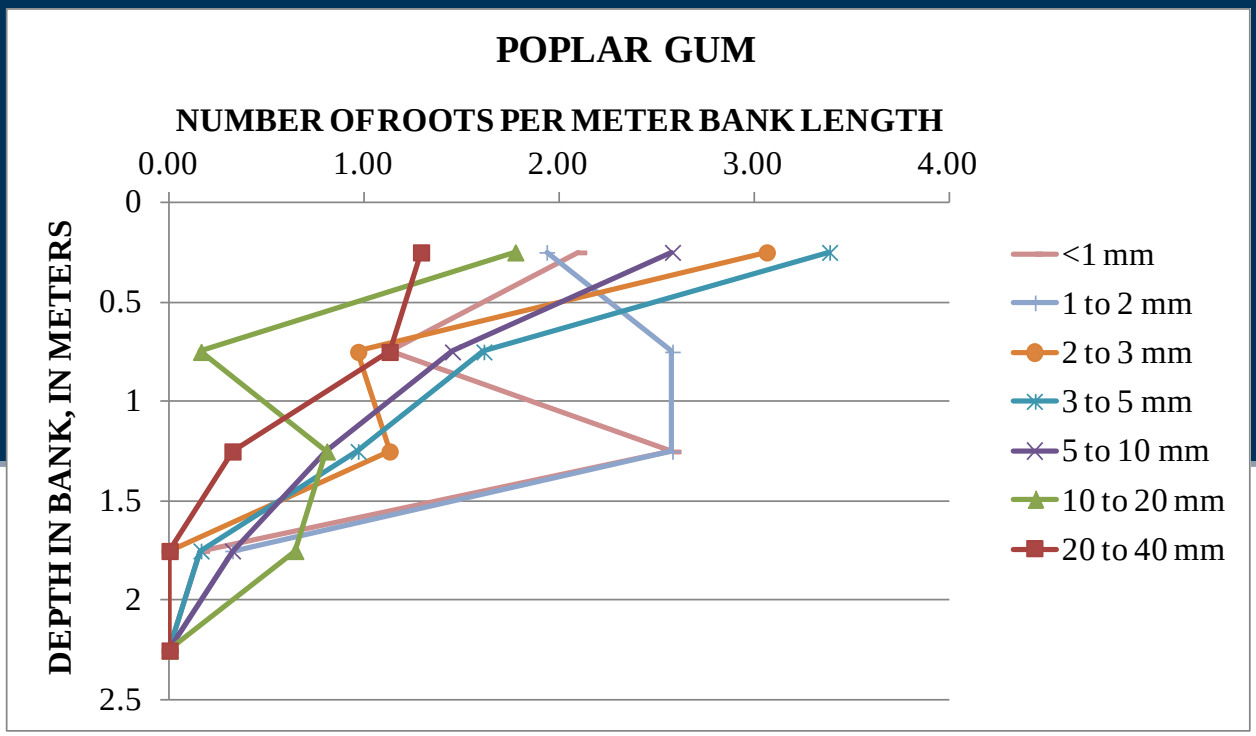
POPLAR GUM
NUMBER OF ROOTS PER METER BANK LENGTH
DEPTH IN BANK, IN METERS
0.00
1.00
2.00
3.00
4.00
0
0.5
1
1.5
2
2.5
<1 mm
1 to 2 mm
2 to 3 mm
3 to 5 mm
5 to 10 mm
10 to 20 mm
20 to 40 mm

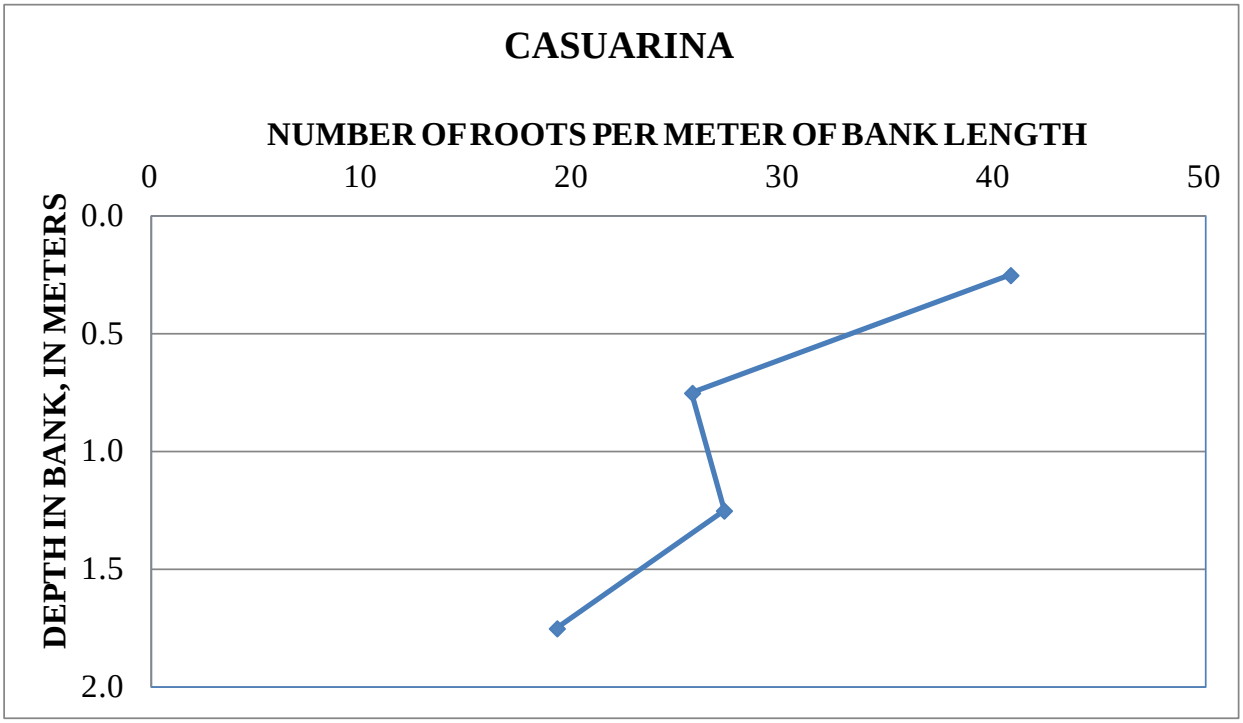
CASUARINA
NUMBER OF ROOTS PER METER OF BANK LENGTH
0
10
20
30
40
50
DEPTH IN BANK, IN METERS
0.0
0.5
1.0
1.5
2.0

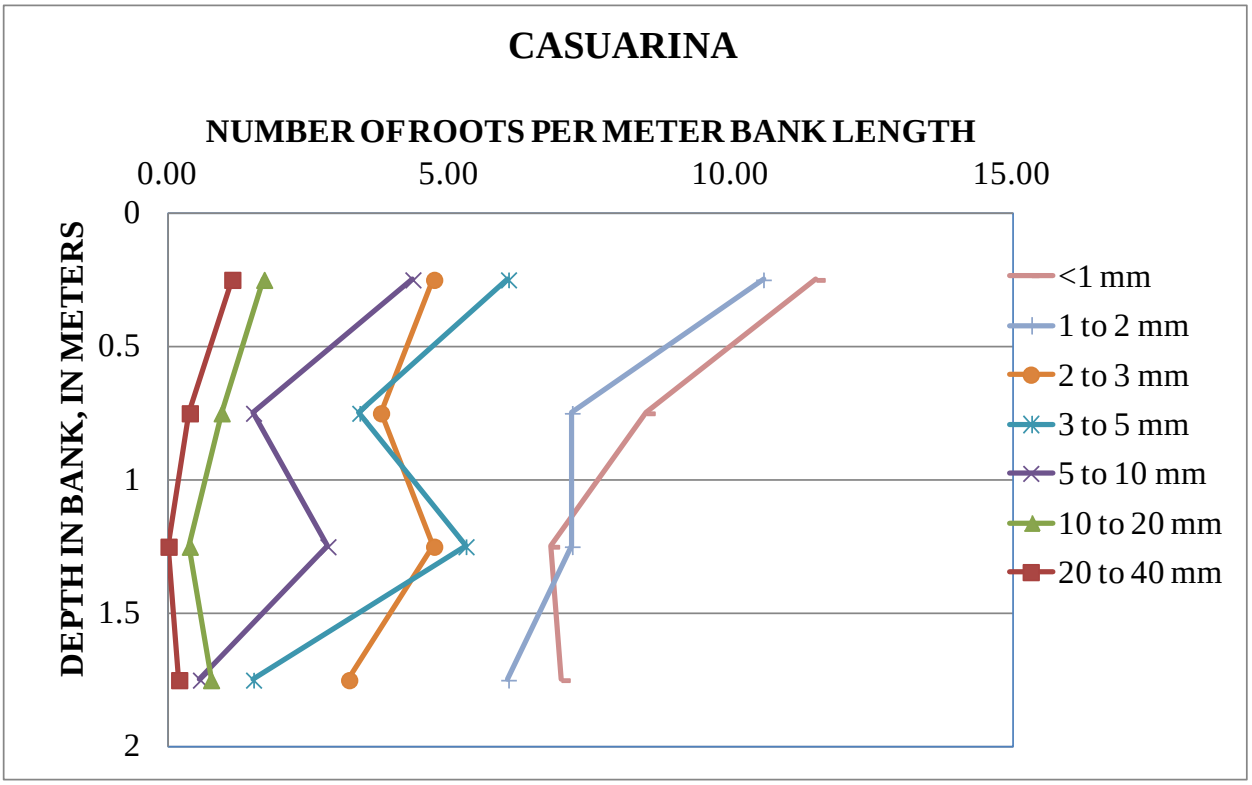
CASUARINA
NUMBER OF ROOTS PER METER BANK LENGTH
0.00
5.00
10.00
15.00
DEPTH IN BANK, IN METERS
0
0.5
1
1.5
2
<1 mm
1 to 2 mm
2 to 3 mm
3 to 5 mm
5 to 10 mm
10 to 20 mm
20 to 40 mm

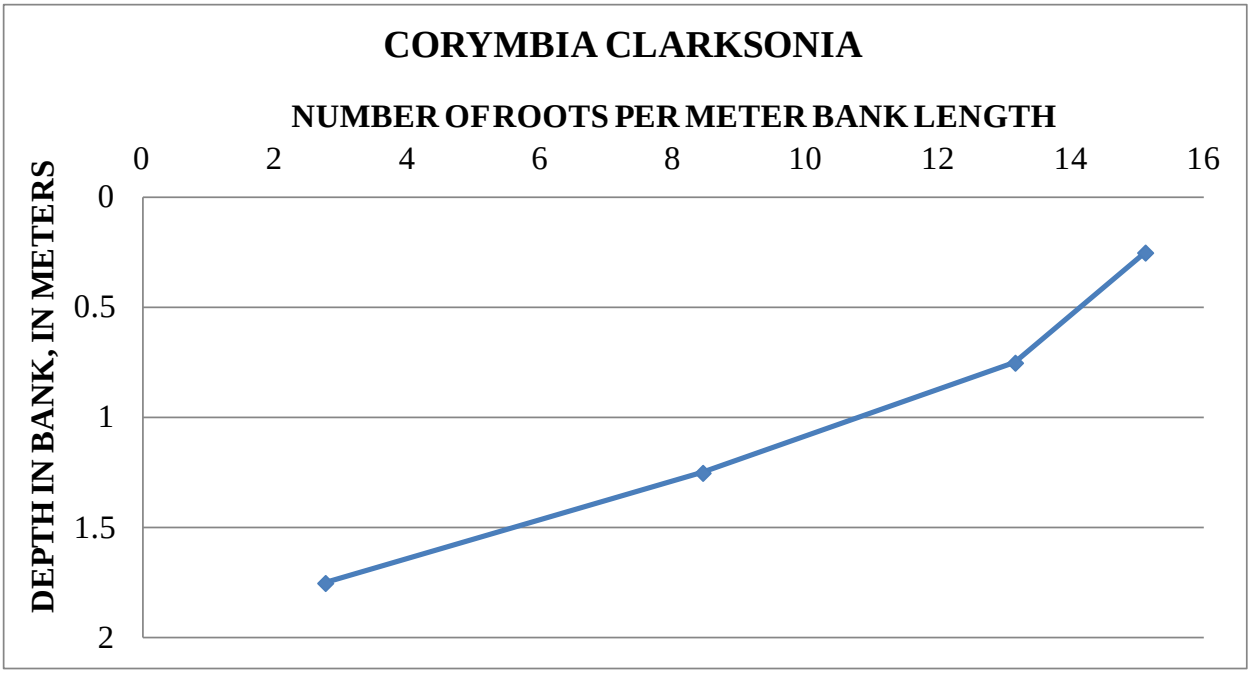
CORYMBIA CLARKSONIA
NUMBER OF ROOTS PER METER BANK LENGTH
0
2
4
6
8
10
12
14
16
DEPTH IN BANK, IN METERS
0
0.5
1
1.5
2

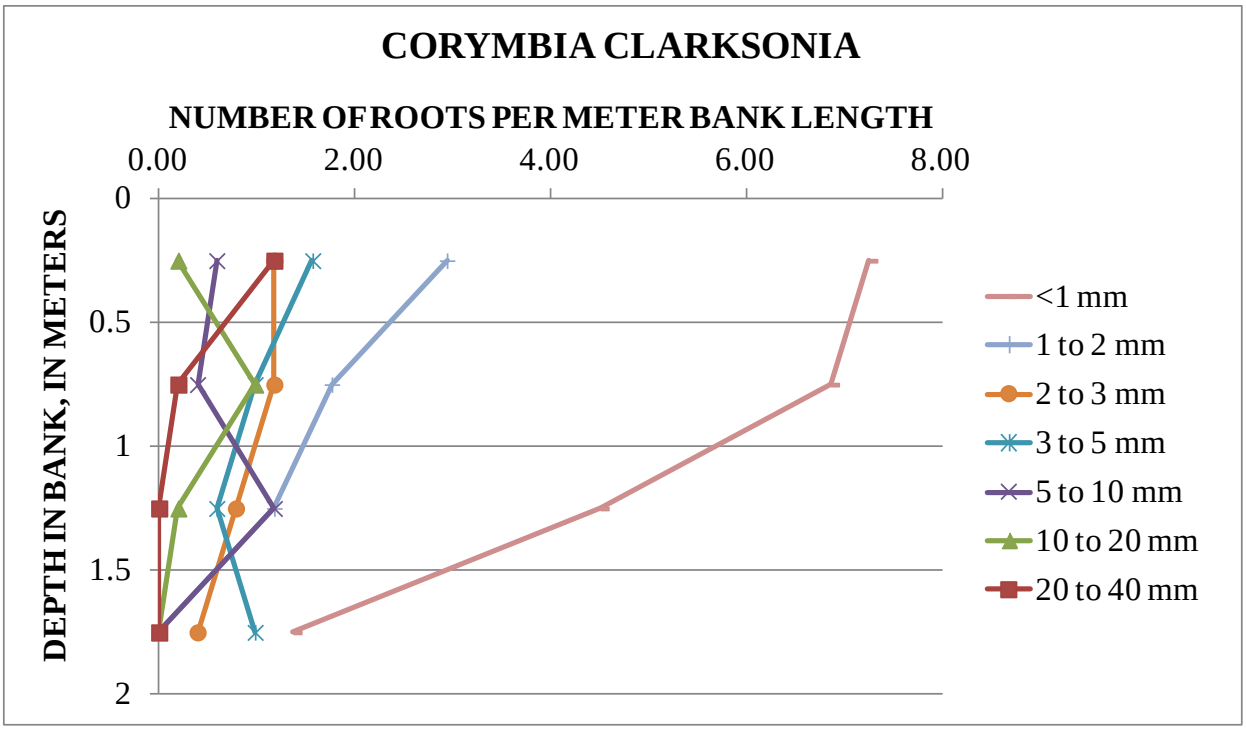
CORYMBIA CLARKSONIA
NUMBER OF ROOTS PER METER BANK LENGTH
0.00
2.00
4.00
6.00
8.00
DEPTH IN BANK, IN METERS
0
0.5
1
1.5
2
<1 mm
1 to 2 mm
2 to 3 mm
3 to 5 mm
5 to 10 mm
10 to 20 mm
20 to 40 mm

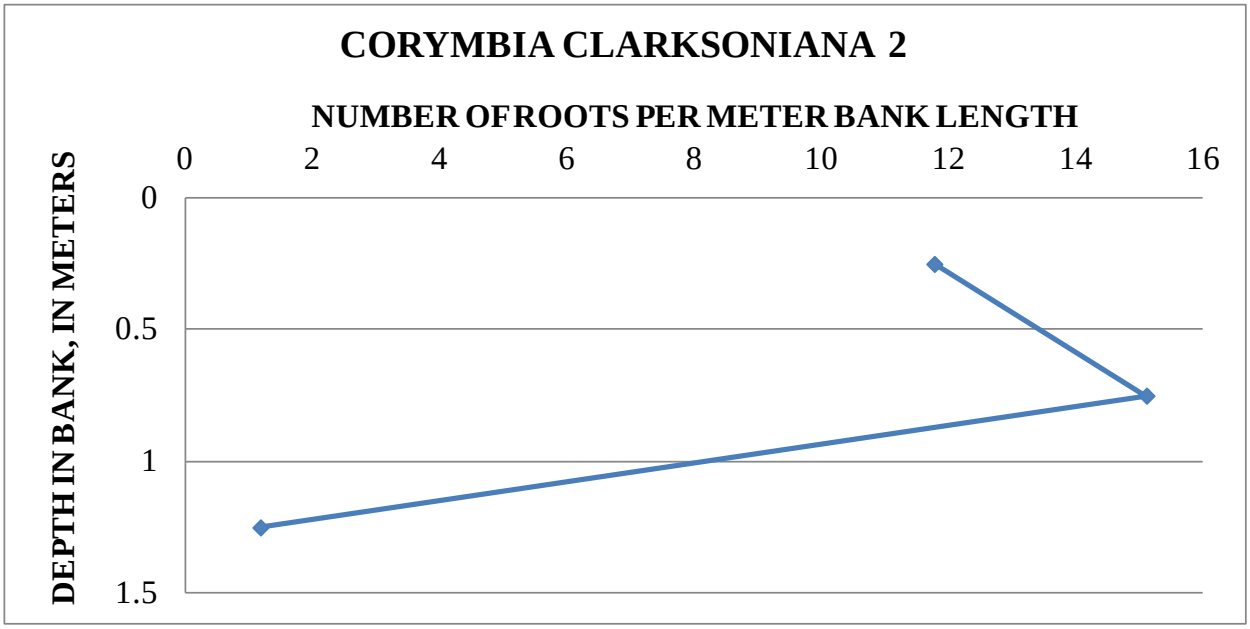
CORYMBIA CLARKSONIANA 2
NUMBER OF ROOTS PER METER BANK LENGTH
0
2
4
6
8
10
12
14
16
DEPTH IN BANK, IN METERS
0
0.5
1
1.5

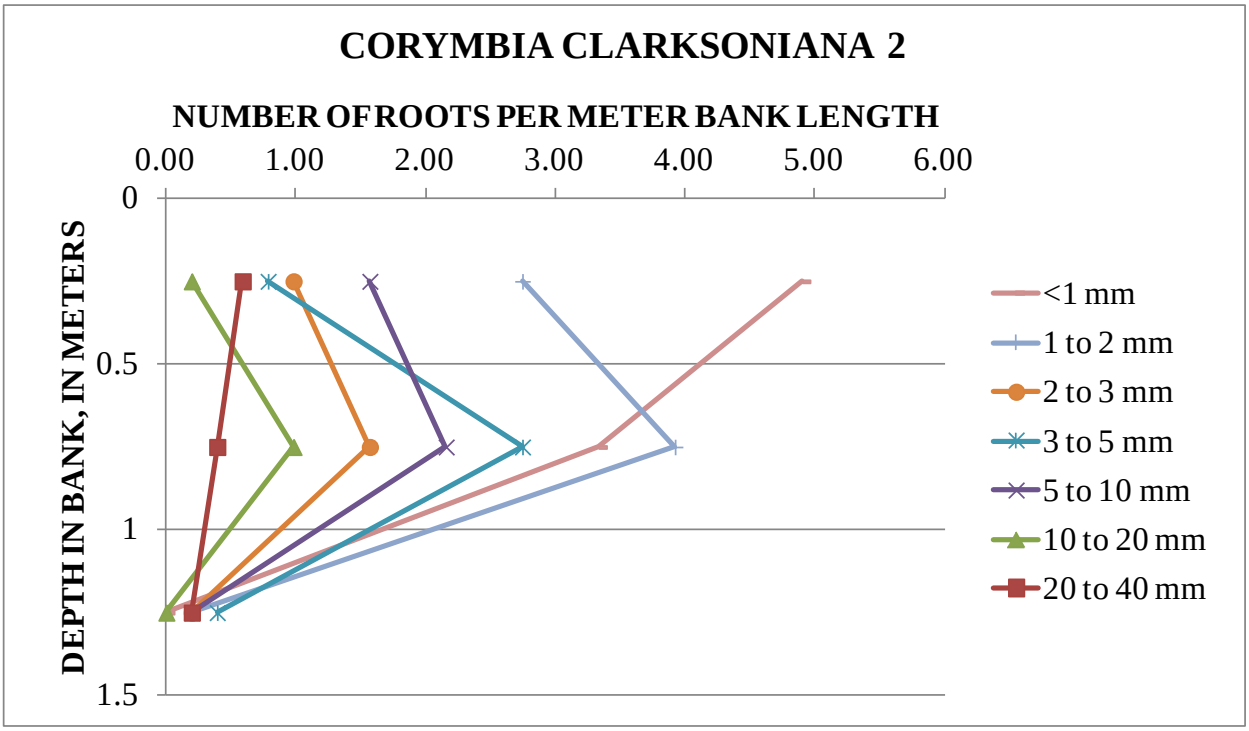
CORYMBIA CLARKSONIANA 2
NUMBER OF ROOTS PER METER BANK LENGTH
0.00
1.00
2.00
3.00
4.00
5.00
6.00
DEPTH IN BANK, IN METERS
0
0.5
1
1.5
<1 mm
1 to 2 mm
2 to 3 mm
3 to 5 mm
5 to 10 mm
10 to 20 mm
20 to 40 mm

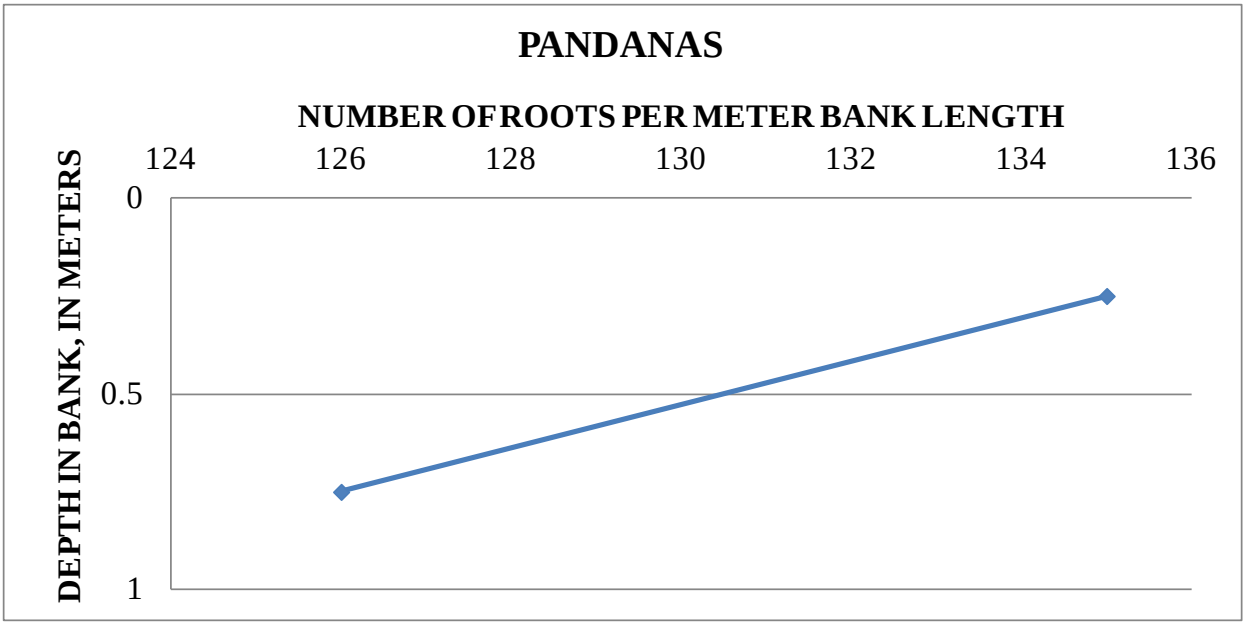
PANDANAS
NUMBER OF ROOTS PER METER BANK LENGTH
124
126
128
130
132
134
136
DEPTH IN BANK, IN METERS
0
0.5
1

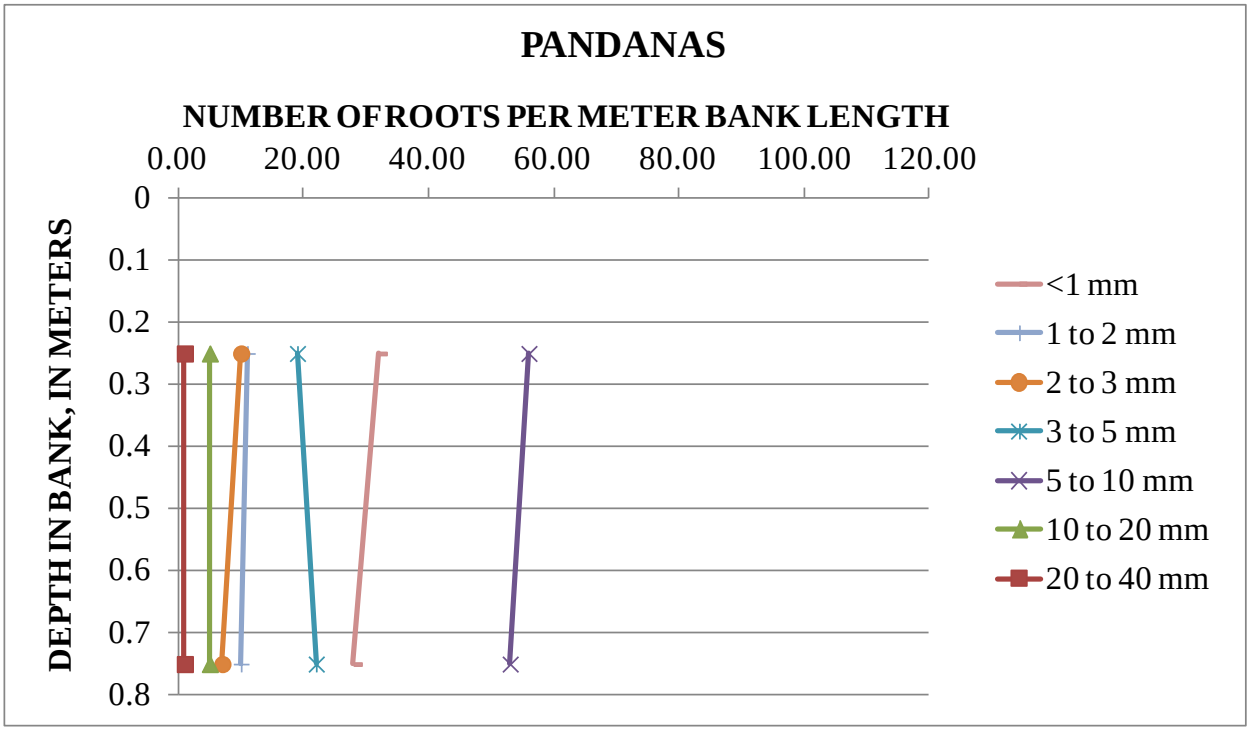
PANDANAS
NUMBER OF ROOTS PER METER BANK LENGTH
0.00
20.00
40.00
60.00
80.00
100.00
120.00
DEPTH IN BANK, IN METERS
0
0.1
0.2
0.3
0.4
0.5
0.6
0.7
0.8
<1 mm
1 to 2 mm
2 to 3 mm
3 to 5 mm
5 to 10 mm
10 to 20 mm
20 to 40 mm

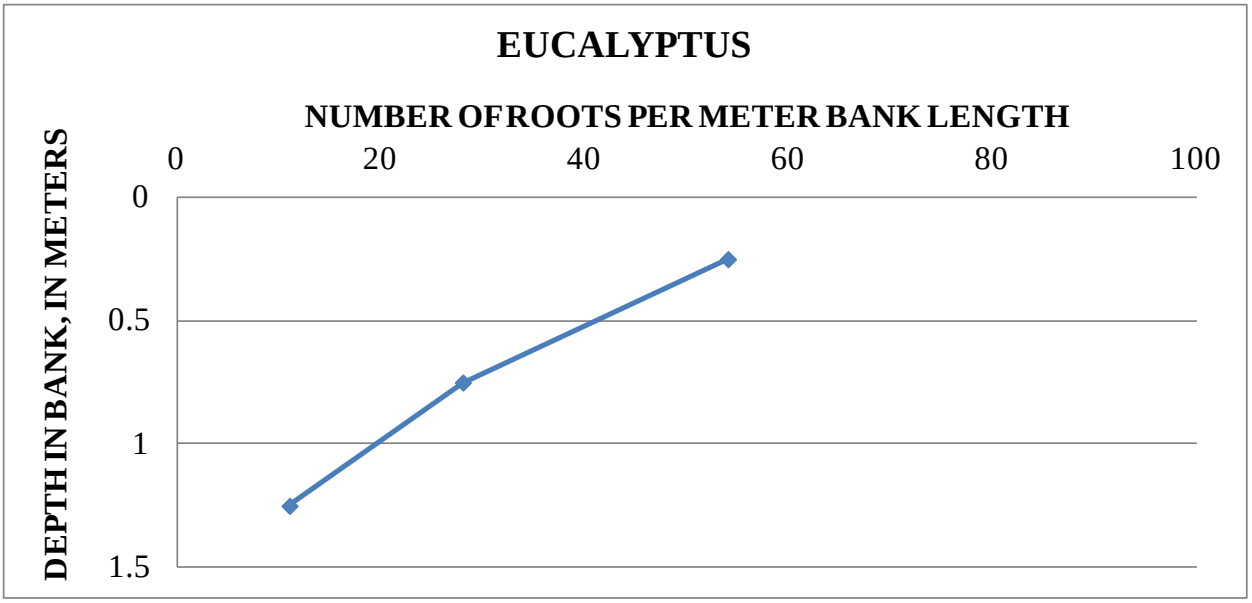
EUCALYPTUS
NUMBER OF ROOTS PER METER BANK LENGTH
0
20
40
60
80
100
DEPTH IN BANK, IN METERS
0
0.5
1
1.5

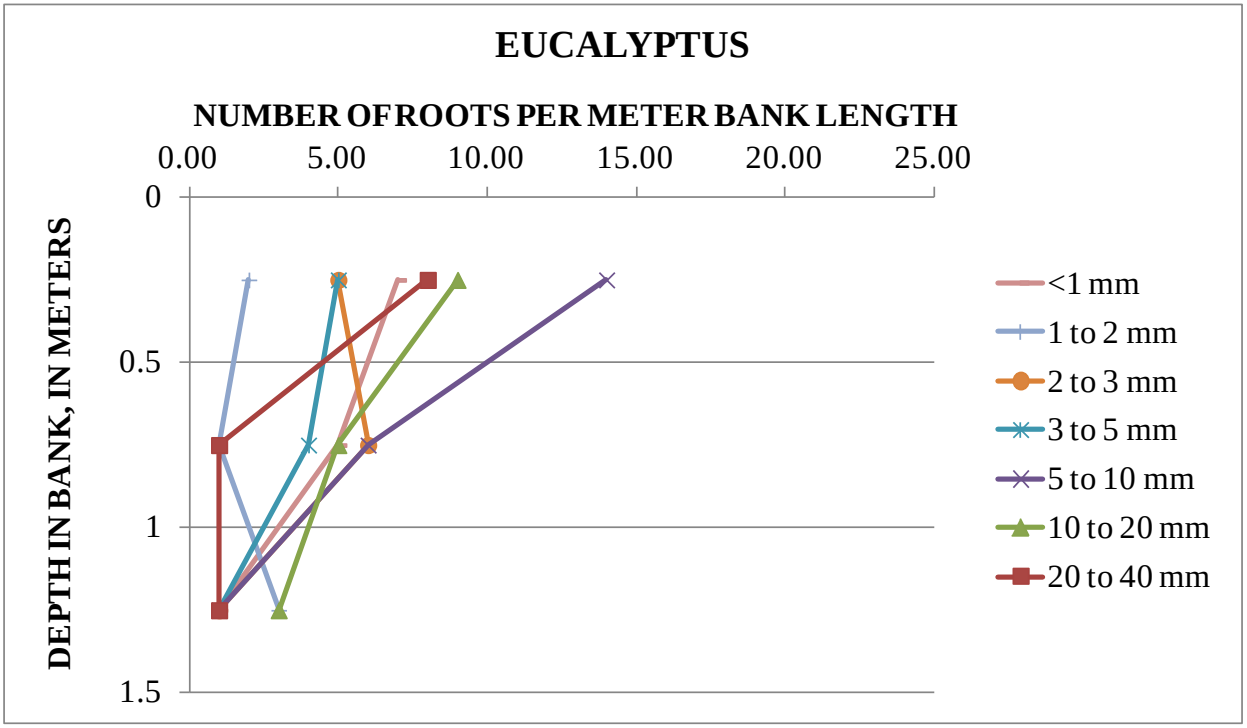
EUCALYPTUS
NUMBER OF ROOTS PER METER BANK LENGTH
0.00
5.00
10.00
15.00
20.00
25.00
DEPTH IN BANK, IN METERS
0
0.5
1
1.5
<1 mm
1 to 2 mm
2 to 3 mm
3 to 5 mm
5 to 10 mm
10 to 20 mm
20 to 40 mm

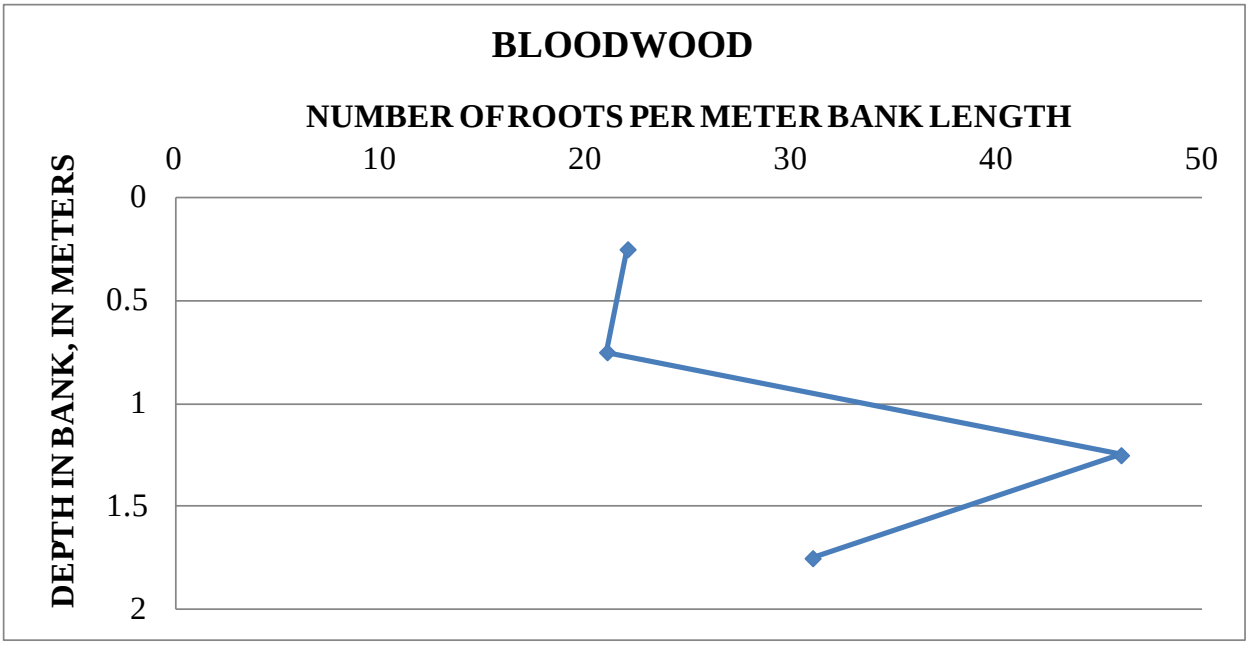
BLOODWOOD
NUMBER OF ROOTS PER METER BANK LENGTH
0
10
20
30
40
50
DEPTH IN BANK, IN METERS
0
0.5
1
1.5
2

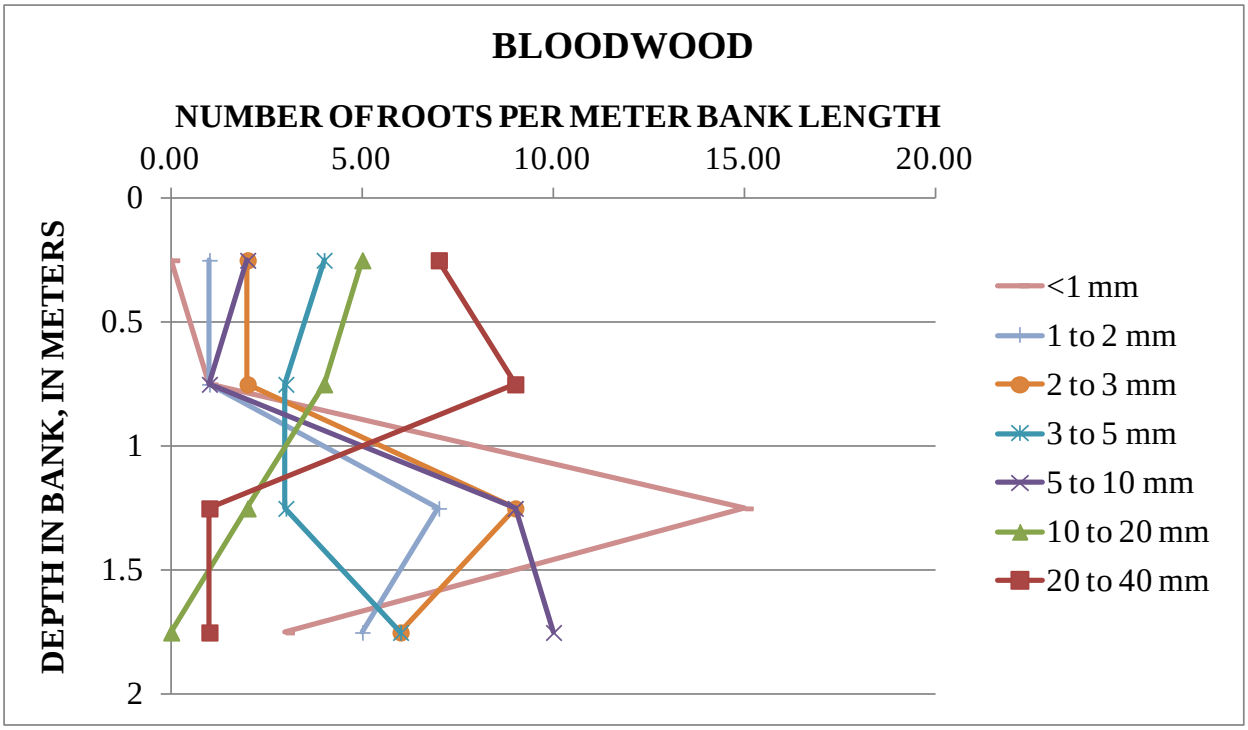
BLOODWOOD
NUMBER OF ROOTS PER METER BANK LENGTH
0.00
5.00
10.00
15.00
20.00
DEPTH IN BANK, IN METERS
0
0.5
1
1.5
2
<1 mm
1 to 2 mm
2 to 3 mm
3 to 5 mm
5 to 10 mm
10 to 20 mm
20 to 40 mm

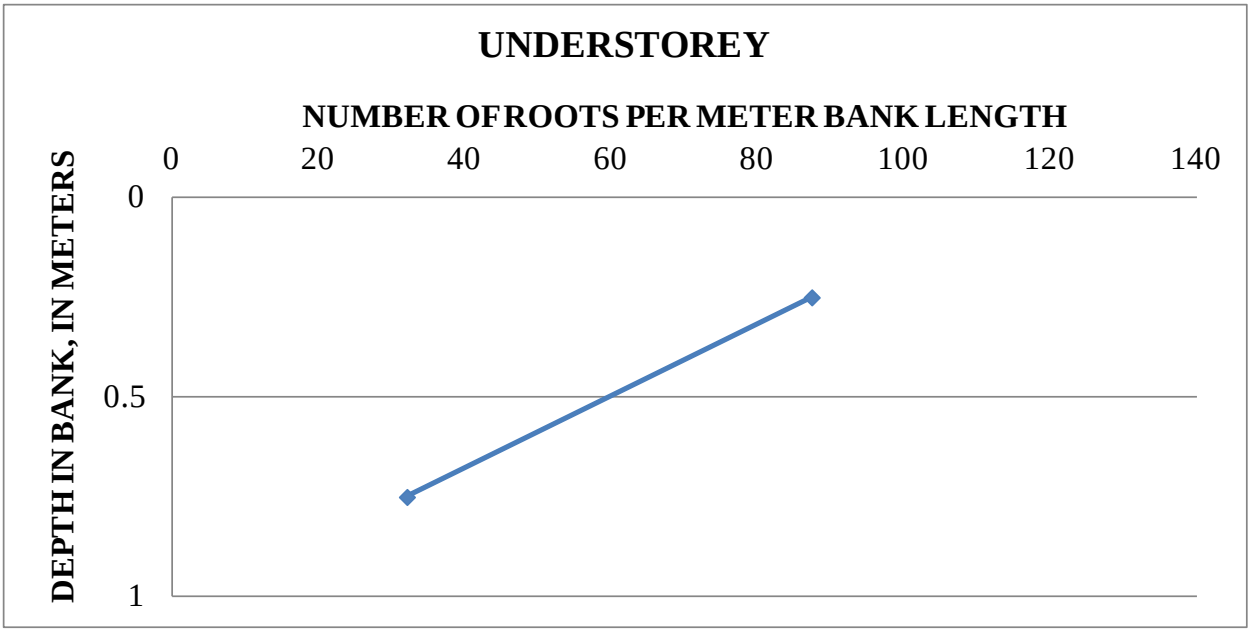
UNDERSTOREY
NUMBER OF ROOTS PER METER BANK LENGTH
0
20
40
60
80
100
120
140
DEPTH IN BANK, IN METERS
0
0.5
1

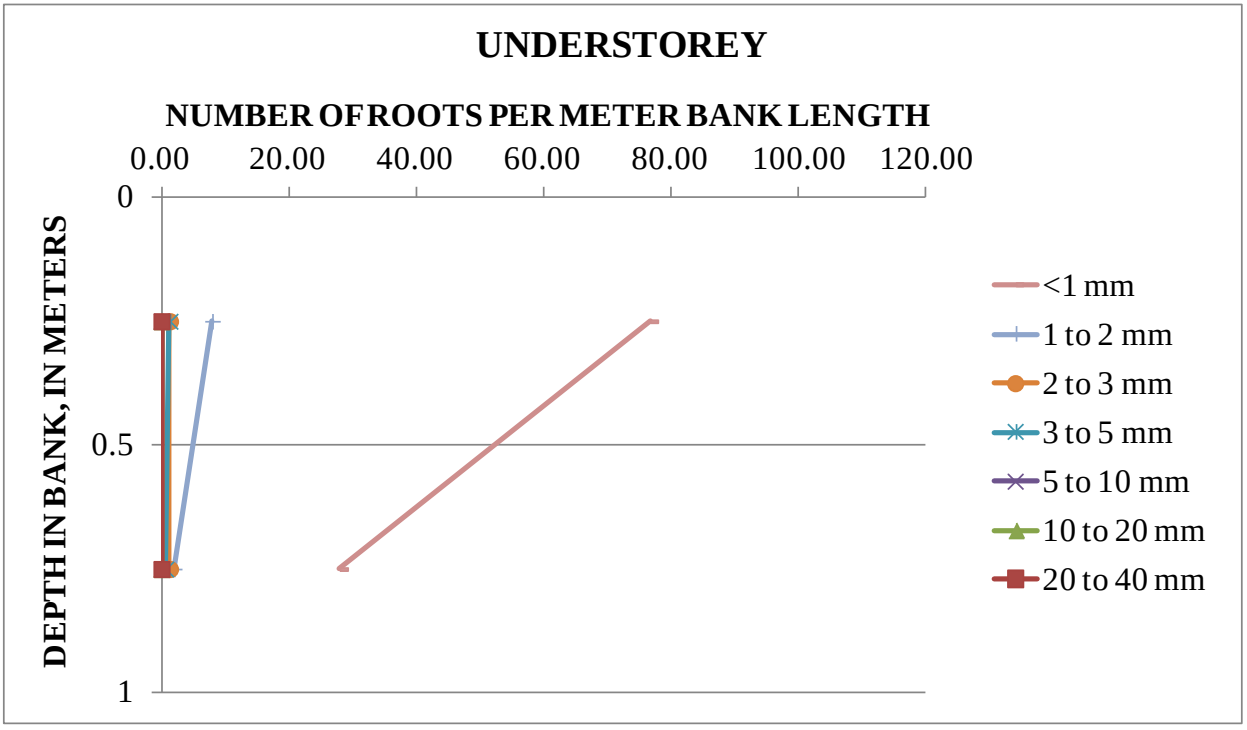
UNDERSTOREY
NUMBER OF ROOTS PER METER BANK LENGTH
0.00
20.00
40.00
60.00
80.00
100.00
120.00
DEPTH IN BANK, IN METERS
0
0.5
1
<1 mm
1 to 2 mm
2 to 3 mm
3 to 5 mm
5 to 10 mm
10 to 20 mm
20 to 40 mm

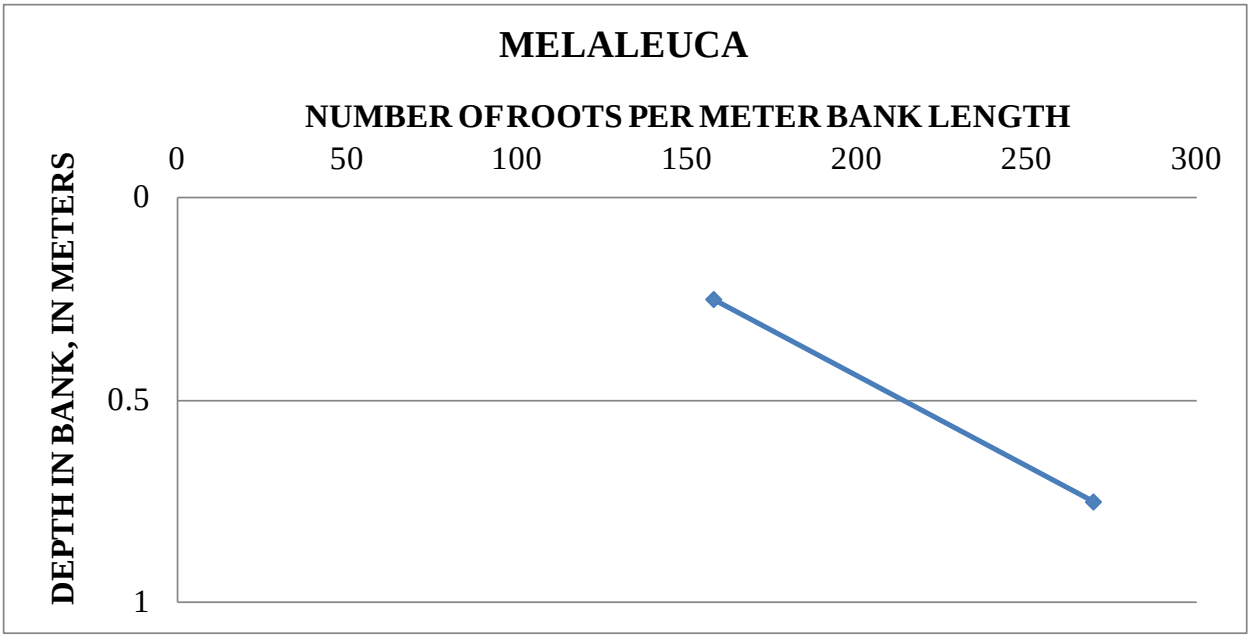
MELALEUCA
NUMBER OF ROOTS PER METER BANK LENGTH
0
50
100
150
200
250
300
DEPTH IN BANK, IN METERS
0
0.5
1

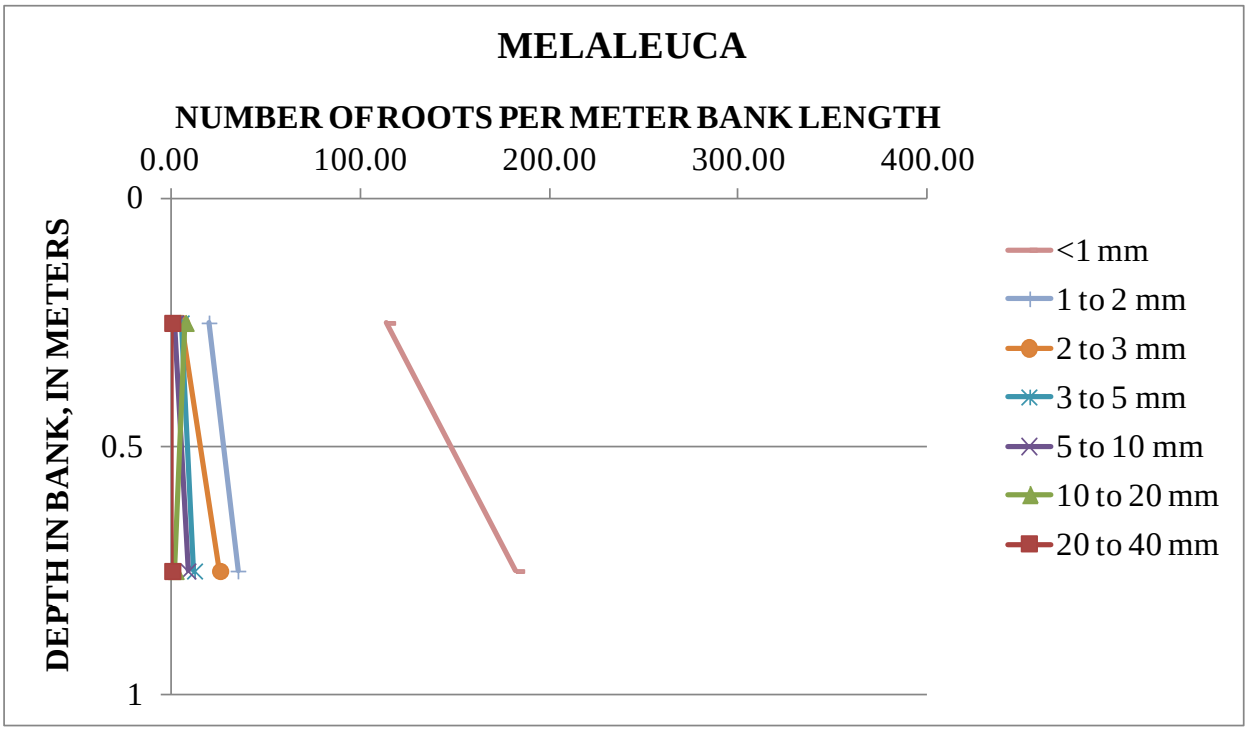
MELALEUCA
NUMBER OF ROOTS PER METER BANK LENGTH
0.00
100.00
200.00
300.00
400.00
DEPTH IN BANK, IN METERS
0
0.5
1
<1 mm
1 to 2 mm
2 to 3 mm
3 to 5 mm
5 to 10 mm
10 to 20 mm
20 to 40 mm

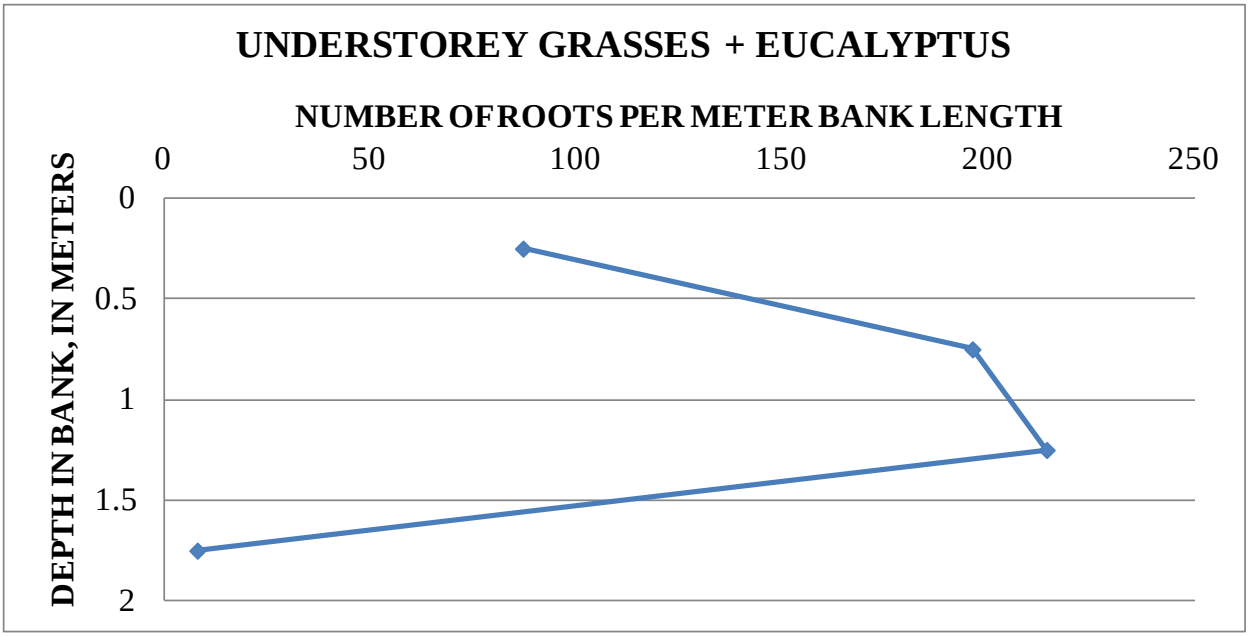
UNDERSTOREY GRASSES + EUCALYPTUS
NUMBER OF ROOTS PER METER BANK LENGTH
0
50
100
150
200
250
DEPTH IN BANK, IN METERS
0
0.5
1
1.5
2

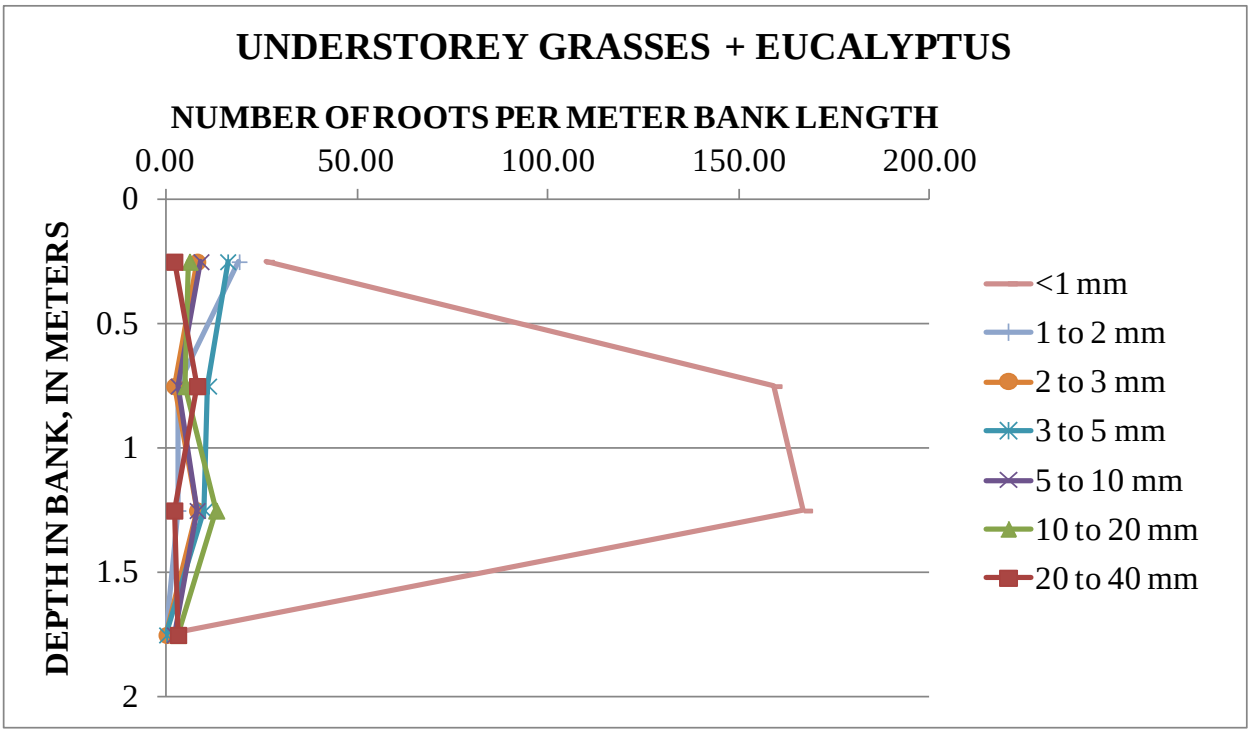
UNDERSTOREY GRASSES + EUCALYPTUS
NUMBER OF ROOTS PER METER BANK LENGTH
0.00
50.00
100.00
150.00
200.00
DEPTH IN BANK, IN METERS
0
0.5
1
1.5
2
<1 mm
1 to 2 mm
2 to 3 mm
3 to 5 mm
5 to 10 mm
10 to 20 mm
20 to 40 mm

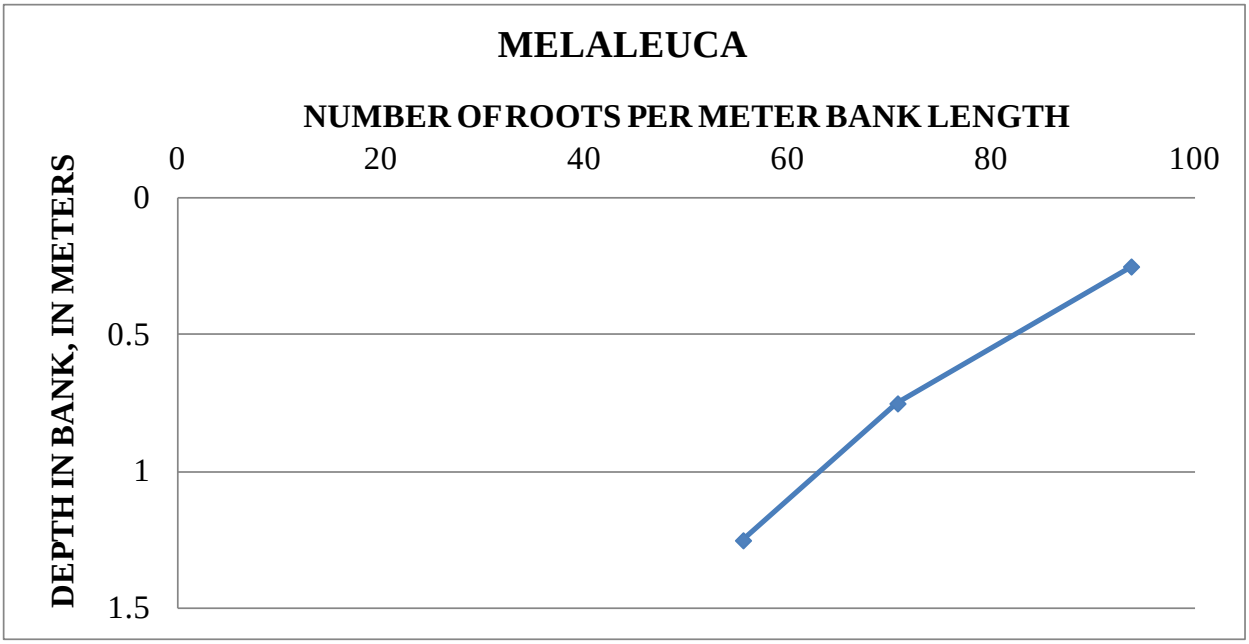
MELALEUCA
NUMBER OF ROOTS PER METER BANK LENGTH
0
20
40
60
80
100
DEPTH IN BANK, IN METERS
0
0.5
1
1.5

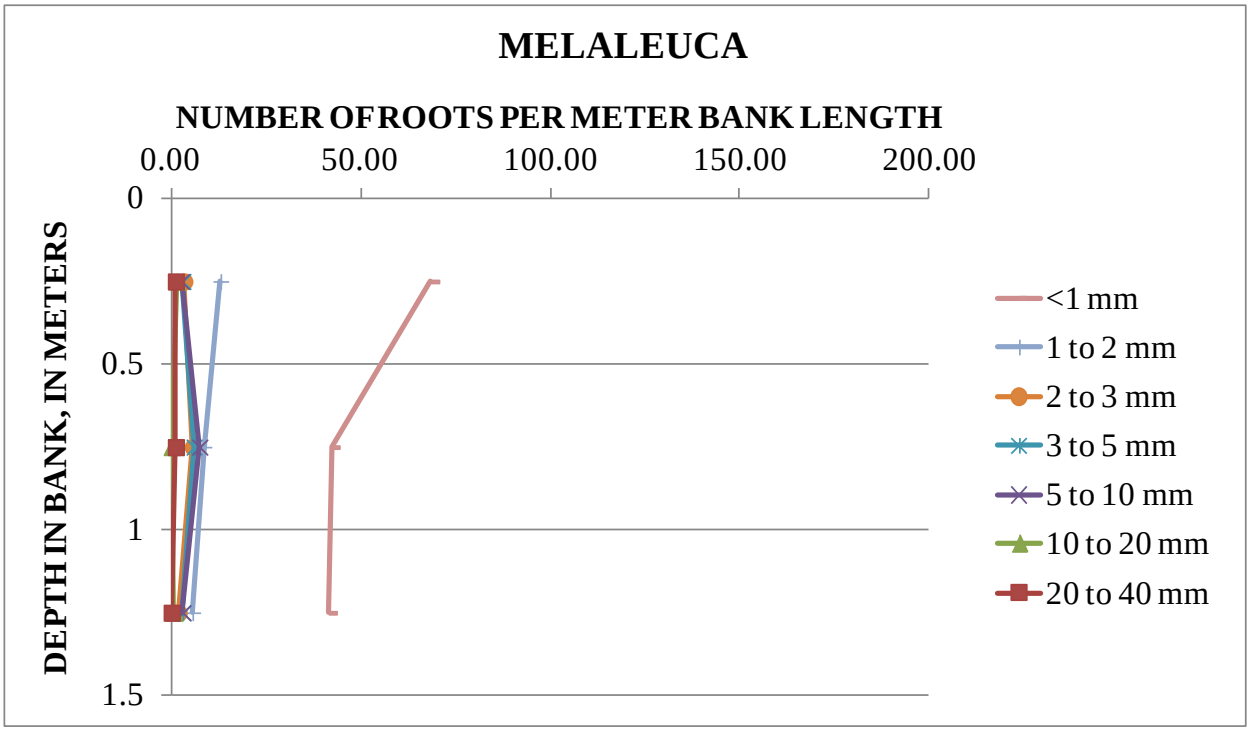
MELALEUCA
NUMBER OF ROOTS PER METER BANK LENGTH
0.00
50.00
100.00
150.00
200.00
DEPTH IN BANK, IN METERS
0
0.5
1
1.5
<1 mm
1 to 2 mm
2 to 3 mm
3 to 5 mm
5 to 10 mm
10 to 20 mm
20 to 40 mm

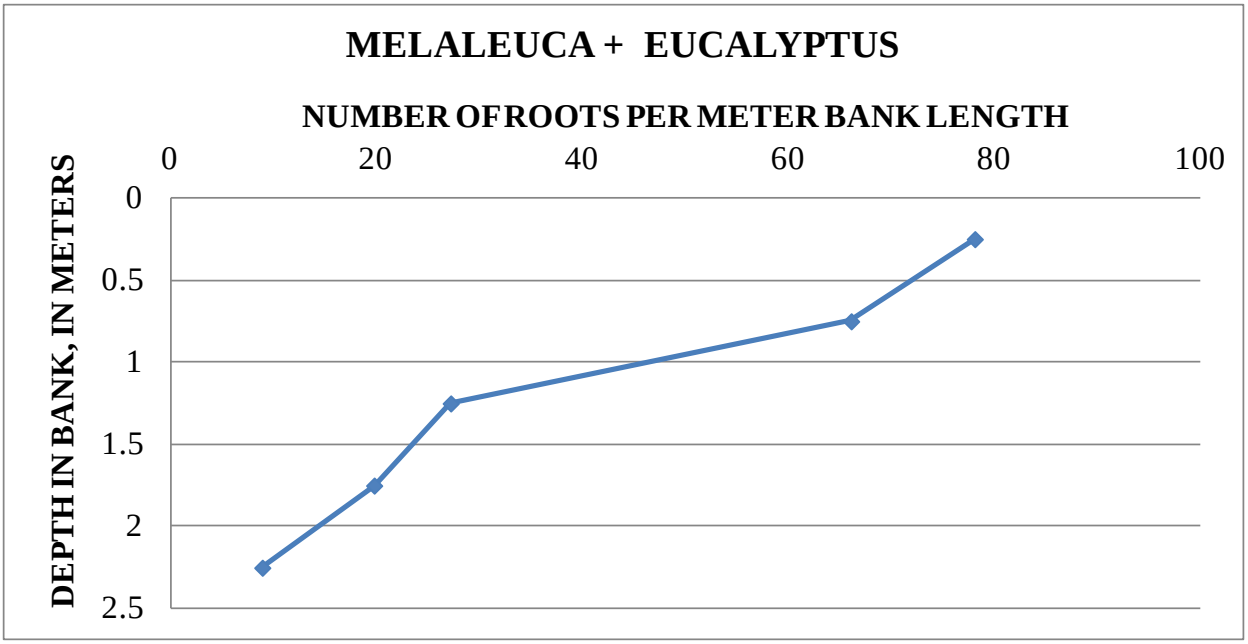
MELALEUCA + EUCALYPTUS
NUMBER OF ROOTS PER METER BANK LENGTH
0
20
40
60
80
100
DEPTH IN BANK, IN METERS
0
0.5
1
1.5
2
2.5

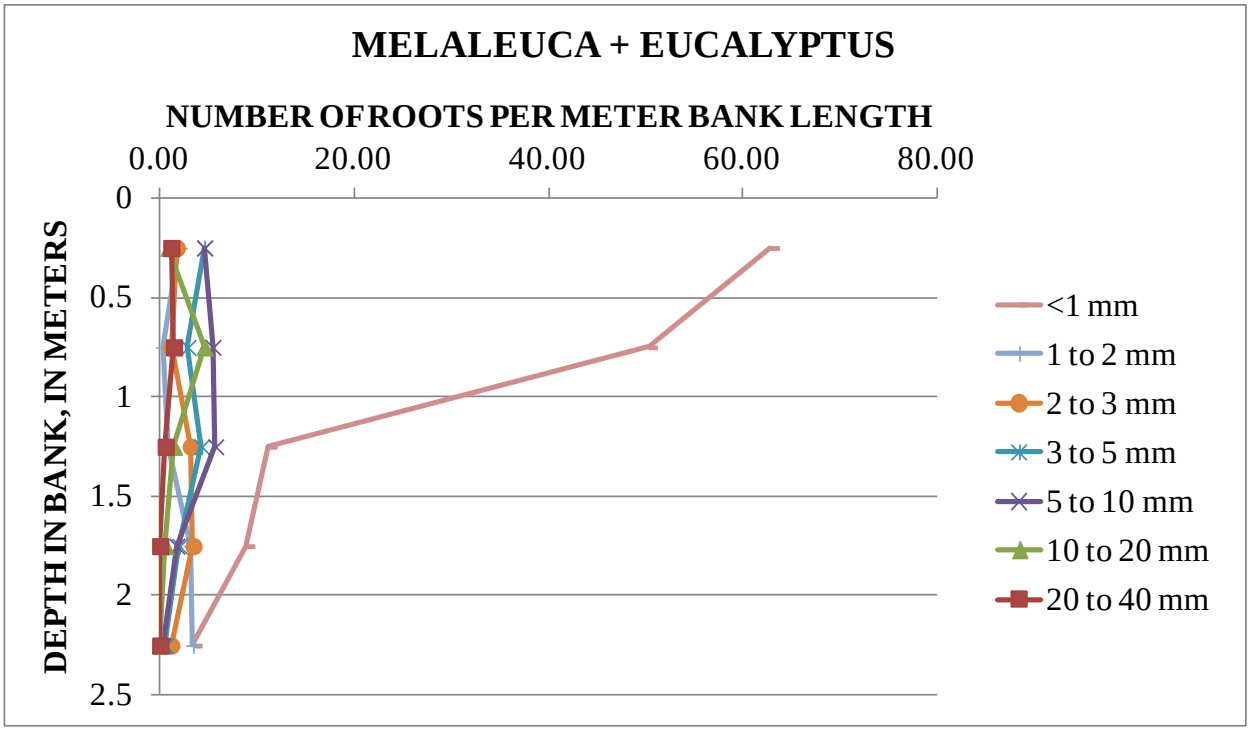
MELALEUCA + EUCALYPTUS
NUMBER OF ROOTS PER METER BANK LENGTH
0.00
20.00
40.00
60.00
80.00
DEPTH IN BANK, IN METERS
0
0.5
1
1.5
2
2.5
<1 mm
1 to 2 mm
2 to 3 mm
3 to 5 mm
5 to 10 mm
10 to 20 mm
20 to 40 mm